The involvement of TRAP1 in the mitochondrial localization of STAT3 in mammalian cells

A dissertation submitted in fulfillment of the requirements for the degree of

MASTER OF SCIENCE
in Biotechnology

for

Rhodes University

Rose Kadye

January 2014

ABSTRACT

STAT3 (signal transducer and activator of transcription 3), an oncogene and transcription factor of genes involved in cellular differentiation, proliferation and immune function, that classically localizes in the cytosol and nucleus has also been found in the mitochondria. However, STAT3 does not have a mitochondrial transit peptide, and its mechanism for mitochondrial localization is unknown. Cytosolic Hsp90s chaperone STAT3 to the nucleus therefore we investigated the involvement of the nuclear-encoded mitochondrial Hsp90 molecular chaperone tumor necrosis receptor associated protein 1 (TRAP1) in STAT3's mitochondrial localization. Using TRAP1 transient over-expression, STAT3 inhibitor S3I-201 and Hsp90 inhibitor geldanamycin, we demonstrate that TRAP1 and STAT3 co-localize and co-immunoprecipitates in mammalian systems. Taken together with the observation that STAT3 potentially directly interacts with TRAP1, these data suggest that TRAP1 plays a role in the mitochondrial localization of STAT3.

ACKNOWLEDGEMENTS

I would like to thank my indispensible supervisor, Dr. Earl Prinsloo for his endless support, invaluable advice, and helpful criticisms which have allowed for me to grow as a critical researcher.

I am indebted to my co-supervisor Prof. Heinrich Hoppe for his expertise and advice.

I also acknowledge the following contributions:

- Dr. Sharon Prince (University of Capetown, South Africa) for MCF7 cells
- Prof. Carminita L Frost (Nelson Mandela Metropolitan University, South Africa) for 3T3-L1 cells
- Prof. Franca Esposito (Università degli Studi di Napoli Federico II, Napoli, Italy) for the TRAP1 construct
- Dr. Christoph Muller (European Molecular Biology Laboratory Heidelberg) for the STAT3 construct
- Dr. Adrienne L. Edkins (Rhodes University, South Africa) for all her assistance with confocal microscopy analysis and flow cytometry
- My colleagues in BioBRU, for being dependent and humorous and for making each day of my laboratory experience enjoyable
- My friends at Rhodes University for making the past 4 years very memorable
- Andrew Mellon Scholarship Foundation
- Rhodes University Prestigious Scholarship Programme
- National Research Foundation (South Africa)

I finally express my gratitude to my husband and daughter, Wilbert and Sally Vimbai Kadye. Their unfailing love and support throughout my academics have inspired me to give my best in everything that I do.

OUTPUTS

Article in press

Kadye, R., Kramer, A. H., Joos-Vandewalle, J., Parsons, M., Njengele, Z., Hoppe, H. and Prinsloo, E. (2013), **Guardian of the Furnace: Mitochondria, TRAP1, ROS and stem cell maintenance.** *IUBMB Life*. doi: 10.1002/iub.1234

TABLE OF CONTENTS

LIST OF FIGURES

CHAPTER 1: Literature Review

CHAPTER 2: Bioinformatic Analysis of TRAP1 and STAT3

CHAPTER 3: The effect of TRAP1 in mitochondrial localization of STAT3 in mouse 3T3L1 pre-adipocytes

LIST OF TABLES

LIST OF ABBREVIATIONS

ABCB1	ATP-binding cassette sub-family B, member 1
ABCG2	ATP-binding cassette sub-family G, member 2
ADP	Adenosine 5´-diphosphate
ATFS-1	activating transcription factor associated with Stress-1
ATP	Adenosine 5´-triphosphate
BSA	bovine serum albumin
Ch1:Ch2	channel 1 to channel 2 ratio
CI	cell index
CSC	cancer stem cell
DCFDA	2',7'-dichlorofluoresein diacetate
DMEM	Dulbecco's modified Eagle's medium
DMSO	dimethyl sulphoxide
DNA	Deoxyribose Nucleic Acid
EDTA	ethylenediamine tetra-acetic acid
EGFR	epidermal growth factor receptor
ESC	embryonic stem cell
ETC	electron transport chai
FPLC	Fast Protein Liquid Chromatography
GA	geldanamycin
GRIM-19	gene associated with retinoic-IFN-induced mortality
GRP94	glucose-regulated protein 94
GTPase	Guanosine-5'-triphosphatase
HA	haemoglutinin
HEPES	N-(2-Hydroxyethyl) piperazine-N'-(2-ethanesulfonic acid)
HIFCS	heat inactivated fetal calf serum
HP1	heterochromatin protein 1
HRP	horse radish peroxidase
Hsp	heat shock protein
ICQ	intensity correlation coefficient
IPTG	Isopropyl β-D-1-thiogalactopyranoside
JAK	Janus Kinase
JTT	Jones-Taylor-Thornton

LB	Luria broth
LIF	leukemia inhibitory factor
M	Methionine
MAFFT	Multiple-Sequence-Alignment using-Fast-Fourier-Transform
MEGA	Molecular Evolutionary Genetics Analysis
ML	maximum likelihood
mtDNA	mitochondrial DNA
MTOR	mammalian target of rapamycin
MUSCLE	Multiple Sequence Comparison by Log-Expectation
NADH	nicotinamide adenine dinucleotide hydride
NCBI	National Center for Biotechnology Information
NP40	Nonidet P40
OD	optical density
PAGE	polyacrylamide gel electrophoresis
PBS	phosphate buffered saline
PDB	Protein data base
PMSF	Phenylmethylsulfonyl fluoride
pSTAT3S727	STAT3 phosphorylated at serine 727
pSTAT3Y705	STAT3 phosphorylated at serine 727
PTEN	Phosphatase and tensin
PVDF	Polyvinylidene fluoride
R	Manders' overlap coefficient
Rac1	Ras-related C3 botulinum toxin substrate 1
REDOX	reduction-oxidation
RGB	red green blue
RIPA	radioimmunoprecipitation assay
ROS	reactive oxygen species
Rr	Pearsons' correlation coefficient
rRNA	ribosomal RNA
RT	room temperature
RTCA	real time cell analysis
SSC	somatic stem cell
SDS	sodium dodecyl sulphate

SPR	surface Plasmon resonance
STAT	signal transducer and activator of transcription
TBS	tris-bufferd saline
TBS-T	tris-bufferd saline-Tween 20
TPR	tetratricopeptide repeat
TRAP1	tumour necrosis factor receptor-associated protein 1
tRNA	transfer RNA
V	Valine
VDAC	Voltage-dependent anion channel

LIST OF SYMBOLS

α	Alpha
β	Beta
°C	degree celcius
M	Molar
mM	millimolar
nM	nanomolar
µg	micrograms
µl	microlitres
L	litres
g	grams
mg	milligrams
kDa	kilo Daltons
min	minutes
mol	mole
ml	millilitre
%	percent or g/100 ml
U	units
V	volts
g	centrifugal force of gravity
rpm	revolutions per minute
v/v	volume to volume ratio
w/v	weight to volume ratio

CHAPTER 1

Literature review

1.1 Introduction

Mitochondria are found in the cytoplasmic matrix where they are the main cellular energy producers for aerobic eukaryotic cells in the form of adenosine tri-phosphate (ATP) through oxidative phosphorylation. In addition to energy production, mitochondria are essential in regulating cellular metabolism, signaling, differentiation, stress response and apoptosis (McBride *et al.*, 2006; Nesti *et al.*, 2007). Because mitochondria are involved in both vital and lethal processes of cellular development, and maintaining homeostasis, defects in both their form and function have negative implications on the cell as a whole (Armstrong, 2007). Dysfunctions of mitochondria are at the core of most human diseases, such as neurodegenerative disorders, premature aging and cancer (Armstrong, 2007). It is therefore crucial to understand the structural processes and signaling pathways that are involved in maintaining mitochondrial homeostasis during periods of both normal and abnormal functioning (Pieczenic and Neustadt, 2007).

Molecular chaperones, also known as stress proteins or heat shock proteins, are important in maintaining proteostasis (Hartl *et al.* 2011). Heat shock proteins are involved in maintaining mitochondrial functioning and homeostasis under normal and stress conditions (Sreedhar and Csermely, 2004; Gesuldi *et al.*, 2007). Furthermore, signaling proteins such as β-catenin have been reported to translocate to the mitochondria during cellular stress to possibly stabilize the mitochondria and promote cell survival and energy production although some of the mechanisms are unknown (Mezhybovska *et al.*, 2009). However, in stem cells, proliferating cancer and cancer stem cells, ATP production shifts from mitochondrial oxidative phosphorylation pathway to cytosolic aerobic glycolysis through the Warburg effect (Warburg, 1927 and 1956). During this process, the mitochondria appear to play less roles in ATP production. Nevertheless, reactive oxygen species (ROS), a by-product of mitochondrial activity through the electron transport chain, have been implicated in driving normal stem cell differentiation and advancing oncogenesis in cancer (Kondoh, 2007; Lopez-Lazaro, 2008). Functional mitochondria are therefore required by both normal and cancer cells (Potikha *et al.*, 1991; Richard *et al.* 2002; Waris and Ahsan, 2006).

1.2 Mitochondria in mammalian cells

1.2.1 Mitochondrial structure

Eukaryotic mitochondria are double-membrane bound cytoplasmic structures that are 0.5-1 micrometer (μm) in diameter (Alberts *et al.,* 1994). The organization of the two membranes divides the mitochondrion into five distinct parts; the inner and outer mitochondrial membranes, the inter-membrane space, the cristae and the matrix (See Figure 1.1A). The inner and outer mitochondrial membranes are each composed of a phospholipid bilayer and proteins in a similar manner as the plasma membrane (Alberts *et al.,* 1994).

The outer mitochondrial membrane contains proteins that allow molecules of 5000 Daltons or less to pass freely (Stein, 1967; Neupert and Herrmann 2007). However, larger proteins may pass through a specific signaling sequence on their N-terminals (Neupert and Herrmann 2007). By comparison, the inner mitochondrial membrane contains proteins that are involved in mitochondrial respiration (oxidative phosphorylation) and constitutes 20 % of the total mitochondrial proteins (Alberts *et al.,* 1994). Due to the activities associated with the electron transport chain, the inner mitochondrial membrane has a membrane potential across it. The mitochondrial resting potential is higher that of the cell membrane as demonstrated by that of rat cortical neurons which has been reported at -139 mV while that of the neuronal cell membrane ranges from -70 to -80 mV (Chen, 1988; Gerencser *et al.,* 2012). Between the inner and outer mitochondrial membranes is the inter-membrane space, whose main function is oxidative phosphorylation (Cooper and Hausman, 2006). While the inward-directed folds of the inner mitochondrial membrane forms the cristae, the matrix, which is the space enclosed by the inner mitochondrial membrane, contains 30-35 % of the total mitochondrial protein and as well as its deoxyribonucleic acid (DNA) (Cooper and Hausman, 2006).

1.2.2 Mitochondrial genome and proteome

Among the cytoplasmic organelles, the mitochondria are unique in that they contain their own DNA, making them semi-autonomous (Cooper and Hausman, 2006). The mitochondrial DNA is usually circular, similar to that of bacteria. Furthermore, each mitochondrion can contain multiple copies of DNA (Weisner *et al.,* 1992; Cooper and Hausman, 2006). There are, however, some variants in the mitochondrial DNA codon usage compared to those of the nuclear DNA. For

example in mammals, the “universal” codons for arginine, AGA and AGG, in nuclear DNA, are stop codons in mitochondrial DNA (Cooper and Hausman, 2006). Furthermore, the mitochondrial DNA only codes for genes of the electron transport chain, oxidative phosphorylation and their translation apparatus (Figure 1.1B) (Bullerwell and Gray, 2004). In humans, mitochondrial DNA codes for a total of 37 genes with no introns. These genes are all for inner mitochondrial membrane proteins; 2 ribosomal RNAs (rRNAs), 22 transfer RNAs (tRNAs), of which 20 are for standard amino acids and an extra gene for leucine and serine (Anderson *et al.*, 1981; Pérez-Martinez *et al.*, 2008). The nuclear genome encodes for the rest of the proteins found in the mitochondria, bringing the mitochondrial proteome in humans to 1500 different proteins (Lonergan *et al.*, 2007; Meisinger *et al.*, 2008).

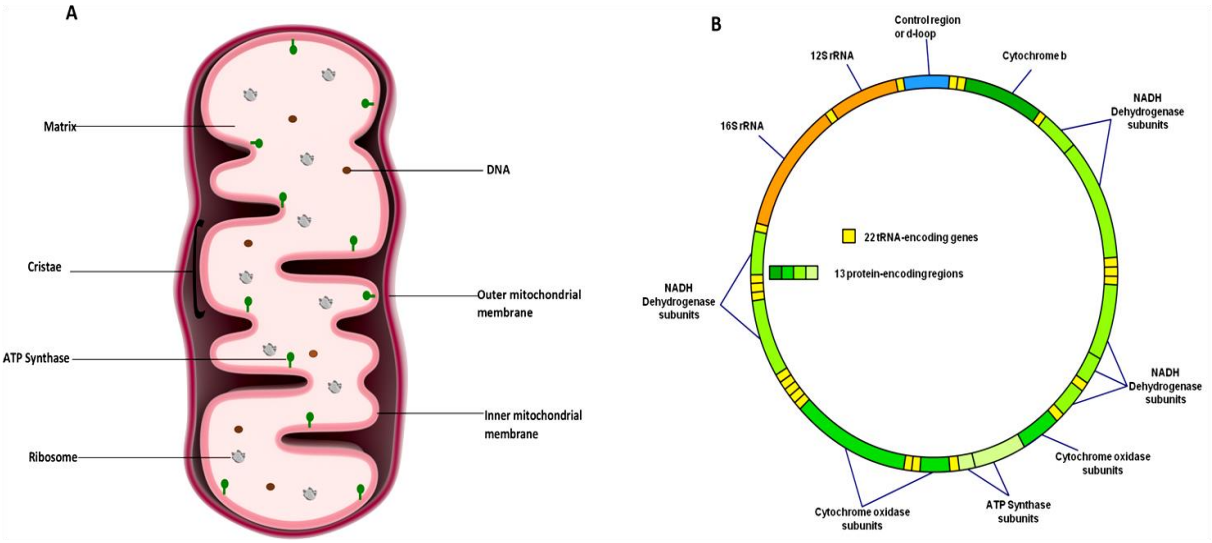

Figure 1.1: A diagram showing (A) the mitochondrion (www.somersault1824.com) and (B) the plasmid map of genes encoded by the mitochondrial DNA. The plasmid map was obtained from Wikimedia Commons authored by Shanel under the GNU Free Documentation License, version 1.2.

1.2.3 Mitochondrial oxidative phosphorylation and ROS

In eukaryotes, oxidative phosphorylation occurs in the mitochondrial cristae where nicotinamide adenine dinucleotide hydride (NADH) produced from the citric acid (TCA) cycle is oxidized in an electron transport chain, establishing a proton gradient across the inner membrane (Figure 1.2) (Lodish *et al.*, 2000). The proton gradient is then used to drive the phosphorylation of adenosine diphosphate (ADP) to ATP using the ATP synthase enzyme.

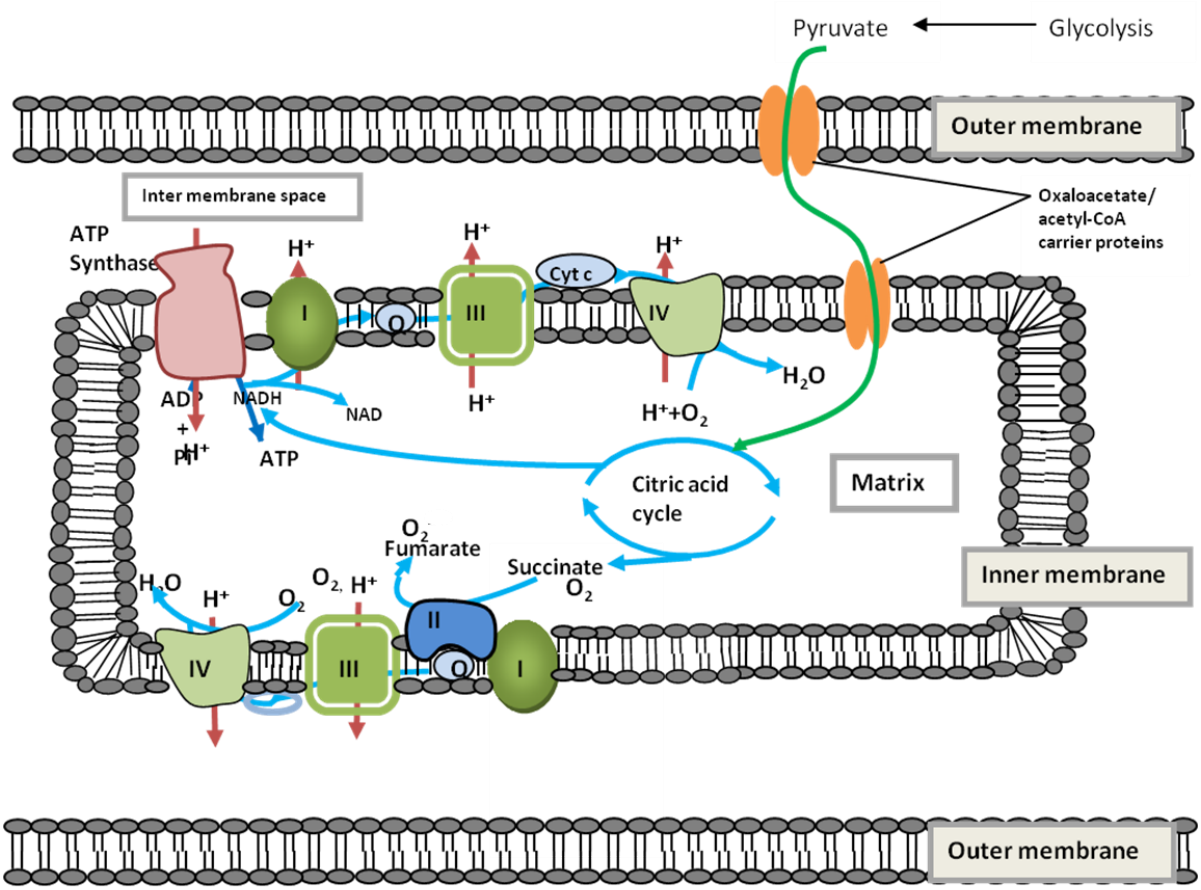

Figure 1.2: Oxidative phosphorylation in eukaryotes. The electron transport chain in the mitochondrion is the site of oxidative phosphorylation, oxidizing nicotinamide adenine dinucleotide hydride (NADH) and succinate that are generated in the citric acid cycle, powering ATP synthase to produce ATP and ROS(O_2^-) (adapted from Turrens, 2003).

The transport chain of electrons released when NADH is oxidized terminates with the transfer of electrons and addition of two protons to exogenous oxygen to form water (Lodish *et al.*, 2000). Furthermore, various respiratory complexes leak electrons to oxygen and reduces it to a ROS superoxide (O_2^-), (see Figure 1.2) (Turrens, 2003; Zhang and Darnell, 2001; Han *et al.*, 2001). Low ROS levels play a key role in normal signaling by regulating reduction-oxidation (REDOX) signaling pathways, whereas high levels have been found to induce permeability of the mitochondrial membrane leading to both arrest of biosynthetic pathways and mitochondrial induced cell death through apoptosis (Schumacker, 2006; Galluzi *et al.*, 2010).

1.2.4 Mitochondrial distribution in cells

Mitochondrial number in a cell varies depending on the organism and cell type, ranging from a single in most unicellular to thousands in multi-cellular organisms (Freitas *et al.*, 1999; Aldon *et al.*, 2009). In higher eukaryotes, the distribution of mitochondria is mediated by the cytoskeleton that provides a structural framework to maintain the position of these organelles and form mitochondrial networks Rappaport, 1998; Okamoto, 2005). In differentiated somatic cells, mitochondrial networks are scattered homogenously throughout the cytoplasm, whereas in embryonic stem and sperm cells they are found in peri-nuclear and around flagella, respectively (Alberts *et al.*, 1994; Lonergan *et al.*, 2006; Facucho-Oliveria and St. John, 2009). The distribution of mitochondria in the cell is therefore important for ATP delivery and cell development (Frazier *et al.*, 2006).

1.2.5 Mitochondrial homeostasis

Properly functioning mitochondria are required by normal and cancer cells for both energy production and normal cell functioning, hence the need to maintain mitochondrial homeostasis and their integrity to prevent processes that lead to cell death. Nonetheless, maintaining mitochondrial homeostasis and integrity involves several mechanisms that are not solely a mitochondrial responsibility (Liu and Butow, 2006; Ryan and Hoogen-raad, 2007). The majority of the mitochondrial proteome is nuclear encoded. Therefore, the proteins involved in their translocation, such as the molecular chaperones of the heat shock family proteins, also have the responsibility of maintaining the proteome during biogenesis. Heat shock proteins, particularly heat shock proteins 60s, 70s and 90s (Hsp60s, Hsp70s and Hsp90s respectively), have been implicated in maintaining proper folding of mitochondrial proteins and assisting in proteolytic degradation of mis-folded or denatured proteins (Murakami *et al.*, 1988; Beckmann *et al.*, 1990; Jäättelä, 1999). Under mitochondrial stress conditions, nuclear-encoded mitochondrial proteins, such as activating transcription factor associated with Stress-1(ATFS-1), have also been reported to accumulate in the nucleus where they activate transcription of stress response genes (Nargund *et al.*, 2012).

1.3 Mammalian Development, Cellular Maintenance and Differentiation

Mammals, being multi-cellular organisms, are derived from stem cells that self-renew through mitotic cell division. These stem cells differentiate into diverse specialized cell types that are tissue- or organ- specific when induced by certain physiological and experimental conditions (Reya *et al.*, 2001). In normal stem cells, differentiation into specialized organs is a staged process while the differentiation potential (potency) of the stem cells decreases at each stage (Odorico *et al.*, 2001; Wang *et al.*, 2009). Since differentiation is a staged process, it therefore results in multi-lineage heterogeneous differentiated cells. These trademarks in normal stem cells have also been described in cancer (Pardal *et al.*, 2003; Dalerba, 2007).

1.3.1 Stem cells and differentiation

Stem cells are classified based on their source and their differentiation potential (potency). In mammals, there are two broad types of stem cells; embryonic stem cells (ESCs) and somatic (adult or fetal) stem cells (SSCs) (Bianco, 2001; Weiss, 2006). While ESCs differentiate into specialized cells (pluripotent), SSCs derived from bone marrow, blood and adipose tissue can differentiate into multiple cell types (multipotent) and act as a repair system that replenishes adult tissues. Table 1.1 highlights the classification of stem cells based on their potency and Figure 1.3 illustrates this further.

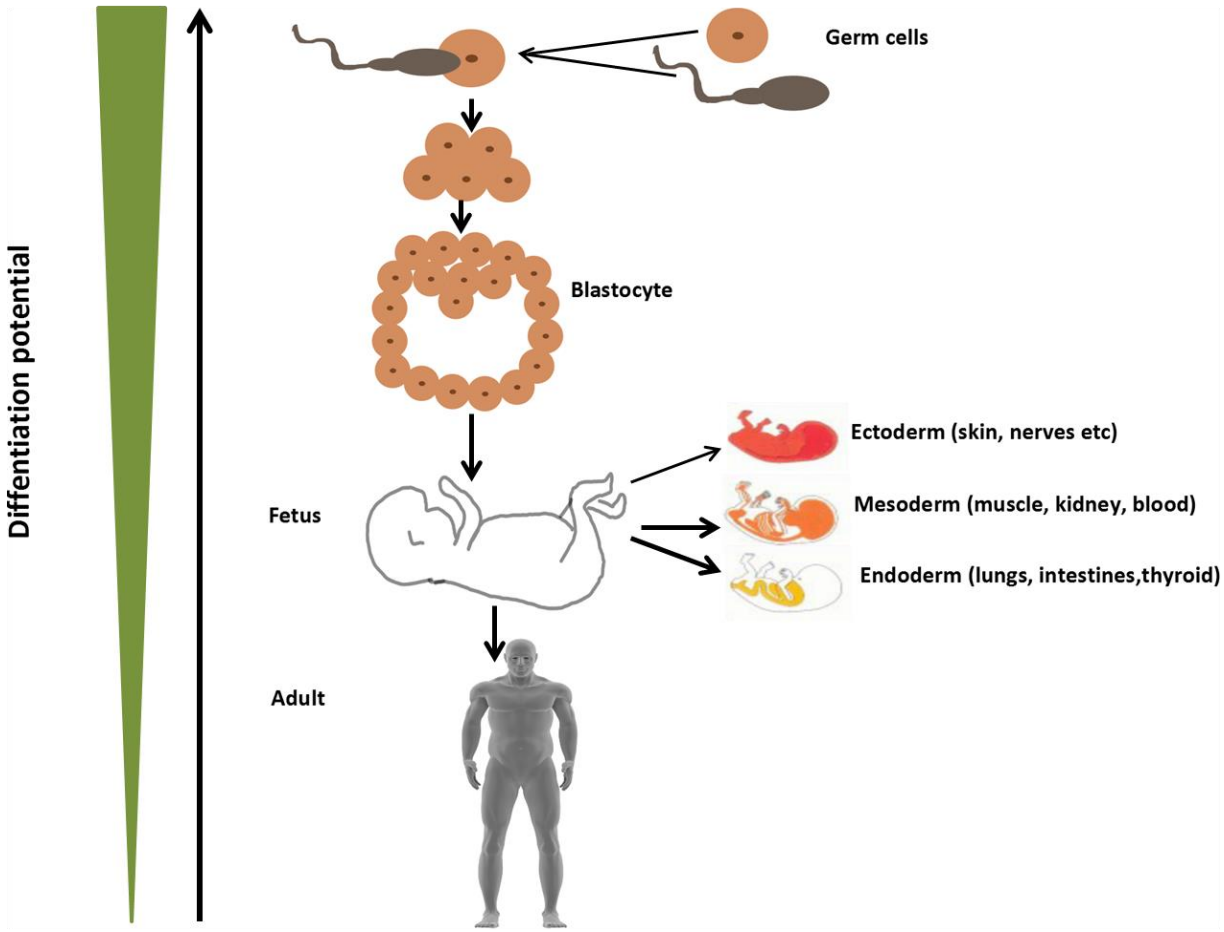

Figure 1.3: Schematic representation of stem cell differentiation potential at different developmental stages (Alison and Islam, 2009; Liras, 2010; www.somersault1824.com).

Table 1.1: Classification of stem cells depending on their differentiation potential (Reya *et al.*, 2001; Alison and Islam, 2009; Liras, 2010).

Class	Definition	Example
Totipotent	Cells that have the ability to develop into a new organism as they can differentiate into all tissue types; all three germ layers (endoderm, mesoderm; ectoderm); germ cells (egg and sperm) and extra-embryonic tissue. In mammals, no single cell is totipotent, only after fertilization of the egg by sperm	Cells of the first four days of cell division of a human fertilized egg.
Pluripotent	Cells that can differentiate into all three germ layers.	Cells of the inner layer of a blastocyst (5+ days old human embryo).
Multipotent	Cells that can differentiate into any cell within a certain type of tissue or organ to replace cells that die or lose their function.	Blood; skin; nerve stem cells.
Unipotent	Cells that can only differentiate into one cell type.	Progenitor cells such as pre-adipocytes; muscle stem cells.

1.3.2 Mitochondria in stem cells

In stem cells, mitochondria are involved in several functions, including ATP production, regulation of apoptosis, signaling and detoxification. Furthermore, oxidative phosphorylation also results in mitochondrial ROS formation (Wang, 2001; McBride *et al.*, 2006). Stem cells have been reported to thrive in both hypoxic and low ROS conditions, and to display the Warburg effect (Kondoh, 2008; Dayem *et al.*, 2010). Hypoxic conditions induce glycolysis and reduce both oxidative phosphorylation and mitochondrial ROS production (Dayem *et al.*, 2010). The Warburg effect

reduces mitochondrial ROS production by shifting ATP production to glycolysis that provides the building blocks for the proliferation of stem cells. It is therefore prudent for stem cells to favor hypoxic conditions and the Warburg effect, and reduce oxidative phosphorylation. In addition to changes in mitochondrial respiration, molecular chaperones have been reported to reduce ROS production and to protect cells from its apoptotic effects (Kim *et al.*, 2008).

1.3.3 Cancer

Normal cells grow, divide and die in an orderly fashion that is regulated by the cell's DNA. In normal cell growth, damaged DNA is either repaired or the cell goes through apoptosis. When the damage is not repaired and the cell continues to grow and divide uncontrollably, the cells form a tumor that can be either benign or malignant (Sell, 1993). Benign tumors have limited control of growth and do not invade the nearby healthy cells. In contrast, malignant tumors grow uncontrollably, destroy nearby healthy cells and can invade other tissues in different parts of the body. In addition to DNA damage, cancer can also be as a result of epigenetic gene deregulation (Malik and Brown, 2000). Cancer can therefore be defined as a class of diseases caused by uncontrolled growth and division of damaged cells.

1.3.3.1 Cancer stem cell theory

In some cancers, small subsets of cells that exhibit stem cell-like properties have been identified as cancer stem cells (CSCs) (Dick, 2003). These are defined as cancer cells that are tumorigenic and exhibit the trademarks of normal somatic stem cells. There are two theories from which CSCs are thought to be derived from. First, they may be derived from normal stem cells that have transformed the regulation of their self-renewal pathways (Sell, 1993; Bjerkvig *et al.*, 2005). Second, they may arise from differentiated cells that acquire the ability to self-renew (de-differentiated cells) (Sell, 1993; Bjerkvig *et al.*, 2005).

CSCs have the ability to divide through mitosis with high proliferation potential, self-renew to produce more stem cells though in a poorly controlled manner, actively express telomerase, activate anti-apoptotic pathways, increase membrane transporter activity, metastasize and differentiate into diverse cell types though generating abnormal tissues (Hamburg and Salmon, 1977; Dick, 2003; Pardal *et al.*, 2003; Wicha *et al.*, 2006; Dalerba, 2007; Visvader and Lindeman, 2008). CSCs are therefore thought to be at the centre of metastatic cancer and have been described

in multiple cancer types, such as brain, lung, leukemia and breast cancer (Reya *et al.*, 2001; Al-Hajj *et al.*, 2003; Clarke *et al.*, 2006). The ability of stem cells to differentiate into multi-lineages is also seen in CSCs where tumors are composed of heterogeneous populations of partially differentiated cell types (Pardal *et al.*, 2003; Dalerba, 2007). The similarities and differences of normal stem cells and CSCs are illustrated in Figure 1.4 that shows the source of stem cells and products of their differentiation.

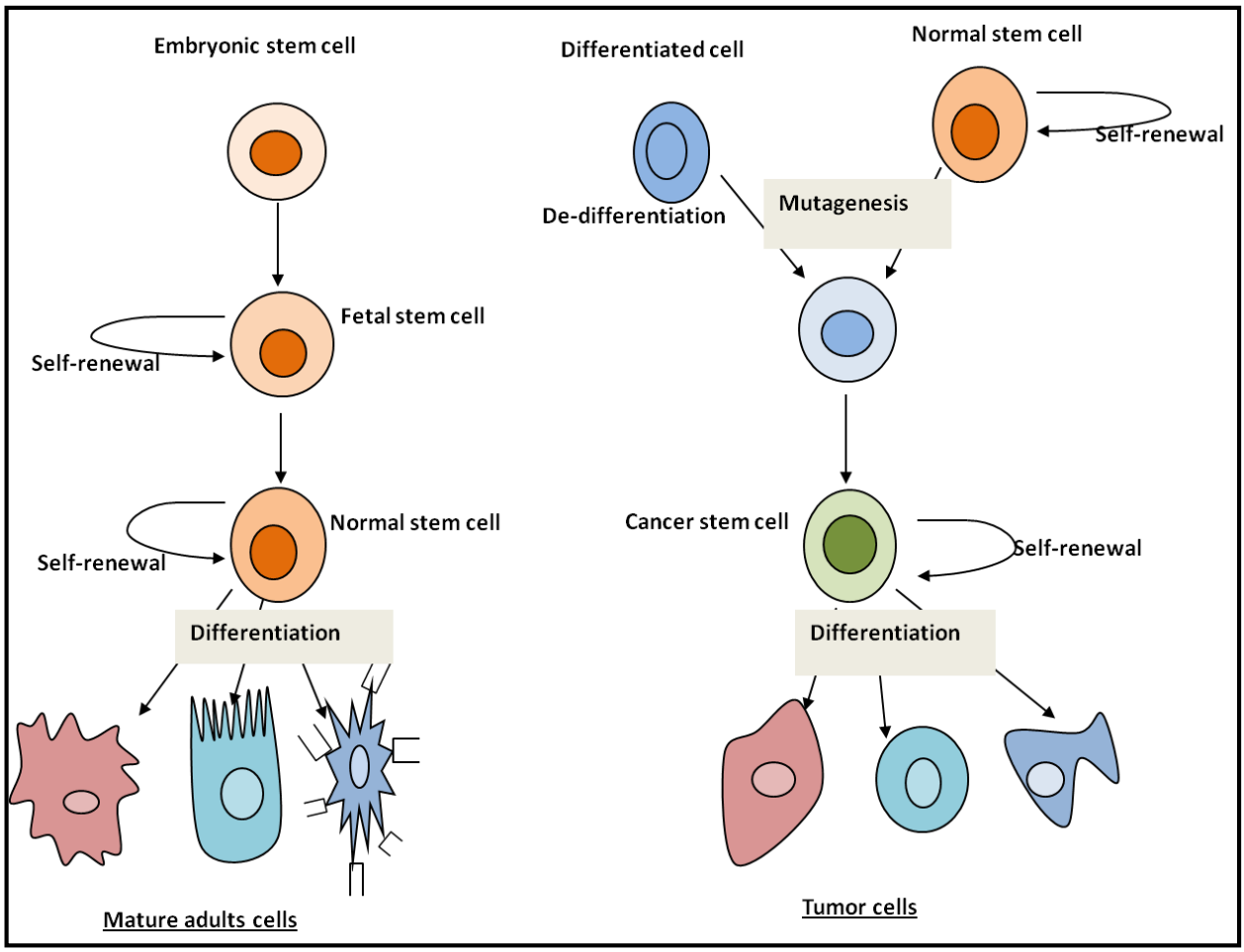

Figure 1.4: Comparison of the characteristics of normal stem cells against those of cancer stem cells (adapted from Pardal *et al.*, 2003).

Despite sharing similar signaling pathways with normal stem cells, CSCs appear to consistently strongly resist regulation of the signaling pathways and the subsequent gene/protein expression (Reya *et al.*, 2001; Clarke *et al.*, 2006). Cancer stem cells are therefore, also more likely to express drug resistance and anti-apoptotic genes that are characteristically expressed by various normal stem cells compared to differentiated cells. Consequently, these cells are more resistant to

chemotherapy, have high resistance to ROS and are therefore less susceptive to apoptotic induction (Vinogradov and Wei, 2012). To effectively treat cancer, it is therefore imperative to come up with therapies that can specifically target and effectively kill the CSCs.

1.3.3.2 Cancer stem cells and chemotherapy

When treating cancer, the goal is both to remove the cancerous cells and to curtail their resurgence. Several therapies are used to treat cancer, either as single or in combination, and these include surgery, chemo, radiation and photodynamic therapy. Most cancer treatments rely on ROS to make cells susceptible to apoptosis induction.

Conventional chemotherapy is targeted on the bulk populations of tumors. This strategy is based on the theory that most cancer cells have the ability to proliferate extensively and form new tumors (Figure 1.5 A). However, evidence suggests that only a small subset of cancer cells have this ability to proliferate (Figure 1.5 B) (Al-Hajj *et al.*, 2003). Chemotherapy, based on model Figure 1.5 A**,** therefore involves drugs that kill tumor cells and result in the shrinking of the tumor, but exclude the cancer stem cells, which leads to the re-growth of the tumor cells. This recurrence of cancer is believed to be a result of drug resistance to chemotherapy drugs by the stem cells (Reya *et al.*, 2001).

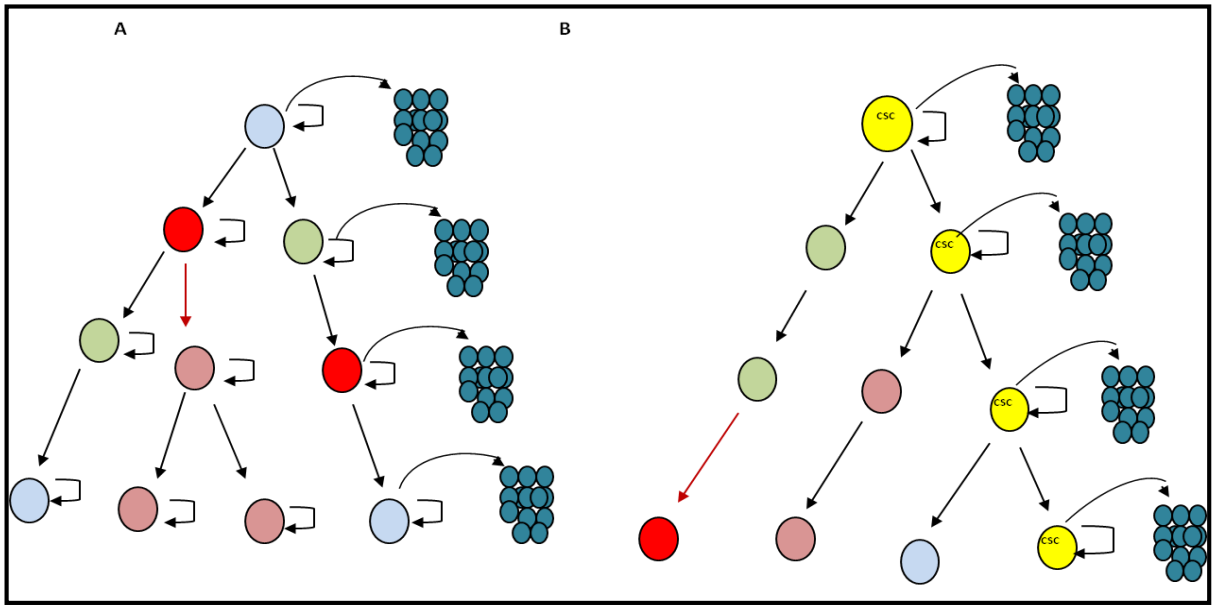

Figure 1.5: Two models of tumor formation. A. Cancer cells of different phenotypes have the ability to self-renew extensively. B. Only a subset of cells (CSC) can proliferate extensively (Reya *et al.*, 2001).

Drug resistance in CSCs has been suggested to be a result of various intrinsic and extrinsic based mechanisms, such as ATP-binding cassette (ABC)-transporter-mediated efflux of drugs, mutation or over expression of the drug target and drug inactivation (Chaudhary and Roninson, 1991; Doyle *et al.*, 1998; Zhou *et al.*, 2001; Chuthapisith *et al.*, 2010). ABC-transporter-mediated efflux in stem cells can has been reported to play a role in protecting and self-renewal of normal and CSCs, which both express high levels of ABC transporters, such as ABC sub-family B, member 1 (ABCB1) and sub-family G, member 2 (ABCG2) (Doyle *et al.*, 1998; Kim *et al.*, 2008; Chuthapisith *et al.*, 2010). Furthermore, quiescence of stem cells makes them inherently more likely to be refractory to drugs that target either the cell cycle or rapidly dividing cells. Apart from the role played by the quiescence of CSCs in the survival of cancer cells, the intrinsic environment of the cells, that of the mitochondria in particular, also contribute to cancer's survival. If chemotherapy can target cancer stem cells, then it may succeed in effectively killing all cancer cells, rendering tumors unable to self-maintain and will therefore completely degenerate.

1.3.4 Mitochondria in cancer

Cancer cells have been reported to utilize the Warburg effect (Warburg, 1927; 1956). The Warburg effect is assumed to be used by cancer cells and normal proliferating cells either for glycolysis that provides most of the building blocks required for cell proliferation or it could be an adaptation to hypoxic conditions in cancer (Lopez-Lazaro, 2008). In cancer, increase in ROS production increases both DNA damage and instability leading to mutations and therefore furthers oncogenesis. Under cellular stress conditions high levels of ROS normally promote apoptosis indirectly by stimulating pro-apoptotic proteins and directly by depolarizing the mitochondrial membrane. However, in cancer the stress sensory system is deregulated allowing for high ROS levels without inducing apoptosis. To prevent apoptosis in cancer, the mitochondria of cancer cells appear to be stabilized against the loss of their homeostasis (Abel *et al.*, 2005; Garedew and Moncada, 2008; Gogvance *et al.*, 2010). Free radical scavenging systems are up-regulated in cancer and signaling proteins have been reported to accumulate in the mitochondria and promote cell survival (Darnell *et al.*, 1994; Ju and Rudolf, 2006; Hiyama and Hiyama, 2007; Wegrzyn *et al.*, 2009). Mechanism of mitochondrial contribution to normal and cancer stem cell self-renewal, differentiation and survival, therefore, requires further investigation.

1.4 Signal transducer and activator of transcription 3 (STAT3)

STAT proteins are DNA binding proteins that are coded for by seven genes in mammals. These proteins mediate cellular differentiation, proliferation, survival and immune function within the cell (Calò *et al.*, 2003). The seven STAT genes coding for the proteins, namely STAT1, STAT2, STAT3 STAT4, STAT5a, STAT5b and STAT6, are canonically inactive as transcription factors in the absence of specific receptor stimulations. These STAT proteins canonically utilize the Janus Kinase (JAK) pathway to regulate trans-activation of genes in response to cytokines (Darnell *et al.*, 1994; Zhang and Darnell, 2001).

1.4.1 STAT3 structure and function

STAT3 is a conserved signal transducer and transcription factor with three major domains; the DNA binding domain, the SH_2 dimerization domain and the trans-activation domain (Becker *et al.*, 1998). STAT3 proteins have been found to have two phosphorylation sites, the canonical tyrosine 705 phosphorylation, and the non-canonical serine 727 phosphorylation.

1.4.2 Canonical function of STAT3

In the canonical JAK/STAT3 signaling pathway, the latent (unphosphorylated) STAT3 localizes in the cytoplasm. The pathway begins when a ligand binds to the transmembrane receptor leading to the activation of the JAK associated with the receptor. JAK phosphorylates tyrosine residues on the cytoplasmic side of glycoprotein 130 (gp130), creating docking sites for the latent cytoplasmic STAT3, which is then recruited to the receptor, phosphorylated at tyrosine 705 (pSTAT3Y705). The phosphorylated STAT3 dimerizes and translocate to the nucleus where it activates the transcription of target genes (Aaronson *et al.*, 2002; Levy *et al.*, 2002). Cytosolic Hsp90 β interacts directly with and chaperones activated STAT3 to the nucleus (Shah *et al.*, 2002; Sato *et al.*, 2003; Setati *et al.*, 2010; Prinsloo *et al.*, 2012). The JAK/STAT3 pathway therefore plays a crucial role in cytokine signaling and immune inflammatory mechanisms (Darnell *et al.*, 1994). Figure 1.6 illustrates the canonical signaling pathway of STAT3.

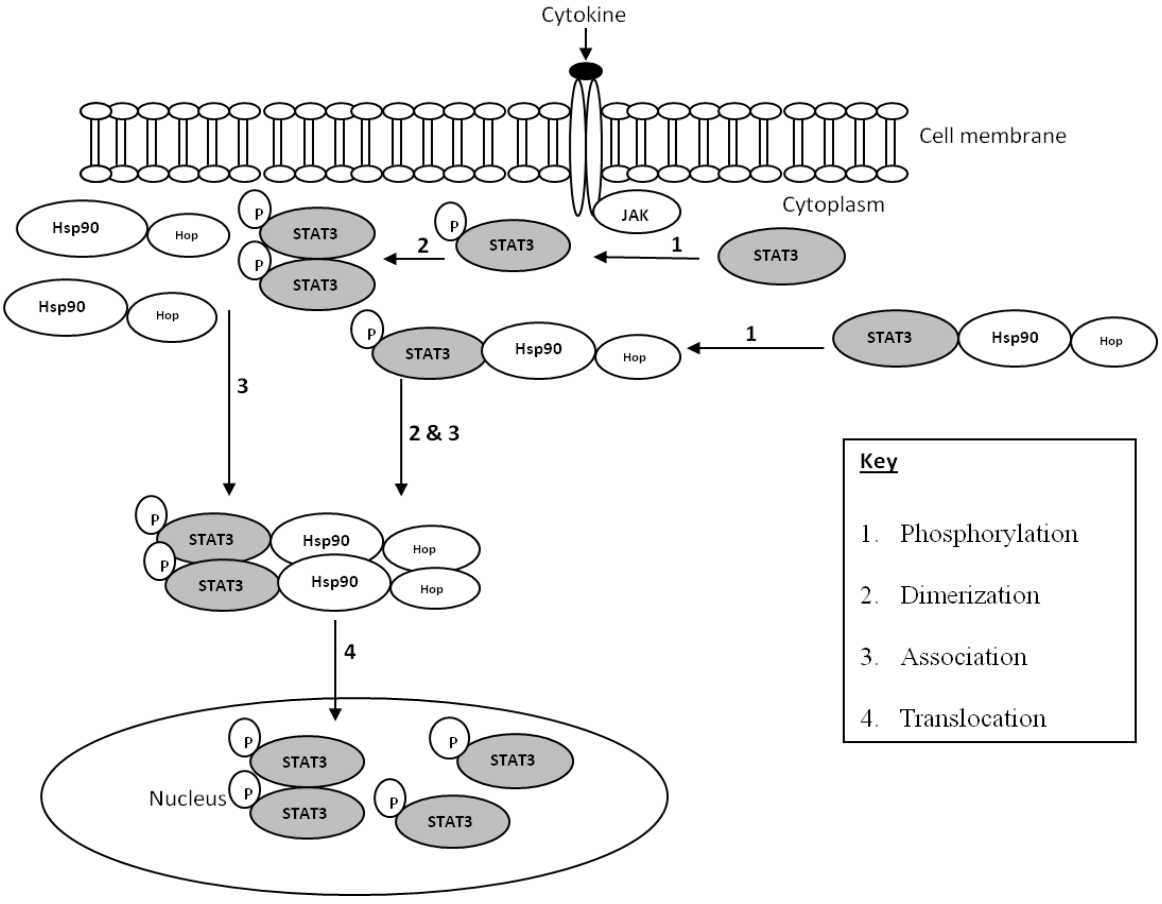

Figure 1.6: The canonical JAK/STAT3 pathway. (The figure was derived from Darnell *et al.*, 1994; Bromberg *et al.*, 1999; Xu *et al.*, 2007).

1.4.3 Non-canonical function of STAT3

In contrast to canonical STAT3 signaling pathway where latent STAT3 localizes in the cytoplasm, latent STAT3 has been found in the nucleus where it has been reported to bind to specific ultra-structural features of DNA, heterochromatin and is essential for the localization of heterochromatin protein 1 (HP1) as well as the stability of heterochromatin (Shi *et al.*, 2008; Timofeeva *et al.*, 2012). Mammalian latent STAT3 has been reported to constantly shuttle between the nucleus and the cytoplasm. Other studies have reported that latent STAT proteins influence gene expression through different mechanism to the canonical way even though JAK has also been reported to translocate to the nucleus to possibly phosphorylate nuclear latent STAT proteins (Reich and Liu *et al.*, 2005; Liu, 2006; Li, 2011). In the canonical pathway, STAT3 is recruited to plasma membrane receptors for phosphorylation on tyrosine 705 which is essential for its interaction with DNA and stimulation of transcription. However, serine 727 phosphorylation differs and according to Wen and Darnell, (1997) does not require recruitment to the membrane and was found to modulate the transcriptional activity of STAT3 even though it was not necessary for DNA binding. STAT3 has also been reported to localize in other organelles such as endosomes and mitochondria (Xu *et al.*, 2007; Wegrzyn *et al.*, 2009).

1.4.4 Mitochondrial STAT3

STAT3's mitochondrial localization has been suggested to be possibly through its association with a cell death regulator gene associated with retinoic-IFN-induced mortality (GRIM-19). Within the mitochondria, STAT3 is suggested to non-transcriptionally regulate the activities of the electron transport chain (ETC) as a monomer by interacting with Complex I and II and necessary for tumor necrosis factor induced necroptosis (Wegrzyn *et al.*, 2009; Shulga and Pastorino, 2012). Recently STAT3 has been reported to localize in the inner mitochondrial membrane chaperoned by GRIM-19 enhancing its integration into complex 1 (Tammineni *et al.*, 2013). These reports of mitochondrial localization of STAT3 suggests the possibility of STAT3 binding to mitochondrial DNA (mtDNA). Wegrzyn *et al.*, (2009) also suggested that mitochondrial STAT3 binds to Complex II and mops up leaked electrons and therefore reduces the mitochondrial production of ROS. STAT3 phosphorylated at serine 727 has been shown to stimulate the interaction of STAT3 and GRIM-19 (Tammineni *et al.*, 2013), increase ROS production and induced cell death in mouse fibrosarcoma cells. Phillips *et al.*, (2010) argued that the STAT3 regulation of oxidative

phosphorylation could not be by direct protein to protein interactions with Complex I and II. Mitochondrial isolations were used in proving the existence of mitochondrial STAT3. However, endosomes may be co-purified resulting in contamination of the sample raising questions whether mitochondrial STAT3 even exist given that it also localizes in endosomes (Xu *et al.*, 2007).

1.4.5 STAT3 and cancer

Studies have shown that STAT proteins play a crucial role in oncogenesis. STAT3 is up-regulated in cancer cells and is constitutively activated by the high ROS levels (Bromberg *et al.*, 1999; Hodge *et al.*, 2005). It therefore acts as an oncogene that causes cell proliferation and expression of genes that renders cells protection against apoptosis.

STAT5, a close family member to STAT3, promotes tumor formation in leukemias, lymphomas, and prostate cancer (Sultan *et al.*, 2005; Gu *et al.*, 2010). Nevertheless, recent evidence shows that it actually plays a suppressive role in breast cancer where its presence in laboratory-grown breast cancer cells was found to prevent them from becoming invasive and aggressive (Sultan *et al.*, 2005; Gu *et al.*, 2010). Peck *et al.* (2011) suggested that the levels of nuclear localized tyrosine-phosphorylated STAT5 in breast cancer can be used as an indicator of breast cancer progression from normal to invasive then metastatic as the levels diminished with the disease's progression.

Gough *et al.*, (2009) showed that mitochondrial STAT3 promoted Ras-dependent cellular transformation and increased electron transport chain activities of complexes II and V. Cellular respiration is important for cell survival and STAT3 activities in the mitochondria supports transformation in oncogenesis by increasing Ras dependent transformation. Although Gough *et al.*, (2009) suggests that STAT3 goes to the mitochondria, a close family member STAT5 demonstrate that STAT proteins can have different functions depending on the cell type. Therefore, STAT3 may localize in the mitochondria in some cells in detectable amounts and not in other cell types.

As no mitochondrial targeting sequence on STAT3 has been reported, its transfer mechanism to this organelle is still unknown. Table 1.2 highlights some of the proteins known to interact with STAT3 experimentally determined through various techniques ranging from fluorescence microscopy, co-immunoprecipitation, and kinase assays to surface plasmon resonance

spectroscopy. A more comprehensive list can be found on (http://en.m.wikipedia.org/wiki/STAT3 on 15/11/2013).

Table 1.2: STAT3 experimentally determined interactions

Nuclear interactions	**Mitochondrial interactions**	**Cytosolic interactions**
Canonical STAT3 activity 1. Gamma activated sequence in gene promoters(Aaronson and Horvath, 2002) 2. Nuclear receptor co-activator 1(Wang, 2005) 3. AT-rich DNA sequences(Timofeeva *et al.*, 2012) Non-canonical STAT3 activity 1. c-Jun(Zhang *et al.*, 1999) 2. Heterochromatin associated protein 1(Timofeeva *et al.*, 2012)	Non-canonical STAT3 activity 1. Complex I(Wegrzyn *et al.*, 2009) 2. Complex II(Wegrzyn *et al.*, 2009) 3. ATP synthase (Complex V) (Gough *et al.*, 2009) 4. GRIM-19 (Tammineni *et al.*, 2013; Zhang *et al.*, 2003)	Canonical STAT3 activity 1. EGFR(Yuan *et al.*, 1996) 2. Hsp90 β (Prinsloo *et al.*, 2012) 3. MTOR(Yokogami *et al.*, 2000) 4. Src(Cao *et al.*, 1996) 5. Janus Kinase(Darnell *et al.*, 1994)

1.5 Tumor necrosis factor receptor-associated protein 1 (TRAP1)

Molecular chaperones of the heat shock protein 90 (Hsp90) family plays an important role in protein folding, degradation and in signal transduction as chaperones of signaling proteins (Shah *et al.*, 2002; Sato *et al.*, 2003; Brown *et al.*, 2007; Schoof *et al.*, 2009). This heat shock protein family exists in major isoforms of Hsp90 α and Hsp90 β in the cytoplasm, glucose-regulated protein 94 (GRP94) in the endoplasmic reticulum and tumor necrosis factor receptor-associated protein 1 (TRAP1) in the mitochondria (Sreedhar and Csermely, 2004). In cancer cells, Hsp90s protect mutated and over-expressed oncogenic 'client' proteins. These include STAT proteins, which are involved in signaling pathways that are crucial for developing and maintaining the tumor phenotype from mis-folding and degrading, consequently becoming a crucial facilitator of cancer cell survival (Whitesell and Lindquist, 2005; Banerji, 2009). Compared to cytosolic Hsp90s,

TRAP1's "client" proteins and co-chaperones, if any, are however not well described (Matassa *et al.*, 2012).

1.5.1 TRAP1 structure and function

TRAP1 is an intra-mitochondrial protein homologous to members of the Hsp90 family with a mitochondrial localization signal on its N-terminus that gets cleaved after it gets into the mitochondria (Felts *et al.*, 2000). Figure 1.6 illustrates the differences between TRAP1 and the canonical Hsp90s. TRAP1 lacks the charged region and the EEVD motif that acts as a flexible linker when binding substrate, and the co-chaperone binding site, respectively. As the interactions of Hsp90 are considered to be charge based, the absence of the charged region in TRAP1 will impact the affinity to which it binds Hsp90 substrates (Meyer *et al.*, 2003).

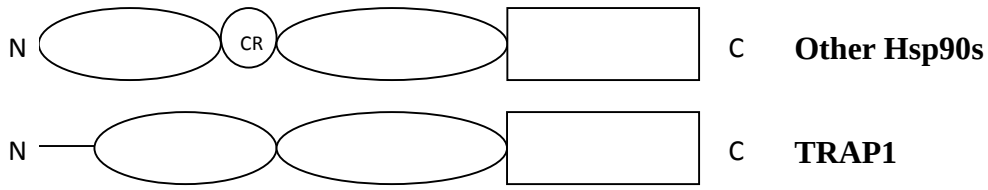

Figure 1.7: Domain organization of Hsp90s. TRAP1 lacks the charged region (CR) and the EEVD motif on the C-terminus.

Phosphorylation is also one of TRAP1's post-translation modifications. Phosphatase and tensin (PTEN)-induced putative kinase 1 has been reported to phosphorylate TRAP1 resulting in protection of cells against oxidative stress-induced apoptosis (Montesano *et al.*, 2007). TRAP1 together with Hsp90 α and β and immunophilin cyclophilin D form a mitochondrial chaperone system that maintains mitochondrial homeostasis and appear to be actively involved in the inhibition of the activities of pro-apoptotic proteins (Kang *et al.*, 2007; Constantino *et al.*, 2009). TRAP1 is therefore involved in cells' resistance to tumor necrosis factor induced apoptosis by antagonizing the activity of cyclophilin D, which is reported to increase the permeability of the mitochondrial membrane (Gesuldi *et al.*, 2007; Landriscina *et al.*, 2010). Within the mitochondria, TRAP1 has been shown to inhibit Complex II, decrease the activity of Complex IV and has been suggested to regulate the metabolic switch from oxidative phosphorylation to glycolysis (Sciocavelli *et al.*, 2013; Yoshida *et al.*, 2013). TRAP1 has also been reported to be involved in the endoplasmic reticulum stress response (Matassa *et al.*, 2013). In hypoxic stem cell niche

environments, TRAP1 is hypothesized to act as buffer that regulates mitochondrial ROS when the cells move from their hypoxic niche to an oxygenated environment (Kadye *et al.*, 2013).

TRAP1 is up-regulated most tumor cells, as compared to normal tissue cells suggesting that it is important for the maintenance of the disease phenotype (Kang *et al.*, 2007; Montesano *et al.*, 2007). Knockdown of this mitochondrial Hsp90 isoform promotes apoptosis and results in a decrease in tyrosine 705-phosphorylated STAT3 in the cell. This not only suggests the importance of TRAP1 in circumventing apoptosis in cancer, and a role in phosphorylated STAT3 stabilization. The involvement of TRAP1 in the STAT3 signaling pathway or localization is another crucial possibility (Kubota *et al.*, 2009). Table 1.3 highlights some of the proteins known to interact with TRAP1 and the total list is less than twenty in comparison to the several hundreds of known Hsp90 *β* client proteins (Song *et al.*, 1995; Chen *et al.*, 1996; Kang, 2011; Matassa *et al.*, 2013; Yoshida *et al.*, 2013). Furthermore, Table 1.3 also point out that TRAP1 is not only functional within the mitochondria but in other subcellular compartments such as the endoplasmic reticulum.

Table 1.3: TRAP1 experimentally determined interactions.

Mitochondrial interactions	**Cytosolic interactions**
Cyclophilin D; Sorcin; c-Src (Tyrosine protein kinase); Succinate dehydrogenase (Complex II)	Translational intiation/elongation factors (ribosomes); TBP7 (endoplasmic reticulum); Tumor necrosis factor receptor; Epidermal growth factor receptor

(Song *et al.*, 1995; Chen *et al.*, 1996; Kang, 2011; Matassa *et al.*, 2013; Yoshida *et al.*, 2013)

1.6 Problem statement

Studies have shown that the signaling protein STAT3 localizes in the mitochondria and promote cell survival and oncogenesis. Nonetheless, the contribution of its mitochondrial localization with regards to self-renewal and maintenance of the tumor initiating cell population is still unclear. Elucidation of this signaling proteins' contribution and targeting mechanisms to the mitochondria would allow for a better understanding of stem cell self-renewal mechanisms and application in the development of more efficient therapeutics targeted at cancer and cancer stem cells. Based on the identified role of Hsp90s in activation and stabilization of signaling proteins, particularly the

involvement of cytosolic Hsp90s in nuclear accumulation of pSTAT3Y705 (Prinsloo *et al.*, 2012), the role of the mitochondrial isoform TRAP1, need to be investigated in the mediation of translocation and stabilization of mitochondrial STAT3.

1.7 Hypothesis

TRAP1 affects the levels of cellular pSTAT3Y705. Furthermore, Hsp90 β chaperones pSTAT3Y705 to the nucleus. However, STAT3 has been reported to localize in the mitochondria even though the mechanism is unknown. Therefore we hypothesize that TRAP1 mediates the transport of STAT3 to the mitochondria.

1.8 Aims

Elucidate how TRAP1 is involved in the mitochondrial translocation of STAT3 and how this affects ROS levels in mammalian cells.

1.8.1 Objectives

a) Determine the localization of STAT3 and TRAP1 before and after over-expression of TRAP1
b) Determine the localization of STAT3 and TRAP1 before and after inhibition of STAT3
c) Determine ROS levels before and after over-expression of TRAP1
d) Analyze the interaction of TRAP1 and STAT3

CHAPTER 2

Bioinformatic Analysis of TRAP1 and STAT3

2.1 Introduction

2.1.1 TRAP1 protein

The human TRAP1 gene is located on chromosome 16 position 13.3, contains 18 exons, encodes a protein that has 704 amino acids, has 14 potential alternate transcripts and is similar to the bacterial Hsp90 homolog high temperature protein (HtpG) (Felts *et al*., 2000; http://www.ncbi.nlm.nih.gov/epigenomics). TRAP1's first 50 amino acids on the N-terminus are highly charged and lack acidic amino acids, a characteristic that is consistent with proteins destined for the mitochondria (Hendrick *et al.* 1989). A striking feature of TRAP1 is that it lacks the highly charged region found immediately after the N-terminal domain that is common for the other Hsp90 homologs (Figure 2.1). Furthermore, TRAP1 lacks the C-terminal EEVD motif that binds classical tetratricopeptide repeat (TPR)-containing Hsp90 co-chaperones, such as Hsp70/Hsp90 organizing protein (Hop) (Felts *et al.* 2000; Olof, 2007). Although some reports suggest that the ATPase domain on the N-terminal also function as a binding site of co-chaperones, TRAP1 neither binds to Hop nor suppresses the aggregation of steroid hormone receptors (SHR), as is common with the cytosolic Hsp90 homologs (Felts *et al.* 2000). Since the suppression of SHRs aggregation is dependent on co-chaperones, this suggests that TRAP1 functions differently because it lacks the co-chaperone binding site. However, TRAP1 previously designated Hsp75, has been reported to fold retinoblastoma protein, suggesting that it has chaperone activity that may utilize a different mechanism and, perhaps different co-chaperones (Chen *et al.*, 1996).

Despite the client proteins and cellular function of TRAP1 being poorly characterized compared to cytosolic Hsp90s, they all bind and hydrolyze ATP and Hsp90-specific inhibitors that act on the ATPase domain also inhibit TRAP1 (Leskovar *et al.* 2008). Therefore, despite the differences in the Hsp90 homologs, there is a potential for sharing common client proteins among these homologs.

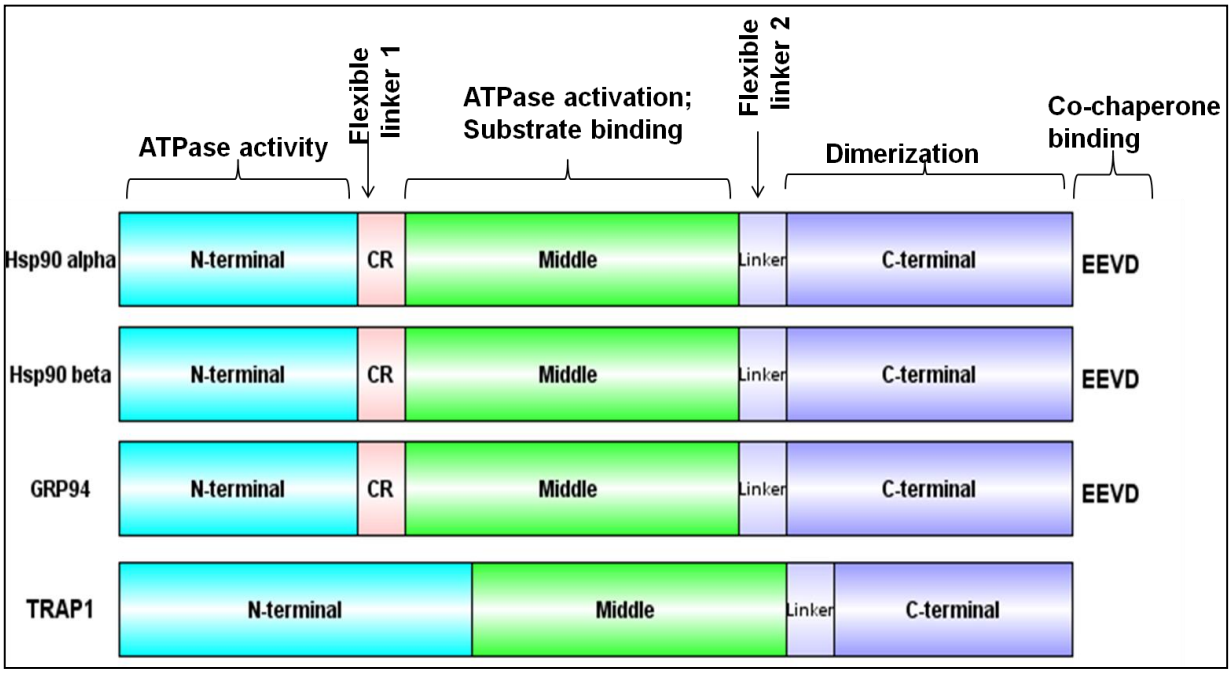

Figure 2.1: Schematic diagram of domain organisation of Hsp90s. CR refers to charged region. Domain functions of interest are also shown however the alignment is not to scale (Whitesell and Lindquist, 2005; Ren *et al.*, 2009).

2.1.2 STAT3 protein

Human STAT3 is located on chromosome 17 position 21.31, contains 24 exons and encodes for a protein that is 770 amino acids long (http://www.ncbi.nlm.nih.gov/epigenomics/Genomes and Maps/Epigenomics). STAT3, a client protein of Hsp90, exist as two major isoforms, namely the 91 kilo Daltons (kDa) α-isoform and the 86 kDa β-isoform (Maritano *et al.*, 2004). It is a highly conserved multi-domain signal transducer protein that has two trans-activation phosphorylation sites tyrosine 705 and serine 727 (Wen *et al.*, 1995; Wen and Darnell, 1997 (Figure 2.2). Proteolytic cleavage of STAT3, a post-translational modification, yields a 72 kDa STAT3γ and a 64 kDa STAT3δ (Chakraborty and Tweardy, 1998; Heveha *et al.*, 2002). Some studies have reported that this protein has a constitutive nuclear localization signal in the coiled-coil domain on the N-terminal that is recognized by importin α3 (Wen and Darnell, 1997; Liu *et al.*, 2005). Nevertheless, other studies show that Arginine residues 414/417 of STAT3 β in the β barrel are essential for nuclear localization, which furthers the nuclear localization mechanism debate (Prinsloo *et al.*, 2012).

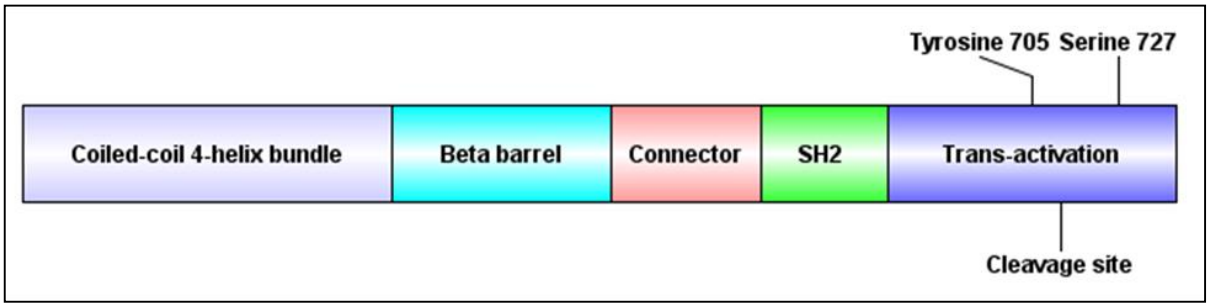

Figure 2.2: Schematic diagram of domain organisation of STAT3 α. The nuclear localization signal has been reported to be in the coiled-coil (Liu *et al.* 2005) region while Arginine 414/417 in the β barrel were essential for nuclear localization and the cleavage site is 55 amino acids from the C-terminus (Darnell *et al*., 1994; Becker *et al.,* 1998; Ren *et al.,* 2009).

Localization of STAT3 to the nucleus has been attributed to a potential for a nuclear localization signal in the coiled-coil domain, residues 414/417 in the β barrel and cytosolic Hsp90s (Ren *et al.,* 2009; Prinsloo *et al.*, 2012). However, mitochondrial localization of STAT3 is less understood. Some studies have suggested that death associated protein GRIM-19 acts as a chaperone and recruits STAT3 to the mitochondria. However, based on the role of cytosolic Hsp90s in the nuclear localization of STAT3, a hypothesis that the mitochondrial isoform of Hsp90 TRAP1, plays a role STAT3's mitochondrial localization was therefore postulated.

2.1.3 Specific Objectives

1. Determine how conserved TRAP1 is in comparison to other Hsp90 isoforms and other species

2. Predict the sub-cellular localization of TRAP1 and STAT3 *in silico*.

2.2 Methods

2.2.1 Sequence retrieval

The FASTA sequences (Table 2.1) of *Homo sapiens*, *Mus musculus*, *Dictyostelium discoideum*, *Saccharomyces cerevisiae* and *Escherichi coli* Hsp90 protein homologs were obtained from National Center for Biotechnology Information (NCBI) Protein Data Base (PDB) (http://www.ncbi.nlm.nih.gov/protein). Human and mouse STAT3 were also obtained from NCBI.

Table 2.1: List of sequences retrieved from NCBI.

Gene	Species	Annotation	Accession Number
HSP90AB	*Homo sapien*	hHsp90-*β*	NP_031381.2
HSP90AB	*Mus musculus*	mHsp90-*β*	NP_032328.2
HSP90AA	*Homo sapien*	hHsp90-*α*	NP_001017963.2
HSP90AA	*Mus musculus*	mHsp90-*α*	NP_034610.1
HSP90B	*Homo sapien*	hGRP94	AAH666561
TRAP1	*Homo sapien*	hTRAP1	AAH23585.1
TRAP1	*Mus musculus*	mTRAP1	NP_080784.1
TRAP1	*Dictyostelium discoideum*	Dd. trap1	Q86L04.1
HSP82	*Saccharomyces cerevisiae*	HSP82	P02829.1
HtpG	*Escherichia coli*	HtpG	AAC73575.1
STAT3	*Homo sapien*	hSTAT3 isoform1	NP_644805.1
STAT3	*Homo sapien*	hSTAT3 isoform2	NP_003141.2
STAT3	*Homo sapien*	hSTAT3 isoform3	NP_998827.1
STAT3	*Mus musculus*	mSTAT3 isoform1	NP_998825.1
STAT3	*Mus musculus*	mSTAT3 isoform2	NP998824.1
STAT3	*Mus musculus*	mSTAT3 isoform3	NP_035616.1

2.2.2 Homology of TRAP1 to Hsp90 and Conservation of domains

The FASTA sequences of the Hsp90 homologs were aligned using Multiple-Sequence-Alignment using-Fast-Fourier-Transform (MAFFT) (Katoh *et al.*, 2002). Similarities and identities were calculated using ClustalW version 2.1 and annotated using BioEdit version (Thompson *et al*., 1994;

Hall, 1999). The homology of TRAP1 to other Hsp90 proteins was inferred based on the sequence identities (Rost, 1999). The domain conservation was assessed using Hsp90 β functional domain divisions according to Chen *et al.*, 2005. The N-terminal domain consisted of residues 1M -236 G, the first charged region domain consisted of residues 237E-271K, the middle domain consisted of residues 272I-617M, the second charged region domain consisted of residues 618G-628I and the C-terminal domain consisted of residues 629N-732D of Hsp90 β.

2.2.3 Phylogenetic analysis of Hsp90s

In order to gain insight into the hypothetical evolutionary place and the sequence in which branching events occurred, for the human, mouse, yeast and bacterial Hsp90s, a phylogenetic tree was generated using Molecular Evolutionary Genetics Analysis (MEGA) version 5.2.2 freely available for downloading at http://www.megasoftware.net/mega.php (Tamura *et al.*, 2011). All other parameters were default, with the exception of sequence alignment that was done using Multiple Sequence Comparison by Log-Expectation (MUSCLE) alignment (Edgar, 2004). This was followed by the maximum likelihood (ML) statistical method based on the Jones-Taylor-Thornton (JTT) model using 1000 bootstrap replications to generate the phylogenetic tree.

2.2.4 Sub-cellular localization prediction

The prediction sub-cellular localization of proteins gives bioinformatic information on where the protein goes within the cell. The sub-cellular localizations and cleavage sites of TRAP1 and STAT3 were predicted using the default settings of PSORT II and TargetP version 1.1, non-plant organism group parameter, to give insight into these proteins' possible locations (Nielsen *et al.*, 1997; Nakai and Horton, 1999; Emmanuelsson *et al.*, 2000).

2.2.5 Secondary structure prediction

The sequences of full length TRAP1 and Hsp90 β were aligned using MAFFT with a FASTA output and the alignment was used to predict the consensus secondary structures of TRAP1 *de novo* and Hsp90 β whose structure has been solved (P08238, www.uniprot.org) using Jpred 3 and the Jnet algorithm (Cuff and Barton, 2000; Katoh *et al.*, 2002; Cole *et al.*, 2008). The predicted secondary structures was then assessed for conservation using the reliability values of the prediction which ranges from 0 – 9 whereby a value closer to 9 implies conservation between the two proteins' secondary structure.

2.3 Results

2.3.1 Homology to Hsp90

To confirm that TRAP1 shared homology with the Hsp90 family, sequence alignments, pair-wise identity and similarity calculations were done and to assess the evolutionary relationship of the Hsp90 homologs, a phylogenetic tree was generated. The results showed that both human and mouse Hsp90 α and β share identical residues ranging from 86.05-99.59 % while TRAP1 shared the least sequence identity with other Hsp90 homologs within the same species sharing 31.95 % identical residues with endoplasmic reticulum Hsp90 (GRP94). The sequence identities observed for human TRAP1 and human Hsp90 β was identical to that of human TRAP1 and mouse Hsp90 β. Similarly, the sequence identities observed for mouse TRAP1 and mouse Hsp90 β was identical to that of mouse TRAP1 and human Hsp90 β indicating that both human and mouse TRAP1s and Hsp90 βs are similar. Human TRAP1 was shown to share homology with human Hsp90 β (Table 2.2), with a 34.2 % sequence identity, and shared the highest sequence identity with yeast Hsp90 (HSP82) with 36.24 % sequence identity (Table 2.2). These results indicate that the structure of a human TRAP1 is likely to be more similar to that of yeast Hsp90 than it is to human Hsp90 β and therefore the functions of human TRAP1 and human Hsp90 β may be less similar compared to those of human TRAP1 and yeast Hsp90. Human and mouse TRAP1 shared 88.49 % identical sequences indicating a high degree of conservation between the two mammalian species.

Table 2.2: Percent Identity Matrix of Hsp90s. The matrix was created by Clustal2.1 after a MAFFT sequence alignment of human (h) and mouse (m) Hsp90 β, Hsp90 α, TRAP1; bacteria (HtpG) and yeast Hsp90 (HSP82).

Identity	hHsp90-β	mHsp90-β	hHsp90-α	mHsp90-α	HSP82	GRP94	HtpG	hTRAP1	mTRAP1
hHsp90-β	100	99.59	86.74	86.05	63.55	48.87	42.39	34.20	34.04
mHsp90-β	99.59	100	87.15	86.46	63.83	49.01	42.55	34.20	34.04
hHsp90-α	86.74	87.15	100	99.18	63.40	45.78	42.88	34.24	34.57
mHsp90-α	86.05	86.46	99.18	100	63.40	49.01	42.72	33.92	34.41
HSP82	63.55	63.83	63.40	63.40	100	49.57	41.57	36.24	35.91
GRP94	48.87	49.01	45.78	49.01	49.57	100	40.95	31.95	31.85
HtpG	42.39	42.55	42.88	42.72	41.57	40.95	100	35.86	36.20
hTRAP1	34.20	34.20	34.24	33.92	36.24	31.95	35.86	100	88.49
mTRAP1	34.04	34.04	34.57	34.41	35.91	31.85	36.20	88.49	100

The phylogenetic tree (Figure 2.3) shows the human and mouse TRAP1 protein sequences analyzed were at the bottom of the tree while those of human and mouse Hsp90 β were at the top of the tree with bacterial Hsp90 (HtpG) above the TRAP1s followed by GRP94 then yeast Hsp90 HSP82 then Hsp90 (Figure 2.3). These results therefore indicate that the TRAP1 gene was more primitive and evolutionary conserved; variations were less among human mitochondrial Hsp90 (TRAP1) and bacterial Hsp90 (HtpG) than when comparing human TRAP1 and human cytosolic Hsp90 (Hsp90 β). This implies that TRAP1 and Hsp90 β in humans had a more divergent and ancient common ancestor compared to human TRAP1 and bacterial Hsp90 homolog HtpG.

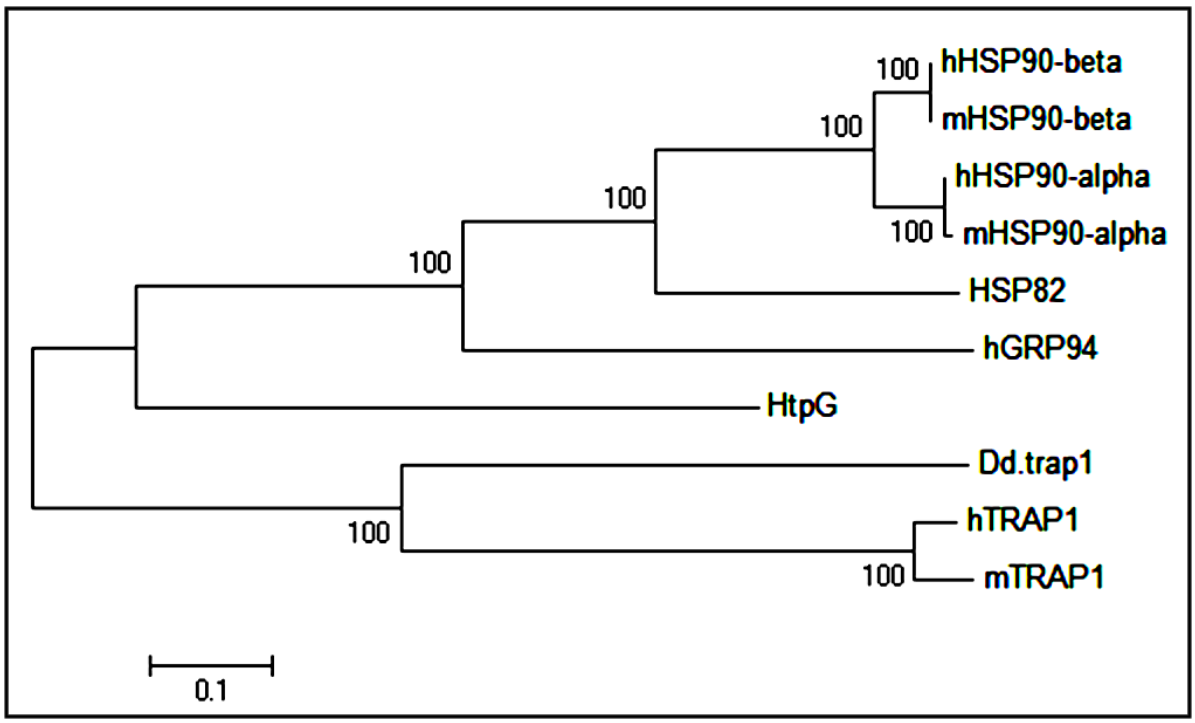

Figure 2.3: Phylogenetic analysis of Hsp90 proteins from human, mouse, yeast and bacteria. The accession numbers are indicated in Table 2.1. Scale bar represents 0.1 DNA distance. (http://www.ncbi.nlm.nih.gov; Tamura *et al*., 2011).

2.3.2 Sequence conservation of the Hsp90 domains

Protein sequence conservation in functional domains suggests conservation of structure and ultimately the function of that domain. To assess how much the Hsp90 domains were conserved; MAFFT sequence alignments were generated and divided into five functional domains as described in Materials and Methods section 2.2.2. The N-terminal domain has been reported as the binding site of ATP. In this study, apart from the first 84 amino acids of human TRAP1 that function as a translocation signal, the N-terminal domain appeared to be the most conserved domain among the aligned Hsp90s as seen by the large proportion of identical residues (*) same colored residues; conserved (:) same colored residues or semi-conserved substitutions (.) residues, implying that surface charges and function of the N-terminal domain were conserved (Figure 2.4).

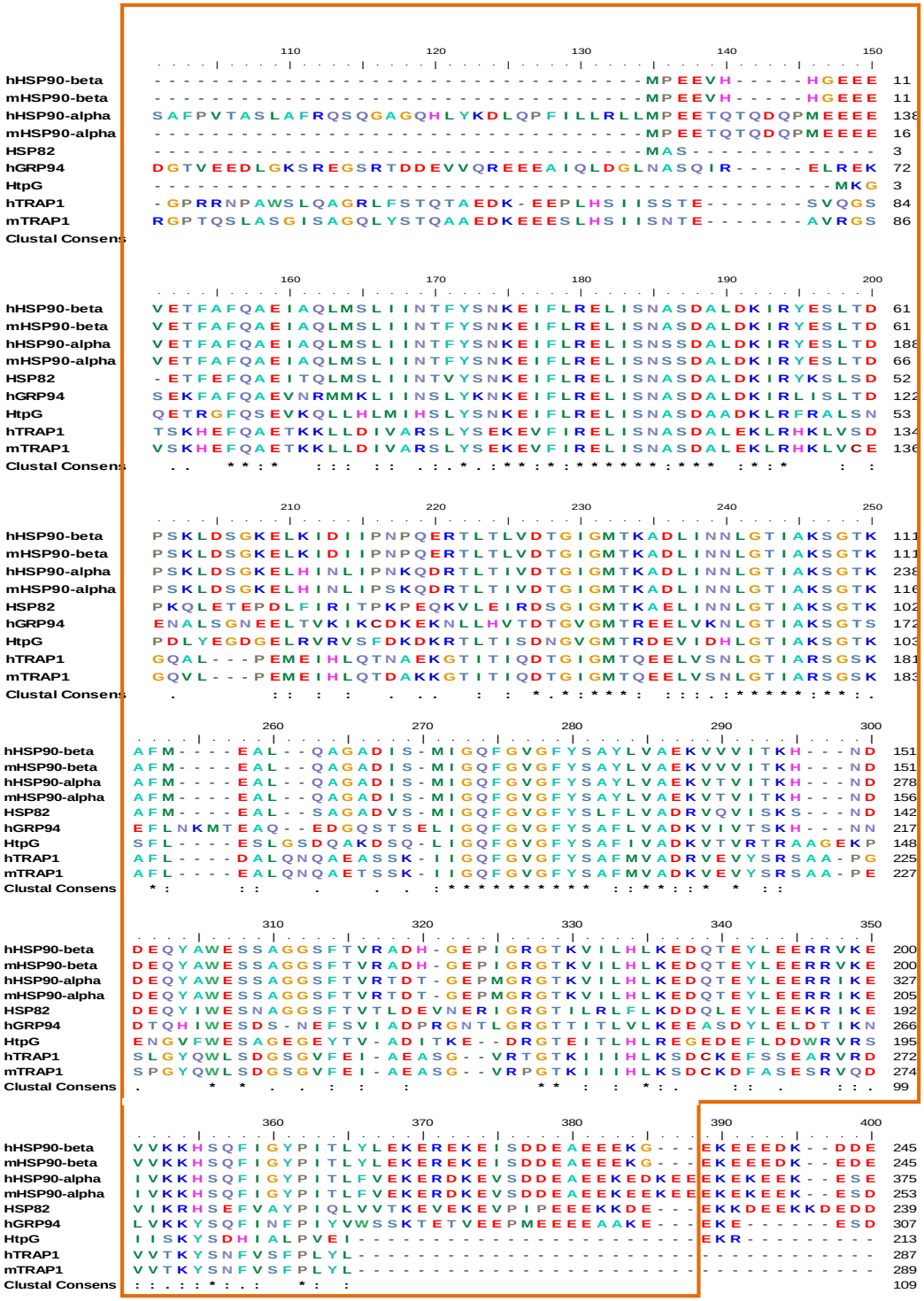

Figure 2.4: Sequence alignment of human cytosolic and mitochondrial Hsp90 proteins against the human N-terminal domain (residues 1-236) of Hsp90 *β* (Katoh *et al*, 2002). The Clustal Consensus (Clustal Consens) highlights the conserved residues. Key: (-) are inserted gaps, (*) are identical residues, (:) are conserved substitutions, (.) are semi-conserved substitutions with similar shapes and same colored residues are conserved. The numbering on top of sequences is a ruler and the sequence position is indicated on the right.

The charged regions of Hsp90 function as flexible linkers that allow for plasticity required for the cooperative domain functions of the protein (Meyer *et al.*, 2003). The results of this study shows that TRAP1 lacked the first charged region that modulates ATP hydrolysis, whereas HtpG carried a few residues within the charged region that was found in the other aligned Hsp90s (Figure 2.5), making the first charged region the least conserved domain.

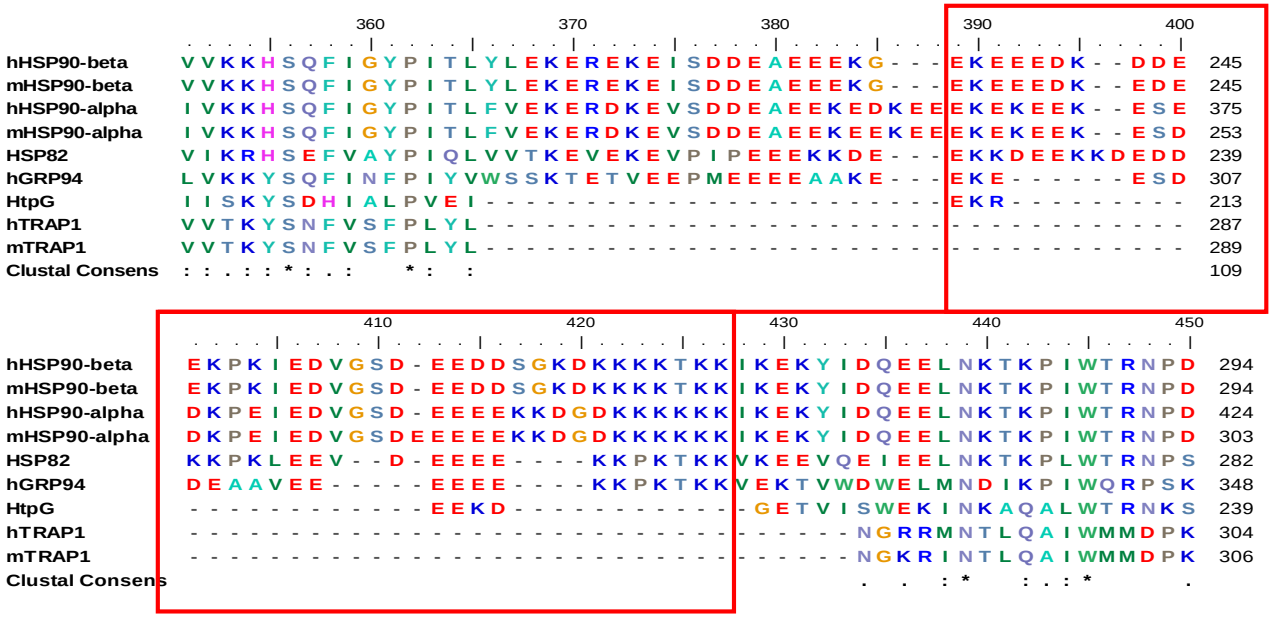

Figure 2.5: Sequence alignment of human cytosolic and mitochondrial Hsp90 proteins against the first Charged Region (residues 237-271) of Hsp90 *β* (Katoh *et al*, 2002). The Clustal Consensus (Clustal Consens) highlights the conserved residues. Key: (-) are inserted gaps, (*) are identical residues, (:) are conserved substitutions, (.) are semi-conserved substitutions with similar shapes and same colored residues are conserved. The numbering on top of sequences is a ruler and the sequence position is indicated on the right.

The middle domain key to binding of Hsp90 to its substrate or "client" proteins in a charge based interaction shows some level of conservation, although it was predominantly via conserved substitutions (Figure 2.6).

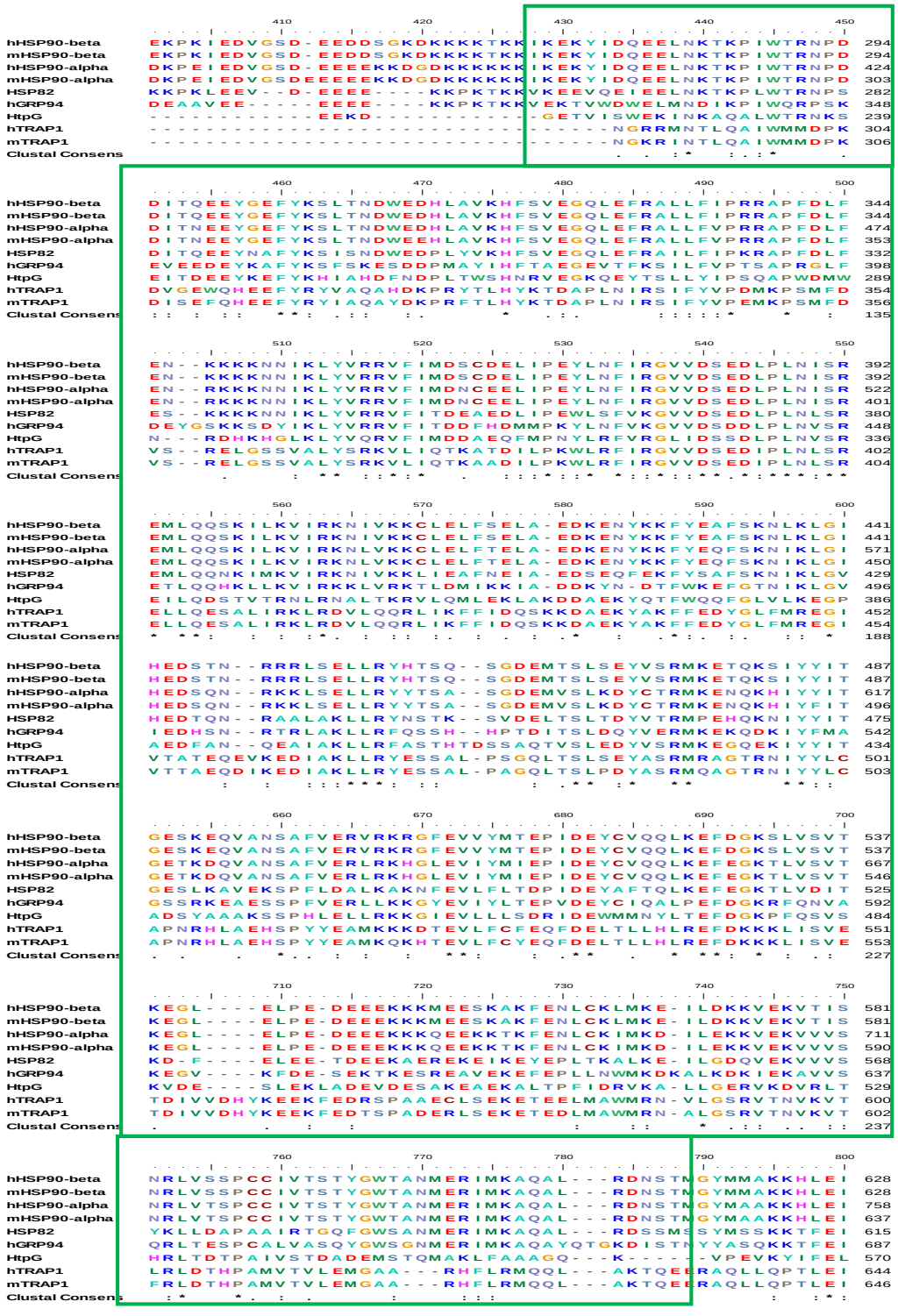

Figure 2.6: Sequence alignment of human cytosolic and mitochondrial Hsp90 proteins against the middle domain of Hsp90 β (Katoh *et al*, 2002). The Clustal Consensus (Clustal Consens) highlights the conserved residues. Key: (-) are inserted gaps, (*) are identical residues, (:) are conserved substitutions, (.) are semi-conserved substitutions with similar shapes and same colored residues are conserved. The numbering on top of sequences is a ruler and the sequence position is indicated on the right.

The second charged region also a flexible linker important for Hsp90 dimers to "clamp" in their substrate only had ten residues with about 40 % of them conserved in TRAP1 (Figure 2.7).

Figure 2.7: Sequence alignment of human cytosolic and mitochondrial Hsp90 proteins against the second Charged Region of Hsp90 *β* (Katoh *et al*, 2002). The Clustal Consensus (Clustal Consens) highlights the conserved residues. Key: (-) are inserted gaps, (*) are identical residues, (:) are conserved substitutions, (.) are semi-conserved substitutions with similar shapes and same colored residues are conserved.

The C-terminal is the dimerization domain where TPR-domain containing co-chaperone binds through the EEVD motif (Olof, 2007). TRAP1 and HtpG lacked the EEVD motif and GRP94 had a conserved substitution for Valine (V) with Methionine (M). Therefore, the results indicate that TRAP1 will not be able to bind to Hsp90 TPR-domain containing co-chaperones (Figure 2.8).

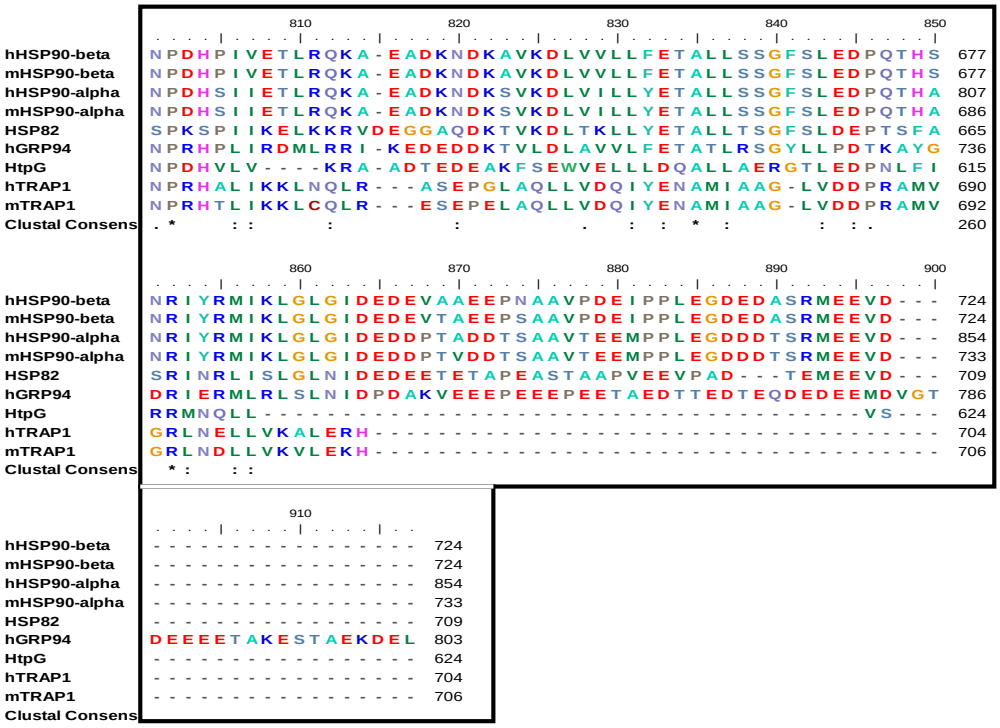

Figure 2.8: Sequence alignment of human cytosolic and mitochondrial Hsp90 proteins against the C-terminal domain (residues 629-732) of Hsp90 *β* (Katoh *et al*, 2002). The Clustal Consensus (Clustal Consens) highlights the conserved residues. Key: (-) are inserted gaps, (*) are identical residues, (:) are conserved substitutions, (.) are semi-conserved substitutions with similar shapes and same colored residues are conserved. The numbering on top of sequences is a ruler and the sequence position is indicated on the right.

2.3.3 Secondary structure prediction

The consensus secondary structure of TRAP1 and Hsp90 *β* was predicted *de novo* to assess if there was conservation of secondary structure which governs the folding of a protein and its function. The predicted secondary structure was based on a consensus sequence of the alignment of these two proteins. Where there are inserted gaps in the sequence (Figure 2.9 HSP90B and TRAP1 rows), the secondary structure predicted (Figure 2.9 jnetpred row) was that of the other protein. Nonetheless, in addition to the reliability of the predicted secondary structure, the reliability values (Figure 2.9 JNETCONF row), also give an indication of how reliable the gap insertion was.

The predicted consensus secondary structure for TRAP1 and Hsp90 *β* had 22 regions of *α*-helices that had at least four helices per region, 15 regions of *β*-sheets that had at least four *β*-sheets per region and 33 regions of random coil or loop regions of random coils or loops that had at least four random coils or loops per region (Figure 2.9 jnetpred row). The predicted consensus secondary

structure for TRAP1 and Hsp90 β had 74.3 % Jnet Reliability values greater than 5, indicating a high level of conservation. The first charged region (Figure 2.9 boxed in blue) was confirmed to be missing in TRAP1 and that it was a loop region. Contrary to the sequence alignment (Figure 2.4-2.8), the middle and the C-terminal domains appeared to be more conserved than the N-terminal domain (Figure 2.9). Although the sequences appeared less conserved, the secondary structures appear to be better conserved between TRAP1 and Hsp90 β indicating that they may share the same tertiary structure. Although TRAP1 was confirmed not to have an EEVD motif (Figure 2.9 boxed in red), the corresponding residues of TRAP1 were also predicted to be random coil residues pointing to the possibility of dimer formation by TRAP1

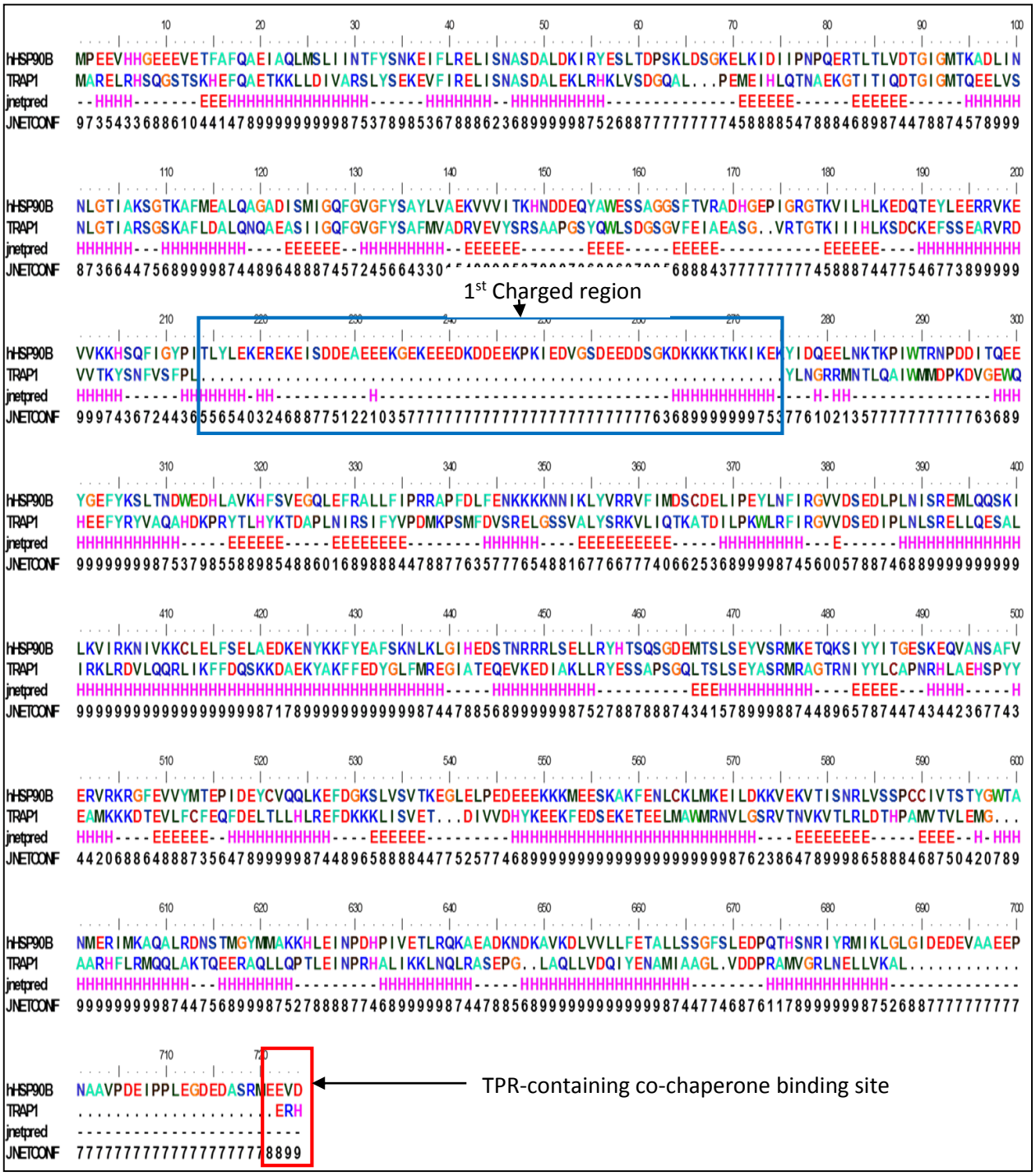

Figure 2.9: The consensus secondary structure prediction of full length TRAP1 and Hsp90 β proteins. Secondary structure prediction was done using JPred and annotated in Bioedit Sequence Alignment Editor. Key: jnetpred is the consensus secondary structure predicted for query; JNETCONF is the Jnet reliability of prediction accuracy ranging from 0 – 9 with 9 being more reliable; α helix (H), β sheet (E) and random coil or loop (-); dot (.) inserted gap.

2.3.4 Sub-cellular localization prediction

The sub-cellular location of a protein also has an effect on its function as membrane bound compartments have different biochemical properties. The prediction sub-cellular localization of proteins gives bioinformatic information on the function of the protein Prediction of sub-cellular localization and cleavage site of TRAP1 and STAT3 were done using PSORT II and TargetP to identify sub-cellular compartments where these proteins are likely to localize and give a bioinformatic insight into the function of these proteins. Using PSORT II, TRAP1 was predicted to be a mitochondrial protein highly likely to localize in the mitochondria with a probability 95.7 %, whereas the chances of STAT3 localizing in the same organelle were much lower at 17.4 % probability (Table 2.3). However, STAT3 was predicted to be predominantly a cytoplasmic protein with cytosolic, nuclear and mitochondrial at 39.1 %, 26.1 % and 17.4 % probability levels, respectively (Table 2.3). These results point to the possibility of TRAP1 and STAT3 sharing mitochondrial and secretory vesicles *in vivo*.

Table 2.3: Sub-cellular localisation prediction of TRAP1 and STAT3 using PSORT II Server.
Key: (CYT is cytoplasm; NUC is nuclear; MIT is mitochondria; PM is plasma membrane and ER is endoplasmic reticulum).

Localization probility (%)								
Protein	CYT	NUC	MIT	Secretory vesicles	Cytoskeletal	PM	ER	Overall decision
STAT3	39.1	26.1	17.4	4.3	4.3	4.3	4.3	Cytoplasmic
TRAP1	-	-	95.7	4.3	-	-	-	Mitochondrial

TargetP predicted TRAP1 to be a mitochondrial protein by a score of 0.905 (Table 2.4). In contrast, STAT3 was predicted to be mitochondrial by a score of 0.136 even though the highest score was for undetermined sub-cellular localizations with a score of 0.874 (Table 2.4). The prediction of STAT3 sub-cellular localization using TargetP was inconclusive and therefore PSORT may be a better sub-cellular localisation prediction server.

Table 2.4: Sub-cellular localisation prediction of TRAP1 and STAT3 using TargetP v 1.1 Server. (MIT is mitochondria and RC is reliability check ranging from 1-5 with 1 being most reliable). The prediction score ranges from 0-1 with 1 being the highest likelyhood.

Localization prediction score							
Protein	MIT	Secretory vesicles	Other	RC	TPlen	Localization	Overall decision
TRAP1	0.905	0.025	0.111	2	59	Mitochondria	Mitochondrial
STAT3	0.136	0.060	0.874	2	-	-	Other

2.3.5 STAT3 conservation

STAT3 isoforms from human and mouse origin were aligned using MAFFT to determine how conserved they were and if human inferences could be made from mouse STAT3 studies. STAT3 proteins had highly conserved sequences between humans and mice (Figure 2.10). Residues important for the STAT3 function such as 414/417R, 705Y and 727S are conserved (Figure 2.10, arrows), although the β isoforms do not have the serine 727 as it is cleaved off as part of the post translation modifications. Such a high level of conservation between human and mouse STAT3s suggest that their structures and functions are also conserved.

Figure 2.10: Multiple sequence alignment of human and mouse STAT3 isoforms. The shaded threshold was set at 90% identity/similarity. The alignment was generated using MAFFT (Katoh *et al*. 1999). Key: hSTAT3 represents human STAT3 and mSTAT3 represents mouse STAT3, (-) are inserted gaps, same shading are identical residues and same colored residues are conserved. Arrows indicate functionally important residues.

2.4 Discussion

Studies have shown that TRAP1 is an Hsp90 homolog although very little is known about its function and interactants. In this study, bioinformatics analysis of TRAP1 and STAT3 were done to assess the similarity of TRAP1 to Hsp90 β, to evaluate the evolutionary relationships of human Hsp90 homologs, and to determine if TRAP1 has the potential to carry out the same functions as Hsp90 β based on structural conservation. In addition, sub-cellular localization prediction of TRAP1 and STAT3 were done to determine the potential sub-cellular localizations of these two proteins. Based on Rost's (1999) guidelines on homologous proteins, TRAP1 was confirmed to be an Hsp90 homolog. The first charged region appeared to be the least conserved domain followed by the C-terminal (Figure 2.5). Both human and mouse TRAP1s (Table 2.2) and STAT3s (Figure 2.10) were highly conserved suggesting that inferences can be made about human cells if mouse TRAP1 and STAT3 are used. Furthermore, human TRAP1 was evolutionary closer to the bacterial Hsp90 homolog, HtpG, than it was to human Hsp90 α. TRAP1 was predicted to localize in the mitochondria, while STAT3 was predicted to localize in the cytoplasm, the nucleus and the mitochondria (Table 2.3-2.4) suggesting that TRAP1 has one cellular localization whist STAT3 has multiple. However, experimental determination of TRAP1 localization has shown that TRAP1 also localizes in the cytoplasm and the ER under certain cellular conditions (Felts *et al*., 2000; Matassa *et al*., 2013). Nonetheless, STAT3 has been reported within organelles such as the mitochondria and endosomes (Xu *et al*., 2007; Wegrezyn *et al*., 2009).

Because the degree to which sequences differ is related to the evolutionary distance from one another, the results of this study showed that TRAP1 and Hsp90 β in humans had a more divergent and ancient common ancestor compared to human TRAP1 and bacterial Hsp90 homolog HtpG. Considering the theory of mitochondrial origin which hypothesize that they originated from bacteria that survived endocytosis, it is important to note the evolutionary DNA distances between the Hsp90s (Figure 2.3). The evolutionary DNA distance between human mitochondrial Hsp90 (TRAP1) and HtpG was smaller than between TRAP1 and Hsp90 β in humans (Figure 2.3). These findings are consistent with Chen *et al.*, (2005; 2006) who suggested that the TRAP1 gene originated from HtpG, whereas the cytosolic Hsp90s arose from GRP94. Furthermore, due to the cyto-protective role that TRAP1 plays, perhaps this gene translocated to the nucleus to ensure expression and conservation of the engulfed bacteria within the eukaryotic cell. The phylogenetic analysis results suggests that human TRAP1 is more likely to function in a manner much more

similar to bacterial Hsp90 than to human Hsp90 β and functional studies can therefore be carried out based on the known functions of bacterial Hsp90.

Sub-cellular localization is related to the protein's function and proteins have signaling peptides that allow them to enter these membrane-bound sub-cellular compartments (Lindgren, 2000). Prediction of sub-cellular localization is therefore important for *in silico* predictions of protein function or identification of drug targets (Yu *et al.*, 2006). The prediction of TRAP1 localization in the mitochondria concurs with other studies where it has been found to mainly localize in the mitochondria (Felts *et al.*, 2000; Kang *et al.*, 2007; Kubota *et al.* 2007). Because low levels of TRAP1 have also been found in other organelles, including the nucleus, lysosomes and endoplasmic reticulum, this may explain the low probabilities detected for other organelles besides the mitochondria (Amoroso *et al.* 2012; Matassa *et al.* 2012).

STAT3 has been canonically reported to localize in the cytoplasm in the absence of activation. When activated by phosphorylation on a tyrosine residue on position 705, STAT3 translocate to the nucleus (Darnell *et al*., 1994; Aaronson and Horvath, 2002; Sehgal, 2003). In this study, STAT3 was predicted to most likely localize in the cytoplasm, followed by the nucleus and then the mitochondria, which is consistent with studies by Wegrzyn *et al*., (2009) on STAT3's localization. Given that there are contesting reports about mitochondrial localization of STAT3, on one side are reports of STAT3 going to the mitochondria (Wegrzyn *et al.*, 2009; Shulga and Pastorino, 2012; Tammineni *et al.*, 2013), and on the other side are reports that it does not go to the mitochondria (Khan *et al.*, 2013), these results suggest that mitochondrial localization is possible however, more studies are required for conclusive results.

The environment of a protein influences its function and given the biochemical differences between the cytoplasm and the mitochondria, proteins found in these locations are likely to behave differently. Therefore, despite the similarities in their sequences and structure, TRAP1 and Hsp90 β may still have different mechanisms of action. Given that the ATPase domain (N-terminal) has been reported to be the most conserved domain among the Hsp90 domains, it is important to note that the predicted secondary structure did not show conservation of structure. This suggests that either these structures were different, or the predicting program had a low predicting power for α helices and loop regions compared to β sheets.

Therefore, the predicted structural differences, in addition to the differences in the sub-cellular localization of TRAP1 and Hsp90 β, perhaps also contribute to the disparity in the proteins' function. Solving the tertiary structure of TRAP1 and comparing it to that of Hsp90 β would give

more insight on the functional differences and shade more light on TRAP1's possible client proteins. Despite TRAP1 and Hsp90 β being imperfectly conserved, it may suffice to coordinate protein function, suggesting that TRAP1 may share some of the Hsp90 client proteins, such as STAT3 possibly through a more ancient mechanism (Süel *et al.* 2003).

To conclude, this study showed a high degree of conservation between human and mouse TRAP1s and STAT3s suggesting that human inference can be drawn from mouse TRAP1 and STAT3. The prediction of STAT3's localization in the mitochondrial implies that STAT3 co-localizes with a mitochondrial protein TRAP1 *in vivo*. However, although STAT3 is a "client" protein of cytosolic Hsp90, the evolutionary distance between TRAP1 and cytosolic Hsp90s and the level of their domains conservation suggests that TRAP1 may or may not function in the same manner when it comes to STAT3. The predicted secondary structure of TRAP1 appeared conserved in comparison to that of Hsp90 β, which suggests the likelihood of similar tertiary structures. Therefore, experimental cellular studies on the localizations and functions of STAT3 and TRAP1 are essential.

CHAPTER 3

The effect of TRAP1 on localization of STAT3 in mammalian cells

3.1 Introduction

STAT3 proteins are canonically known to localize in the cytoplasm and undergo post-transcriptional modifications such as cleavage and phosphorylation (Bromberg *et al*., 1999). When activated, through phosphorylation of Tyrosine 705 (pSTAT3Y705) and/or Serine 727 (pSTAT3S727), STAT3 translocate to the nucleus to activate the transcription of genes (Darnell *et al*., 1994; Aaronson and Horvath, 2002; Sehgal, 2003). The translocation of STAT3 to the nucleus is reported to be facilitated by the molecular chaperone Hsp90 β that is found in the cytoplasm (Shah *et al*., 2002; Sato *et al*., 2003; Prinsloo *et al.*, 2012). Hsp90 β's role as a molecular chaperone has been shown through both inhibition and disruption of interaction studies (Shah *et al*., 2002). These studies have shown that either inhibiting the molecular chaperone's activity or disrupting STAT3's interaction with Hsp90 is associated with a decrease in STAT3 nuclear localization (Prinsloo *et al.*, 2012).

Both latent and activated STAT3 have been reported to localize in other cellular organelles, including the mitochondria (Gough *et al*., 2007; Xu *et al.*, 2007; Wegrzyn *et al*., 2009). Because STAT3 localizes predominantly in the cytoplasm, its occurrence within the mitochondria suggests a chaperone-mediated translocation mechanism as proteins have to be unfolded and refolded during mitochondrial translocation. Molecular chaperones of the Hsp60 and Hsp70 class have been shown to facilitate mitochondrial trafficking of nuclear encoded proteins (Craig *et al*., 2003; Wang *et al*., 2004). It is therefore likely that TRAP1, an Hsp90 isoform that mainly localizes in the mitochondria (Felts *et al.*, 2000; Ni and Lee, 2007; Taherian *et al*., 2007), is involved in STAT3 translocation. TRAP1's mitochondrial localization appears to be a naturally occurring process as this protein has a mitochondrial transit peptide on the N-terminal (Santos *et al.*, 2004). The previous study (Chapter 2) confirmed that TRAP1 contains a mitochondrial localization signal on its N-teminal. This mitochondrial protein has also been reported to have protein-chaperoning functions (Chen *et al*., 1996). There is nevertheless debate over the mitochondrial localization of STAT3 because other studies suggest that this protein does not translocate to the mitochondria (Khan *et al*., 2013). However, *in silico* prediction of STAT3 sub-cellular localization (Chapter 2), suggests that this protein has the potential for other sub-cellular localizations including the mitochondria. The *in silico* prediction of the sub-cellular location of proteins was based on experimentally determined amino acid sequences and predicted the presence of any N-terminal sub-cellular pre-sequences.

3.1.1 Specific Objectives

1. Determine the cellular localization of TRAP1 and STAT3 in 3T3L1 pre-adipocytes and MCF7 human breast carcinoma.

2. Investigate the effect of TRAP1 and STAT3 inhibition on the localization of STAT3.

3. Determine the effect of over-expressing TRAP1 on the localization of STAT3.

3.2 Materials and Methods

3.2.1 Materials

All chemicals, culture media, molecular biology reagents, suppliers, catalogue numbers and equipment are listed in Table A1. The antibodies used in this study are listed Table A2&A3.

3.2.2 Methods

3.2.2.1 Cell culture and maintenance of murine 3T3L1 mouse pre-adipocytes and MCF7 breast cancer cells

The 3T3L1 mouse pre-adipocytes were a gift from Prof Carminita L. Frost (Department of Biochemistry and Microbiology, Nelson Mandela Metropolitan University, South Africa), and MCF7 human breast epithelial cancer cells were a gift from Dr Sharon Prince (Department of Human Biology, University of Cape Town, Cape Town, South Africa). Cells were initially seeded onto 25 cm^3 tissue culture flasks (Corning) to increase cell number as determined by light microscopy. The cells were then passaged by trypsinization onto 75 cm^3 tissue culture flasks (Corning) and maintained in complete media comprising Dulbecco's modified Eagle's medium (DMEM), 5 % (v/v) heat-inactivated fetal calf serum (HIFCS), 50/50 penicillin/streptomycin (100 U/ml). The cells were incubated in a humidified incubator at 37 °C, in a 5 % CO_2 atmosphere for 3T3L1 cells and 9 % CO_2 atmosphere for MCF7 cells.

Cell cultures were split 1:2 once 80 % confluency was reached, as judged by light microscopy. Cells were split by washing with phosphate-buffered saline (PBS) pH 7.4, after which trypsin/ethylenediaminetetraacetic acid (EDTA) was added for 5-7 minutes at 37 °C to generate a cell suspension. Complete media was added to the trypsin suspension to inhibit further trypsinization, and the cell suspension was transferred to a sterile 15 ml tube. An aliquot of 20 µl

was removed from the cell suspension, which was used for cell counting using a 0.1µl Bright-Line hemacytometer (Hausser Scientific, USA). Trypan Blue was used to stain dead cells. Centrifugation of the cell suspension was carried out at 650 *g* at 4 °C for 2 minutes. The supernatant was poured-off the pelleted cells, and the cells were re-suspended in the residual volume to create a single cell suspension, after which more complete media (20 ml) was added. The cells were then seeded onto 2 × 75 cm^3 tissue culture flasks. All cell cultures were routinely checked microscopically for *Mycoplasma* contamination (Section A2 for protocol).

3.2.2.2 Cell lysate preparation

Trypsinized cells were immediately pelleted at 650 *g* for 2 minutes. After centrifugation, the supernatant was removed and the pelleted cells were re-suspended in the residual volume. This was followed by addition of 200 µl of ice-cold radio-immunoprecipitation assay (RIPA) buffer (50 mM Tris-HCl pH 7.4, 150 mM sodium chloride (NaCl), 1 mM ethylenediaminetetraacetic acid (EDTA), 1mM sodium deoxycholate ($C_{24}H_{39}O_4Na$), 1 % (v/v) Nonidet P40 (NP40), 2 µg/ml protease inhibitor cocktail). Lysis was allowed to occur on ice, on a rocking platform for 30 to 60 minutes. Cell debris was discarded by centrifugation at 12 000 *g* and 4 °C for 30 minutes. Protein was quantified using the NanoDrop 2000 at 280 nm (Thermo Scientific). The RIPA lysate was boiled for 10 minutes in 1 × sodium dodecyl sulphate (SDS) sample loading buffer (0.2 M Tris pH 6.8, 20 v/v % glycerol, 10 % w/v SDS, 0.05 w/v % bromophenol blue, 10 mM β-mercaptoethanol). After boiling, the sample (15 µl) was resolved by SDS-polyacrylamide gel electrophoresis (PAGE) (12 % acrylamide) according to Laemmli (1970) at 135 V for approximately 1 hour 30 minutes in 1 × SDS-PAGE running buffer (0.3 M Tris, 44 % (w/v) glycine, 0.1 % (w/v) SDS) for Western blot analysis according Towbin *et al*., 1979.

3.2.2.3 Mitochondrial isolation

Trypsinized cells ($2\text{-}5\times10^7$) were immediately pelleted at 650 *g* for 2 minutes. After centrifugation, the supernatant was removed and the pellet was re-suspended in 5 × the volume of the pellet with Mitochondrial isolation buffer (0.3 M mannitol, 0.1 % (w/v) bovine serum albumin (BSA), 10 mM 4-(2-Hydroxyethyl)piperazine-1-etahesulonic acid, N-(2-Hydroxyethyl) piperazine-N'-(2-ethanesulfonic acid) (HEPES) pH 7.4, 1 × protease inhibitor cocktail that inhibit serine, cysteine,aspartic proteases and amino peptidases)

(www.hci.utah.edu/publicweb/content/grossman/protocols/ March 2012). The cells were homogenized on ice using a dounce-homogenizer, after which an aliquot was stained with trypan blue. The cells were counted under a microscope (magnification × 20) until at least 50% damaged cells were observed. Whole cells and nuclei debris were discarded by centrifugation at 1000 *g* and 4 °C for 10 minutes, and the supernatant was collected. The cytosolic fraction was obtained as the supernatant following centrifugation at 14000 *g* for 15 minutes at 4°C, whereas the pellet represented the mitochondrial fraction that was washed twice with ice-cold isolation buffer. Protein concentration was assessed using the NanoDrop 2000 at 280 nm absorbance (Thermo Scientific). Samples were mixed with 50 µl of × 5 SDS sample loading buffer and boiled for 10 min before resolving by SDS-PAGE.

3.2.2.4 Western blot analysis

Western blot analysis was performed according to Towbin *et al*. (1979). Samples were resolved on 12 % acrylamide gel by SDS-PAGE. Prior to electro-blotting, the gel was washed in ice-cold transfer buffer (25 mM Tris, 192 mM glycine and 20 % (v/v) methanol) to remove excess SDS. Transfer of the resolved proteins was performed onto a methanol activated Immun-Blot® transfer Polyvinylidene fluoride (PVDF) membrane (BioRad, South Africa) in transfer buffer for 1 hr 30 min at 70 V (400 mA) with stirring and cooling. Ponceau (0.1 % (w/v) Ponceau S, 1 % (v/v) glacial acetic acid) staining was used to confirm protein transfer. Non-specific binding sites were blocked for 1 hr in 5 % blocking solution (5 % (w/v) fat-free milk powder in tris-buffered saline (TBS) (50 mM Tris-Cl, pH 7.5, 150 mM NaCl) in plastic zip-lock bags on a shaker at 180-200 rpm at room temperature (RT). Primary antibody (see Table A1) was added to the 2 % blocking solution and the membrane was further incubated overnight on the shaker at high speed at 4 °C. The membrane was then washed for 1 hour in TBS with 0.1 % Tween 20 (TBS-T), at 15 min intervals followed by incubation with secondary antibody (see Table A2) for 1 hour at RT on the shaker. Three 15 minute rinses were performed before detection using the Clarity™ western ECL substrate (BioRad, USA) in UVIproChemi™ (UVItec, UK). Voltage-dependent anion channel (VDAC) proteins located on the outer membrane of the mitochondria were used as the mitochondrial marker while Actin was a cytosolic marker.

3.2.2.5 Immunofluorescence microscopy

Cells that were grown on a glass coverslip in a 24 well plate were washed with PBS. These cells were fixed by incubating with 4 % (w/v) paraformaldehyde for 30 minutes at room temperature (RT). PBS was used to wash the cells for 5 minutes after which they were permeabilized by incubation with 0.1 % (v/v) Triton^{TM} X100 in PBS for 5 minutes followed by two washes with PBS for 5 minutes. The cells were blocked using 1 % (w/v) bovine serum albumin (BSA) in TBS for 30 minutes at RT followed by incubating with the appropriate primary antibody (Table A1) in 0.1 % BSA in TBS at a dilution of 1:500 for 2 hours at RT. The cells were washed twice with PBS for 5 minutes followed by incubation in FITC-labeled secondary antibodies (Table A2) at a 1: 1000 dilution in 0.1 % BSA in PBS for 45 minutes at RT. The cells were washed twice with PBS for 5 minutes at RT followed by nuclear counterstaining with Hoechst 33342 at a 1:1000 dilution in water for 90 seconds at RT. The moisture was allowed to evaporate in dark cupboard after which glass coverslips were mounted with cells side down on glass slides using a small drop of DAKO mounting medium (Invitrogen). Immunofluorescence images were captured using Zeiss AxioVert.A1 FL-LED Microscope and a confocal laser-scanning Zeiss Laser Scanning Microscope (LSM) 510 Meta Confocal microscope. Images were recorded and processed digitally with Zen Blue and Zeiss LSM Image Browser software (Zeiss, Germany). Voltage-dependent anion channel (VADC) staining was used as the mitochondrial marker. The same procedure was performed with primary or secondary antibody only as negative controls.

3.2.2.6 Inhibition studies

3.2.2.6.1 Cell growth assay and determination of the half maximal inhibitory concentration (IC_{50}) of inhibitors

The IC_{50} of the inhibitors geldanamycin (Roe *et al*., 1999) and S3I-201 (Siddiquee *et al.*, 2007) was determined using the ACEA xCELLigence Real-time Cell Analyser (RTCA) biosensor system (Roche). Cells were seeded in an E-plate 96 with micro gold electrodes covering the bottom of the wells. This system is a label free assay based on an electrical cell substrate impedance and measured electrical impedance at given time points (Z_i) in relation to the background reading (Z_0) to calculate arbitrary cell index (CI) units as: $CI \approx \left(\frac{Zi - Z0}{15} \right)$.

The more cells attached on the electrodes, the larger the impedance on the electrode. Cell densities of 1×10^3, 2×10^3, 4×10^3 or 8×10^3 were seeded in quadruplicate in each well. Cell index was recorded every 15 minutes for 24 hours before adding 6 dilutions of inhibitor (250, 125, 62.5, 31.25, 15.625 and 7.8125 µM S3I-201; 50, 5, 12.5, 6.25, 3.125 and 1.5126 µM GA). Following addition of inhibiting compound, the cell index was monitored and recorded for 24 hours and 72 hours for geldanamycin and S3I-201, respectively. The RTCA software (The RTCA Software Package 2.0) was used to analyze the data. The calculation of IC_{50} values was done using non-linear regression analysis and DRC (area under the curve in a time period versus concentration) curve type.

3.2.2.6.2 Effect of geldanamycin and S3I-201 on mitochondrial localization of STAT3

Murine 3T3L1 cells (1×10^4 cells/ml) were seeded in a 24 well culture plate with cover slips for 24 hours before treating with IC_{50} concentrations of geldanamycin or S3I-201 for 24 hours at 37 °C, 5 % CO_2. Following treatment, the cells were stained and coverslips mounted on microscope slides as described in section 3.2.2.5.

3.2.2.7 Transient transfection of 3T3L1 cells with TRAP1 encoding construct

The pRc-CMV-TRAP1-HA plasmid (obtained from Professor Franca Esposito (Università degli Studi di Napoli Federico II, Napoli, Italy) encoding for human TRAP1 and a Haemoglutinin (HA) tag was confirmed to carry the TRAP1 gene by automated DNA sequencing (inqaba biotec, RSA) using the T7 forward primer and the SP6 reverse primer. Endotoxin-free plasmid was isolated using GenElute™ endotoxin-free plasmid midiprep kit (Sigma-Aldrich) before transfection into 3T3L1 cells. Transient transfections of about 2×10^5 3T3L1 cells with 10 µg/ml of TRAP1-HA were done in PBS using 4 mm electroporation cuvette and a Gene Pulser Xcell electroporation system at 180 Volts and 950 microfarads (µF) capacitance (Imamura *et al*., 2001). Transfected cells were plated in 6 well culture dishes for 72 hours before staining for either fluorescence microscopy or ROS assay. The HA-tag was used to detect transfected cells as it is a viral protein not expected to be endogenously expressed by 3T3L1 cells.

3.2.2.9 Cellular localization analysis

Immuno-fluorescence images, captured using an immunofluorescence microscope, were used to analyze potential co-localization of VDAC and TRAP1 with STAT3 and their expression profiles

across a cell. Images were processed using ImageJ v1.421 (MacBiophotonics, Canada). A red, green and blue (RGB) color composite image was generated and used to plot profiles using the Color Functions Plugin (Collins, 2007).

3.2.2.10 ROS determination

To measure total cellular ROS, cells at about 70 % confluency were trypsinized to single cell suspension and washed three times before incubation with 100µM 2',7'-dichlorofluoresein diacetate (DCFDA) (Sigma-Aldrich) in PBS for 30 minutes at 37 °C. After incubation with DCFDA, cells were analyzed on a flow cytometer (BD FACSAria^{TM}, CA, USA) to measure the fluorescence after excitation at wavelength of 488 nm and emission at 530 nm. .

3.3 Results

3.3.1 Protein expression in 3T3L1 cells

To determine if proteins were present at detectable protein levels and if its signalling pathway was activated in 3T3L1 cells, western blot analysis of the total cell lysate was conducted to detect total STAT3, STAT3 phosphorylated at serine 727 (pSTAT3S727) and STAT3 phosphorylated at tyrosine 705 (pSTAT3Y705), TRAP1, VDAC and Actin. Total STAT3 (Figure 3.1 left panel, Total cell lysate lane) and post transcriptional modifications pSTAT3S727 (Figure 3.1 middle panel, Total cell lysate lane) and pSTAT3Y705 (Figure 3.1 right panel, Total cell lysate lane) were detected between 75 and 100 kDa as expected indicated by the top arrows (Figure 3.1). However, lower molecular weight bands were also detected at 50 kDa (Figure 3.1 middle panel, Total cell lysate lane) and below the 37 kDa mark (Figure 3.1 right panel, Total cell lysate lane), indicating possible proteolytic cleavage or non-specific binding of the antibody.

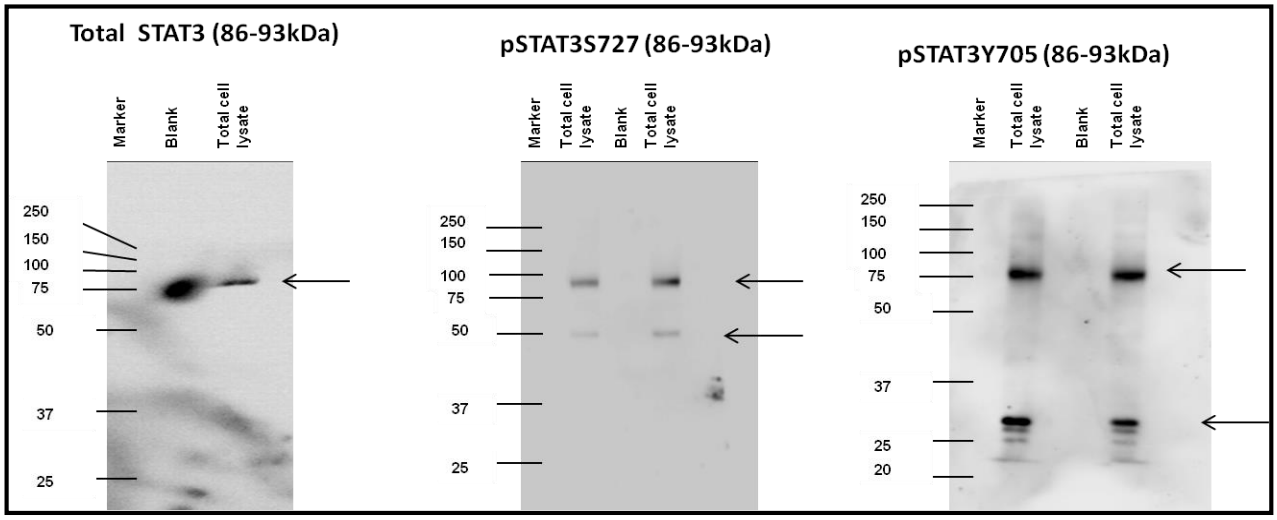

Figure 3.1: Western blot detection of total STAT3, pSTAT3Y705 and pSTAT3S727 in murine 3T3L1 cells. Equal amounts of total cell lysate protein were loaded in each well for 12 % SDS-PAGE. The antibodies used (Table A2) were expected to detect total STAT3 (STAT3 α and STAT3 β) at 93 and 86 kDa molecular weight respectively.

TRAP1 was detected at approximately 75 kDa as expected (Figure 3.2, left panel, Total cell lysate lane). VDAC, the mitochondrial marker was detected was detected at approximately 100, 60 and 35 kDa (Figure 3.2, middle, Total cell lysate lane) indicating higher molecular weight isoforms of VDAC. Actin, a cytosolic marker, was detected above the 37 kDa mark (Figure 3.2, right panel, Total cell lysate lane).

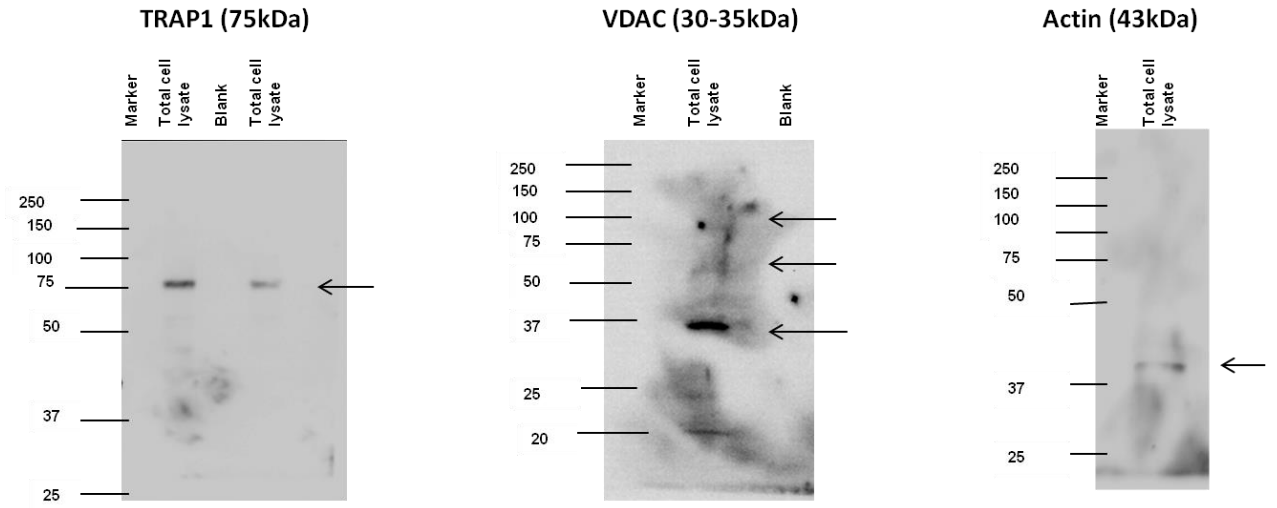

Figure 3.2: Western blot detection of TRAP1, VDAC and Actin in murine 3T3L1 cells Equal amounts of total cell lysate protein were loaded in each well for 12 % SDS-PAGE. The antibodies used (Table A2) were expected to detect TRAP1, VDAC and Actin proteins at 75, 30-35 and 43 kDa respectively.

3.3.2 *In vivo* expression of HA-tagged TRAP1 protein

To verify if recombinant protein encoded by the pRc-CMV-TRAP1-HA was being expressed in transfected cells, western blot analysis and immunofluorescence microscopy were carried out to detect the C-terminal HA-tag and TRAP1. The expression plasmid pRc-CMV-TRAP1-HA was confirmed to carry the TRAP1 gene by automated DNA sequencing (Section A3). Cells (3T3L1) were transfected with a plasmid encoding for the TRAP1 gene tagged with a haemoglutinin peptide at the C-terminal. Western blot analysis of the total cell lysate of non-transfected cells did not detect HA (Figure 3.3A NT panel) but HA was detected at multiple molecular weights in transfected 3T3L1 cells as highlighted by the arrows in Figure 3.3A T panel, indicating that the TRAP1 gene was possibly fully translated and potential post translational proteolytic cleavage as the HA tag is on the C-terminus.

Furthermore, fluorescence microscopy also detected HA (Figure 3.3B HA panel) compared to the non-transfected control that did not detect HA (Figure A2), therefore both western blotting and fluorescence microscopy indicate that the TRAP1 gene was potentially being transcribed (Figure 3.3). VDAC staining was used to mark the position of the mitochondria (Figure 3.3B VDAC panel). TRAP1-HA was found to localize in both the cytoplasm and nucleus of transfected 3T3L1 cells (Figure 3.3B HA panel) and all cells present appeared to express TRAP1-HA (Figure 3.3B 10× magnification). Endogenous TRAP1 was localized in perinuclear punctuate structure (Figure 3.3C Untreated, TRAP1 panel), in a pattern similar to that observed for the mitochondrial marker VDAC (Figure 3.3B VDAC panel), indicating a mitochondrial localization in untreated cells. However; over-expression of TRAP1 appeared to result in more nuclear localization as the morphology of cells become more rounded (Figure 3.3C TRAP1 over-expression TRAP1 panel).

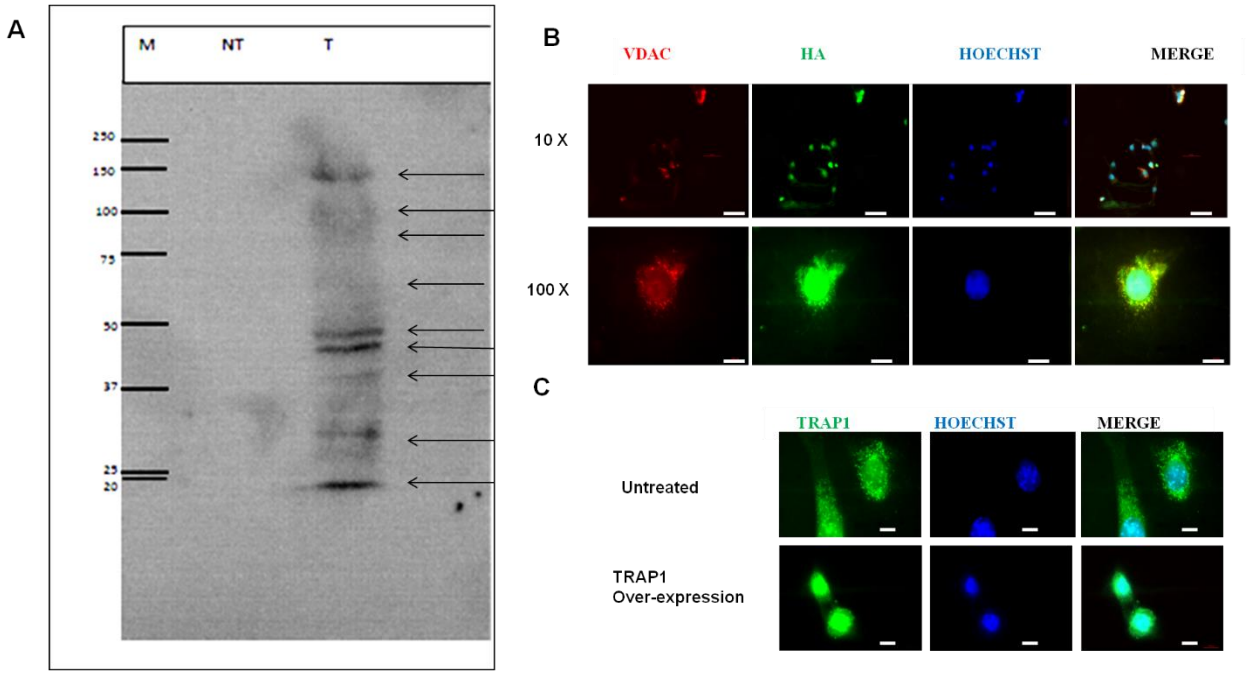

Figure 3.3: Confirmation of transfection success by (A) western blot analysis in total cell lysate, (B) microscopy using antibody against the HA tag on adherent cells and (C) microscopy using antibody against TRAP1 on adherent cells respectively 72 hour after transfection. Microscopy images were captured using a Zeiss AxioVert.A1 FL-LED Microscope at 10 × and 100 × magnification (B top panel and B bottom panel to C respectively). Scale bars represent 200 µm and 20 µm for 10 × and 100 × magnifications respectively.

3.3.3 Determining the IC_{50} of geldanamycin and S3I-201 in murine 3T3L1 cells

Mouse cell model 3T3L1 pre-adipocytes were compared to a human cell model MCF7 breast cancer cells because cancer cells are known to be sensitive to STAT3 and Hsp90 inhibition (Bromberg *et al*., 1999; Hodge *et al*., 2005; Whitesell *et al*., 2005; Banerji, 2009). Prior to the inhibition assays, the seeding density of cells were determined by growth assays of both 3T3L1 and MCF7. For 3T3L1 cells, the best seeding density was 2×10^4 cells/well, whereas that of MCF7 cells was 8×10^4 cells/well (Section A4). It was imperative to determine the IC_{50} concentrations of inhibitory compounds so that concentrations lower than the IC_{50} but high enough to elicit cellular response without killing most of the cells could be used to assess their effect on STAT3 and TRAP1 localization. The IC_{50} of the inhibitors was calculated using the CI of the time period starting from the red vertical line to the end of the experiment (Figures 3.4-3.6).

The IC_{50} of the STAT3 inhibitor S3I-201 was calculated to be 9.05 µM with R^2 of 0.925 for 3T3L1 pre-adipocyte cells (Figure 3.4), seeded at a density of 2×10^4 cells/well as that seeding

density had an R^2 value closest to 1 indicating it was the most reliable plot (n=4) (Figure A3). MCF7 breast cancer epithelial cells had an IC_{50} of 56.03 µM with R^2 of 0.931 (Figure 3.5) (n=4), for cells seeded at a density of 8×10^4 cells/well as that seeding density had an R^2 value closest to 1 indicating it was the most reliable plot (Figure A5). The Hsp90 inhibitor geldanamycin (GA) was calculated to have an IC50 of 0.872 µM with an R^2 value of 0.907 for 3T3L1 pre-adipocyte cells seeded at a density of 2×10^4 cells/well (Figure 3.6) (n=4).

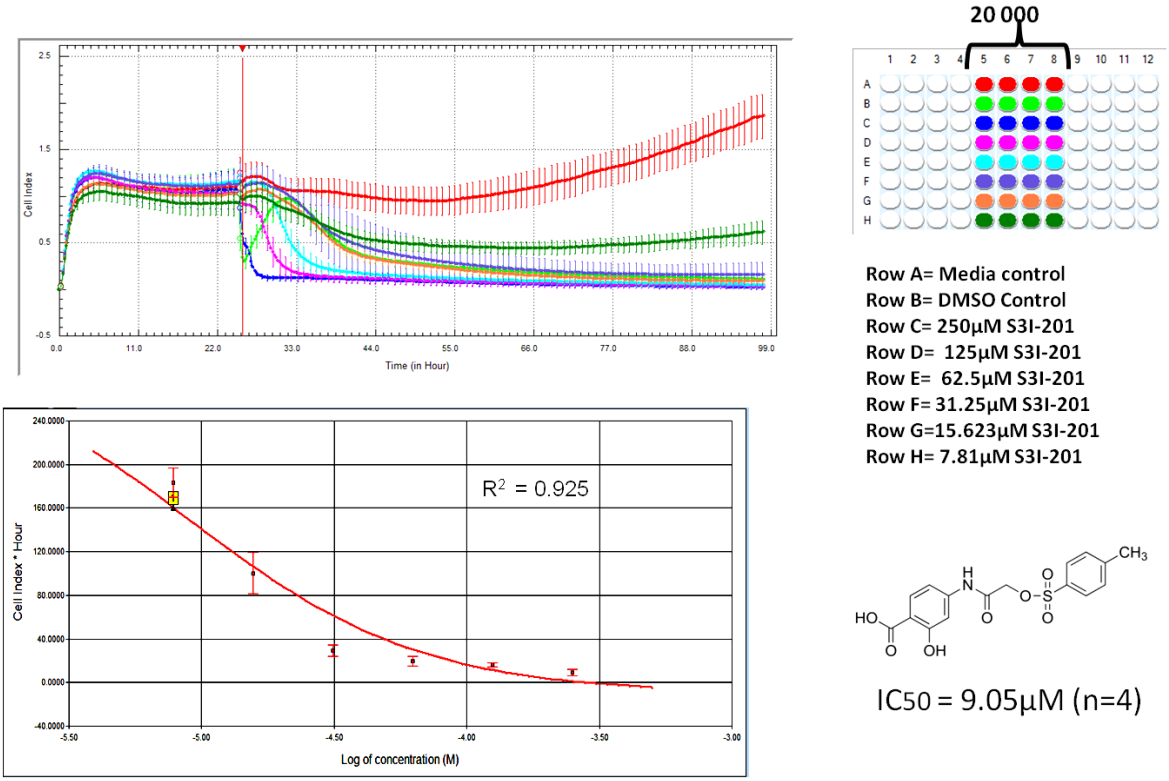

Figure 3.4: Dynamic monitoring of compound S3I-201 interaction with 3T3L1 pre-adipocyte cells. The effect of the different concentrations of S3I-201 on 3T2L1 cells was monitored in real time using xCELLigence Real Time Cell Analyzer with media as a negative control and DMSO as a solvent control.

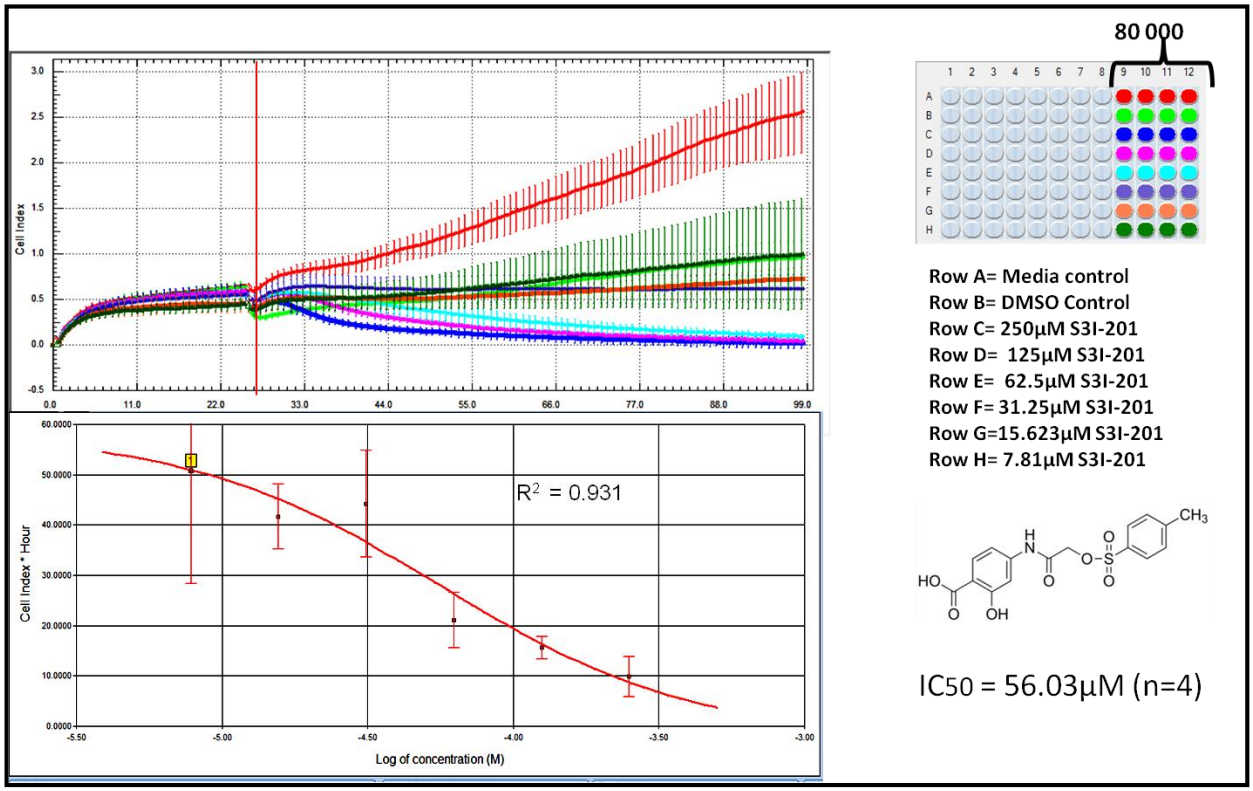

Figure 3.5: Dynamic monitoring of compound S3I-201 interaction with breast cancer MCF7 epithelial cells. The effect of the different concentrations of S3I-201 on MCF7 cells was monitored in real time using xCELLigence Real Time Cell Analyzer with media as a negative control and 0.2 % (v/v) DMSO as a solvent control.

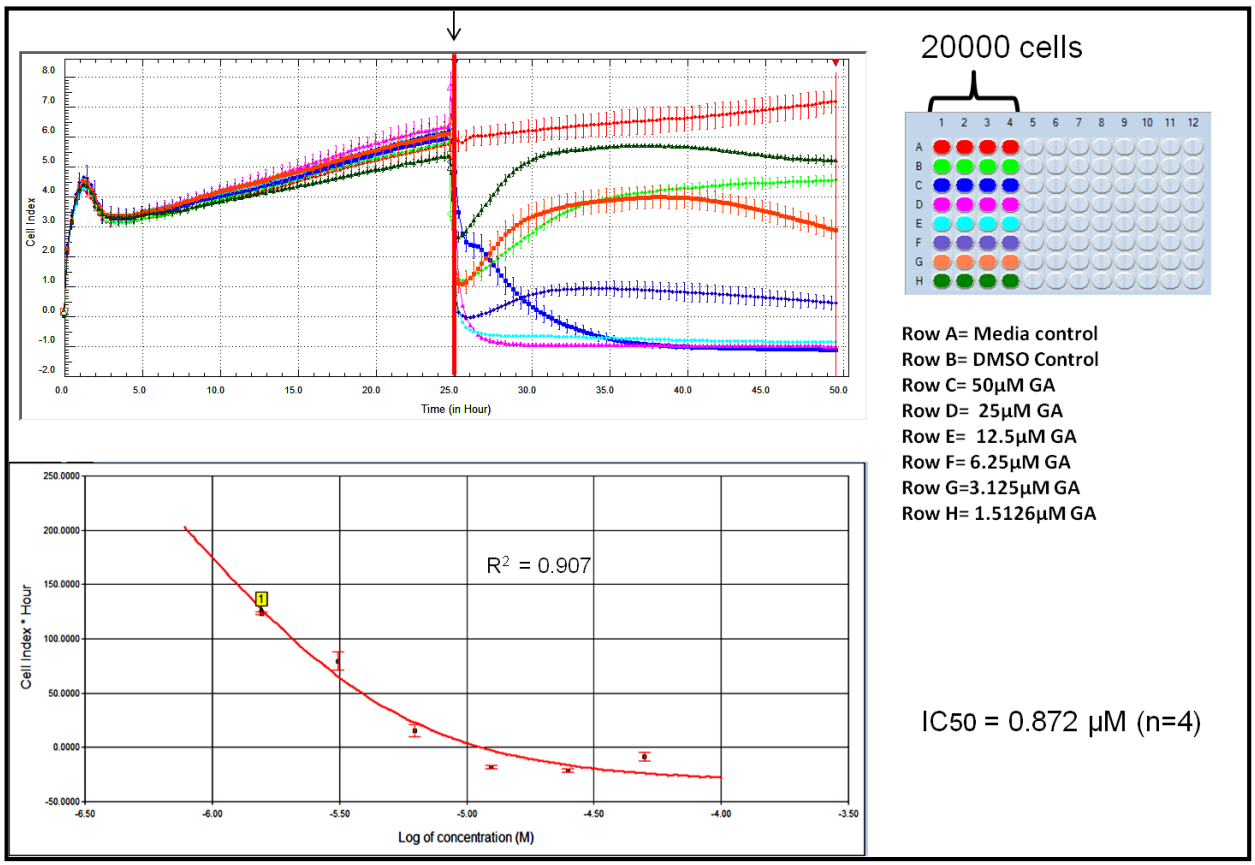

Figure 3.6: Dynamic monitoring of compound geldamycin interaction with 3T3L1 pre-adipocyte cells. The effect of the different concentrations of GA on 3T2L1 cells was monitored in real time using xCELLigence Real Time Cell Analyzer with media as a negative control and DMSO as a solvent control.

3.3.4 Mitochondrial distribution in 3T3L1 cells

Immunofluorescence detection of VDAC, an outer mitochondrial protein, was used to identify the position of the mitochondria (Figure 3.7 red fluorescence). The position of the mitochondria was assessed in relation to that of the nucleus (Figure 3.7 blue fluorescence). Mitochondria of untreated cells displayed punctuate perinuclear distribution with a high intensity towards the nucleus that dropped towards the cell periphery (Figure 3.7 untreated panel). Cells treated with the STAT3 inhibitor displayed loss of the punctuate staining (Figure 3.7 STAT3 Inhibition panel) observed in untreated cells and appeared to be lifting off indicating that the cells' mitochondrial outer membrane's integrity may possibly have been impaired. However, over-expressing TRAP1 appeared to result in perinuclear arrangement of mitochondria (Figure 3.7 TRAP1 over-expression

panel) and a reduction in the size of the cells as shown by the cell sizes in relation to the 20 µm scale bar. Cells treated with the Hsp90 inhibitor also appeared to lose the punctuate staining (Figure 3.7 Hsp90 Inhibition panel) observed in untreated cells indicating that the cells' mitochondrial outer membrane's integrity may possibly have been impaired.

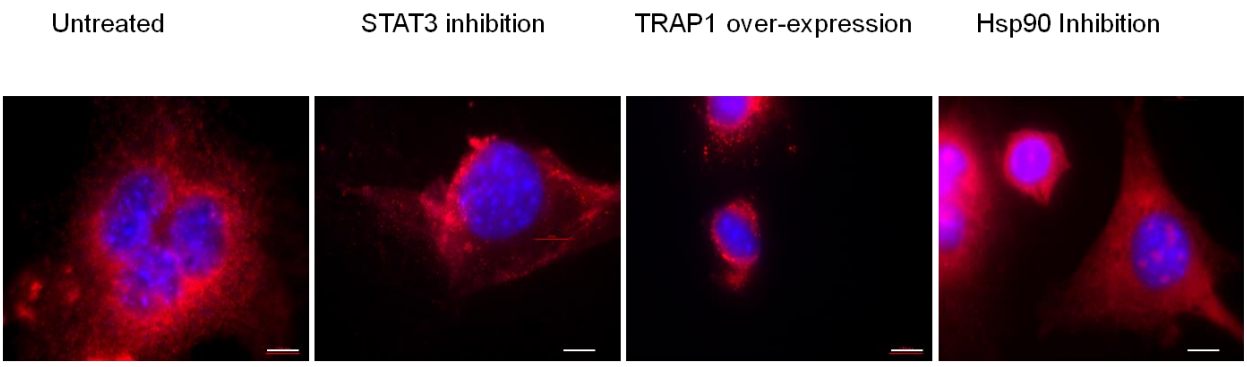

Figure 3.7: Cellular localization of mitochondria. Epi-fluorescence microscopy images of stained 3T3L1 cells captured using a Zeiss AxioVert.A1 FL-LED Microscope at 100× magnification showing the distribution of mitochondria using VDAC (red) staining as a mitochondrial marker and Hoechst (blue) as nuclear marker. Scale bars represent 20 µm.

3.3.5 Localization of total STAT3

Localization of STAT3 was assessed using VDAC staining (Figure 3.8 VDAC panel), to mark the mitochondria for which the staining pattern observed was similar to that observed in Figure 3.7. Hoechst staining was used to mark the position of the nucleus (Figure 3.8 Hoechst panel). Total STAT3 localized in the nucleus and in punctuate structures in the cytoplasm of untreated cells (Figure 3.8 UNTREATED, STAT3 panel) and the results indicate that most of the punctate STAT3 structures also overlap with the staining of VDAC indicating that both STAT3 and VDAC are located within the same region, which points to a confirmation of STAT3 localization in mitochondria. STAT3 in S3I-201 treated cells was found to be predominantly localized in the nuclei of most cells (Figure 3.8 STAT3 inhibition, STAT3 panel). However, TRAP over-expression does not seem to alter the distribution of STAT3 (Figure 3.8 TRAP1 OVER-EXPRESSION, STAT3 panel). Within cells treated with GA, STAT3 staining was observed to have lost the punctate staining which co-localized with VDAC, in agreement with previous result (Figure 3.7) indicating that mitochondrial membrane integrity may be compromised (as assessed

by VDAC staining) and, consequently, the STAT3 localization to the mitochondria may have been affected also (Figure 3.8 Hsp90 Inhibition, STAT3 panel).

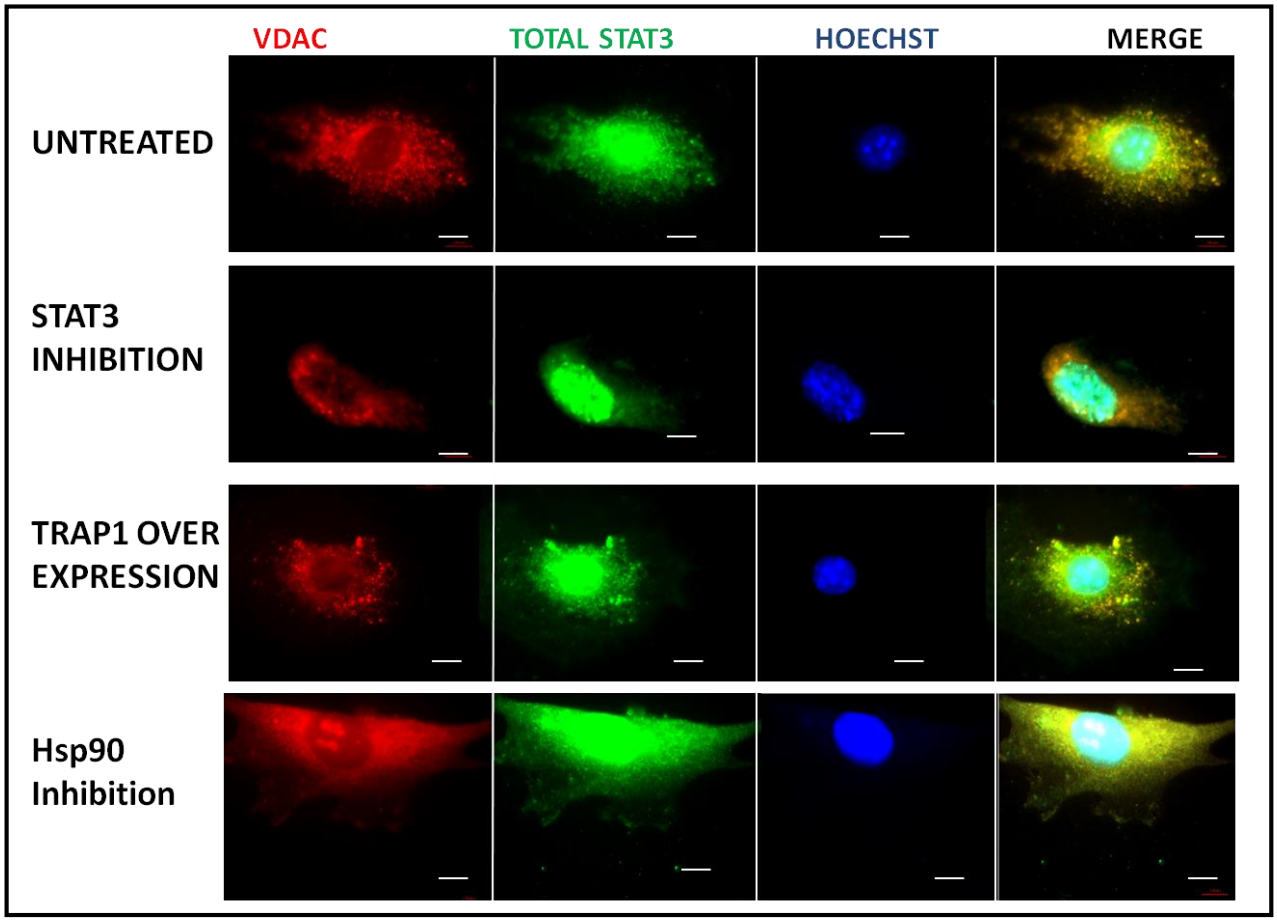

Figure 3.8: The sub-cellular localization of Total STAT3 in 3T3L1 cells. Epi-fluorescence microscopy images of stained 3T3L1 cells captured using a Zeiss AxioVert.A1 FL-LED Microscope at 100× magnification. VDAC is red; total STAT3 green; Nuclei blue; Merge is the overlap of Nuclei, VDAC and total STAT3 signals with the yellow regions highlighting co-localization of VDAC and total STAT3. Scale bars represent 20 µm.

3.3.6 Localization of pSTAT3Y705

Localization of tyrosine 705 phosphorylated STAT3 (pSTAT3Y705), was assessed using VDAC staining (Figure 3.9 VDAC panel), to mark the mitochondria and Hoechst staining to mark the position of the nucleus (Figure 3.9 Hoechst panel) to determine its presence in both the nucleus and the mitochondria. STAT3 phosphorylated at tyrosine 705 was also found in punctate structures around the nucleus (Figure 3.9 UNTREATED, pSTAT3Y705 panel) that appeared to be very similar to the VDAC puncta, strongly indicating extensive mitochondrial localization. This

suggests that the pSTAT3Y705 localization was similar to that of total STAT3 (Figure 3.8 UNTREATED, TOTAL STAT3 panel), with perhaps more intense staining in the nucleus (Figure 3.9 UNTREATED, pSTAT3Y705 panel). Treating cells with the STAT3 inhibitor for 24 hours appeared to have no effect on the cytoplasmic localization of pSTAT3Y705 although the levels seem to decrease indicating that the inhibitor may have prevented further phosphorylation (Figure 3.9 S3I-201, pSTAT3Y705 panel). The results also show that the pSTAT3Y705 localization in the nucleus (Figure 3.9 S3I-201, pSTAT3Y705 panel), seem unchanged. Furthermore, there are punctate structures in the perinuclear region that seem to partially co-localize with VDAC (Figure 3.9 S3I-201, pSTAT3Y705 panel), indicating that the inhibitor seemed not to have an effect on mitochondria or potential pSTAT3Y705's mitochondrial localization. Because the STAT3 inhibitor does not disrupt phosphorylation but only prevents new phosphorylation events, the cytosolic pSTAT3Y705 decreased substantially, whereas the phosphorylated form was retained in the nucleus. Cells over-expressing TRAP1 were smaller and showed a punctate cytoplasmic localization of pSTAT3Y705 (Figure 3.9 TRAP1 OVER-EXPRESSION, pSTAT3Y705 panel), which appears to be in the same region as VDAC, indicating that more pSTAT3Y705 may potentially be localizing in the mitochondria compared to untreated cells. These results (Figure 3.9 TRAP1 OVER-EXPRESSION, pSTAT3Y705 panel), point to the involvement of TRAP1 in the potential mitochondrial localization of pSTAT3Y705. Within cells treated with GA, pSTAT3Y705 staining was observed to have lost the punctate staining (Figure 3.9 Hsp90 Inhibition, pSTAT3Y705 panel), similar to the pattern observed in Figure 3.8 Hsp90 Inhibition, STAT3 panel, indicating loss of mitochondrial membrane integrity.

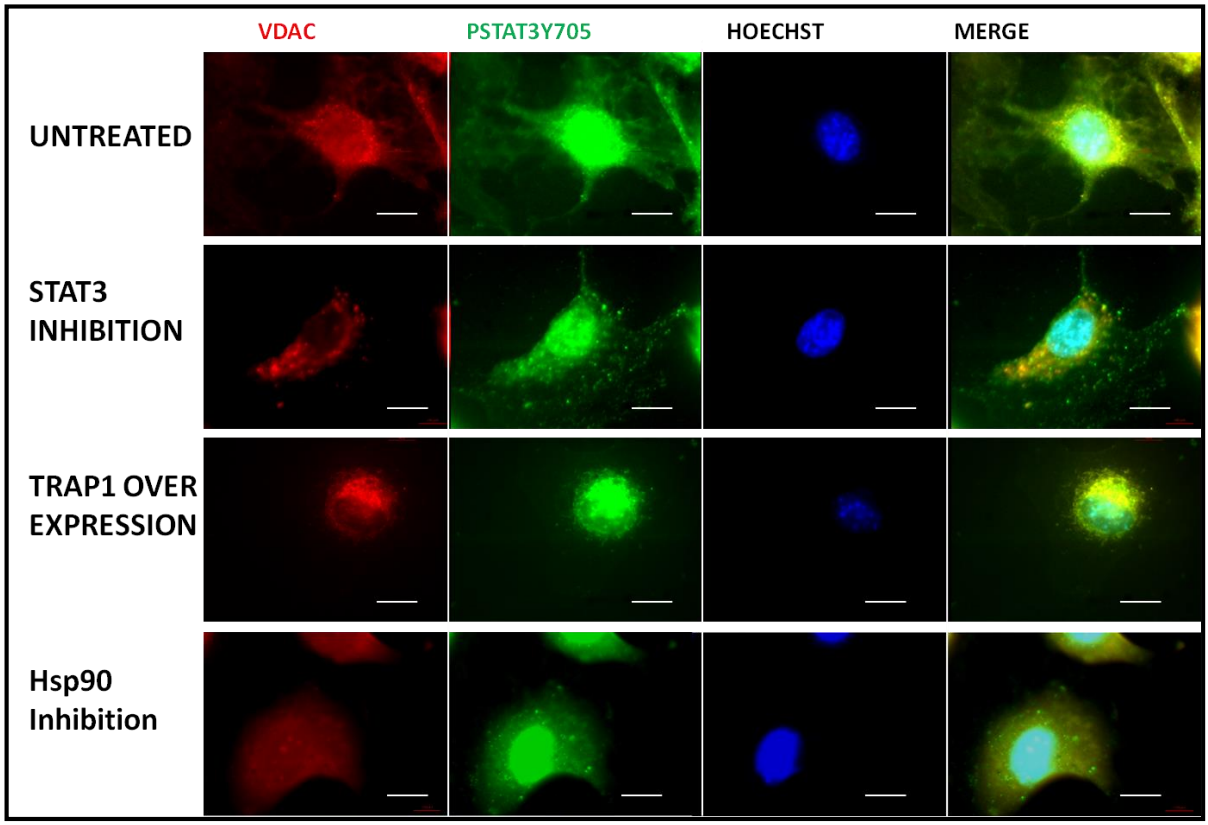

Figure 3.9: The sub-cellular localization of pSTAT3Y705 in 3T3L1 cells. Epi-fluorescence microscopy images of stained 3T3L1 cells captured using Zeiss AxioVert.A1 FL-LED Microscope at 100 × magnification. VDAC is red; pSTAT3Y705 green; Nuclei blue; Merge is the overlap of Nuclei, VDAC and pSTAT3Y705 signals with the yellow regions highlighting co-localization of VDAC and pSTAT3Y705. Scale bars represent 20 µm.

3.3.7 Localization of STAT3S727

Punctate cytoplasmic localization was observed for pSTAT3S727 untreated 3T3L1 cells (Figure 3.9 UNTREATED, pSTAT3S727 panel), and its cytoplasmic localization appeared similar to VDAC, indicating possible mitochondrial localization (Figure 3.10). Similar to pSTAT3Y705 levels whose levels also appeared to decrease in the presence S3I-201 (Figure 3.9 S3I-201, pSTAT3Y705 panel), the localization of pSTAT3S727 appeared unaffected by the presence of the inhibitor (Figure 3.10 S3I-201, pSTAT3S727 panel). Cells over-expressing TRAP1 were smaller and showed a condensed nuclear localization of pSTAT3S727 (Figure 310 TRAP1 OVER-EXPRESSION, pSTAT3S727 panel), similar to the observation in indicating a possible TRAP1 effect on morphology, cell viability and phospho-activated STAT3 but also still had some mitochondrial localisation evident, particularly in the top cell. Within cells treated with GA (Figure 3.10 Hsp90 Inhibition, pSTAT3S727 panel), pSTAT3S727 staining was observed to have lost the

punctate staining observed in untreated cells (Figure 3.10 UNTREATED, pSTAT3S727 panel), similar to the pattern observed in Figure 3.8 Hsp90 Inhibition, STAT3 panel, indicating that mitochondrial membrane integrity may be compromised. Nonetheless, experimental controls such as cells that were treated with DMSO or cells that were transfected with an empty vector, would allow for concrete conclusions to be drawn from these results.

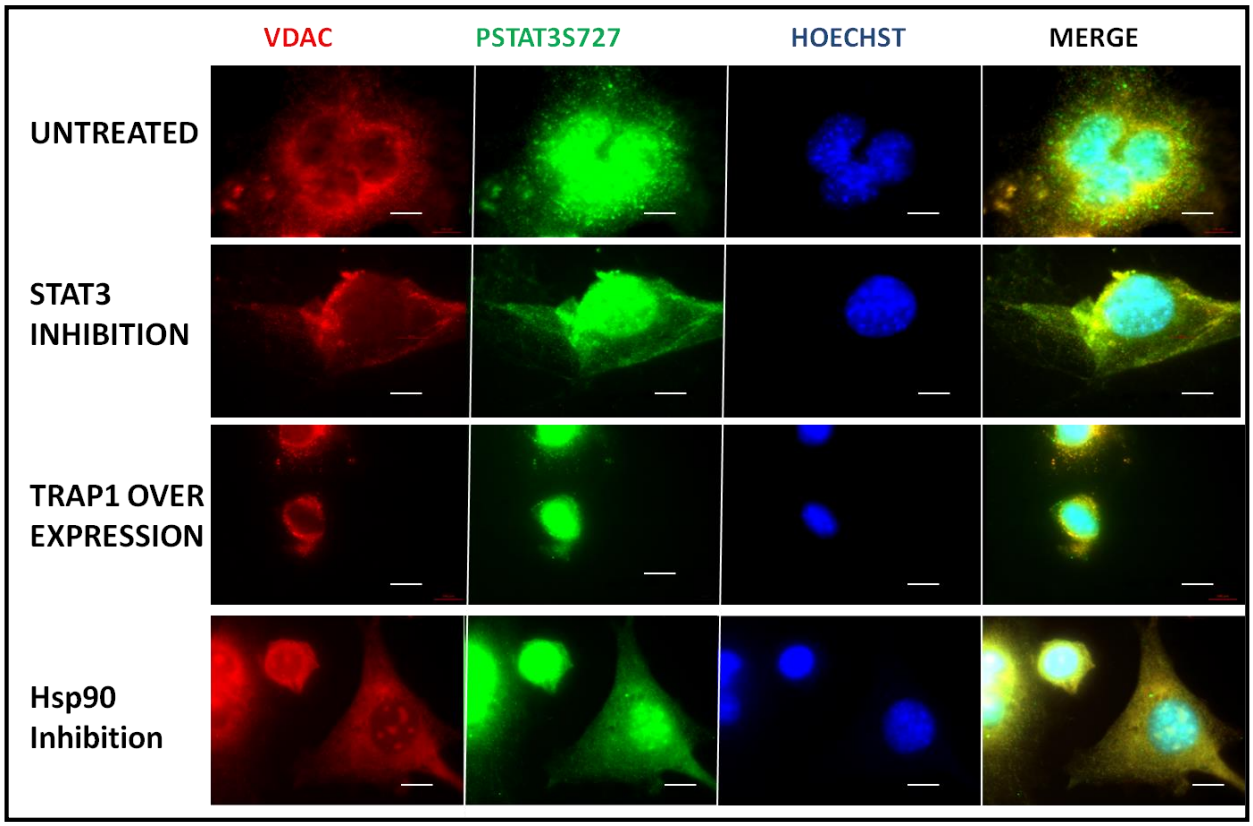

Figure 3.10: The sub-cellular localization of pSTAT3S727 in 3T3L1 cells. Epi-fluorescence microscopy images of stained 3T3L1 cells captured using a Zeiss AxioVert.A1 FL-LED Microscope at 100 × magnification. VDAC is red; pSTAT3S727 green; Nuclei blue; Merge is the overlap of Nuclei, VDAC and pSTAT3S727 signals with the yellow regions highlighting co-localization of VDAC and pSTAT3S727. Scale bars represent 20 µm.

Because of low intensities, the unequal intensities of fluorescence and high background, the images captured using the confocal microscope (Figure 3.11A), could not be used for co-localization analysis. Instead, intensity profiles were plotted (Figure 3.11B) to further explore the morphological changes of the cells. Compared to untreated cells, the nuclear region appeared to become larger with S3I-201, GA and TRAP1 over-expression treatments with TRAP1 over-

expression having the largest nuclear region (Figure 3.11B), indicating that the cytoplasmic becomes smaller and biomolecular concentrations may become higher.

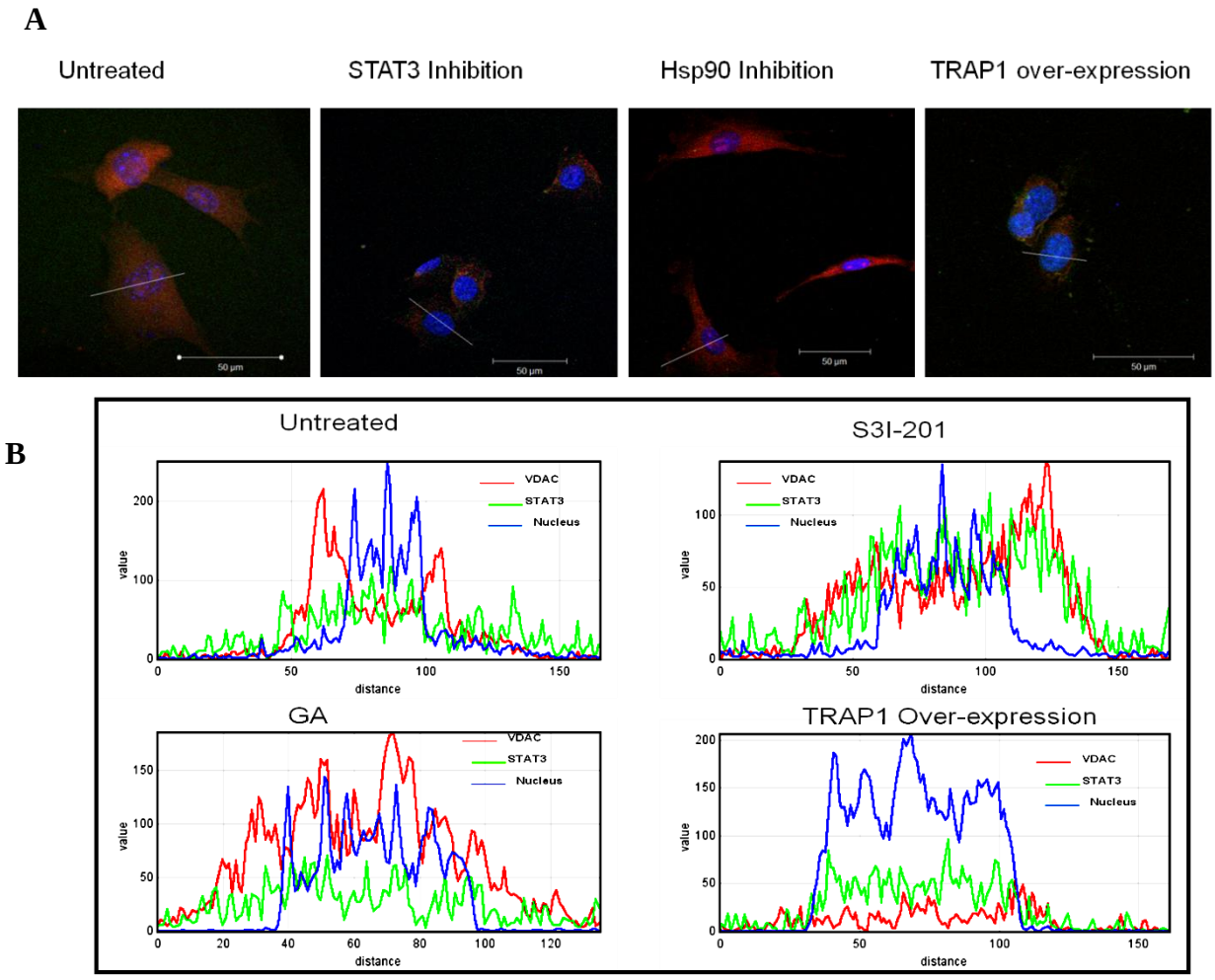

Figure 3.11: Fluorescence profiles of VDAC and STAT3 in treated 3T3L1 cells. (A)Images captured using a Zeiss LSM 510 confocal microscope was used to plot the profiles (B). The scale bar represents 50 µm. Distance shown on profile is in micrometers (µm).

3.3.8 Localization of Total STAT3, pSTAT3Y705, pSTAT3S727 and TRAP1 untreated murine 3T3L1 cells using western blotting analysis

Cell fractionation and separate western blotting of the same samples were done to determine in which sample fractions total STAT3, pSTAT3S72, pSTAT3Y705 and TRAP1 were located using VDAC, Actin and Histone as the mitochondrial, cytosolic and nuclear marker respectively. Total STAT3 was detected in total cell lysate and all three fractions; the plasma membrane and nuclei fraction, the cytoplasmic fraction and the mitochondrial fraction (Figure 3.12 total STAT3 panel). TRAP1 (Figure 3.12 TRAP1 panel), pSTAT3S727 (Figure 3.12 pSTAT3S727 panel) and

pSTAT3Y705 (Figure 3.12 pSTAT3Y705 panel) were also detected in all the cell fractions. In addition to STAT3 detection within the mitochondrial fraction, the membrane and nuclear fractions had reduced Actin (Figure 3.12 Actin, mitochondria panel) and VDAC (Figure 3.12 VDAC, PM + Nuclei panel) respectively indicating mitochondrial isolation and a fairly conclusive mitochondrial detection of STAT3.

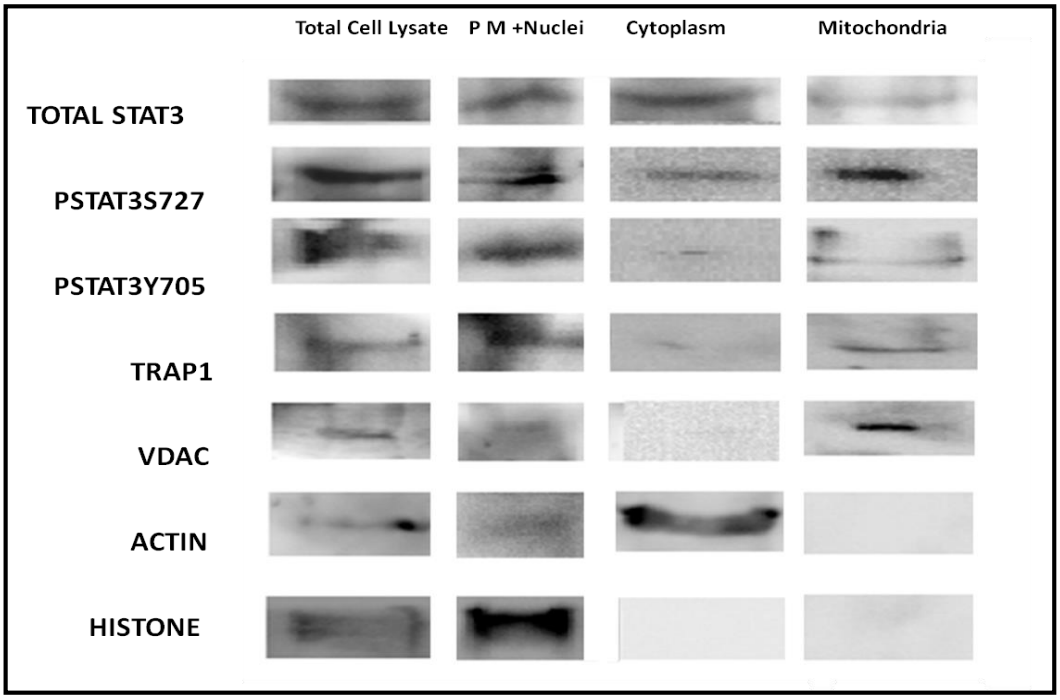

Figure 3.12: Detection of STAT3 in the mitochondria by western blot. Mitochondria isolations of murine 3T3L1 cells expressing STAT3 were prepared as described in Material and Methods section 3.2.2.3 starting with the same number of cells. Western blotting for total STAT3, pSTAT3S727, pSTAT3Y705, TRAP1, mitochondrial protein VDAC, cytosolic protein Actin and nuclear protein Histone were done.

3.3.9 Effect of S3I-201 and TRAP1 over-expression on Reactive oxygen species (ROS) in murine 3T3L1 pre-adipocyte cells

Both STAT3 and TRAP1 have been reported to reduce cellular ROS levels therefore inhibiting STAT3 would result in an increase in ROS levels and over-expressing TRAP1 would result in a reduction of ROS compared to untreated cells. Untreated cells stained with DCF-DA were used as a negative control to assess the effect of treatments on ROS. The 3T3L1 cells had two ROS populations as indicated by the two peaks on the DCF-DA histogram (Figure 3.13A untreated, ROS low and ROS high). Calculations of the ROS low or ROS high were made using the replicates. Analysis of ROS populations defined in untreated cells showed that the low ROS population

increased (Figure 3.13E STAT3 inhibition) from untreated (Figure 3.13B) to S3I-201 inhibited cells (Figure 3.13C) while the high ROS population did not appear to change (Figure 3.13E STAT3 inhibition). In comparison, cells that were over-expressing TRAP1 showed a reduction in both the low and high ROS populations (Figure 3.13D TRAP1 over-expression ROS low and ROS high; Figure 3.13F TRAP1 over-expression) suggesting that TRAP1 was being over-expressed.

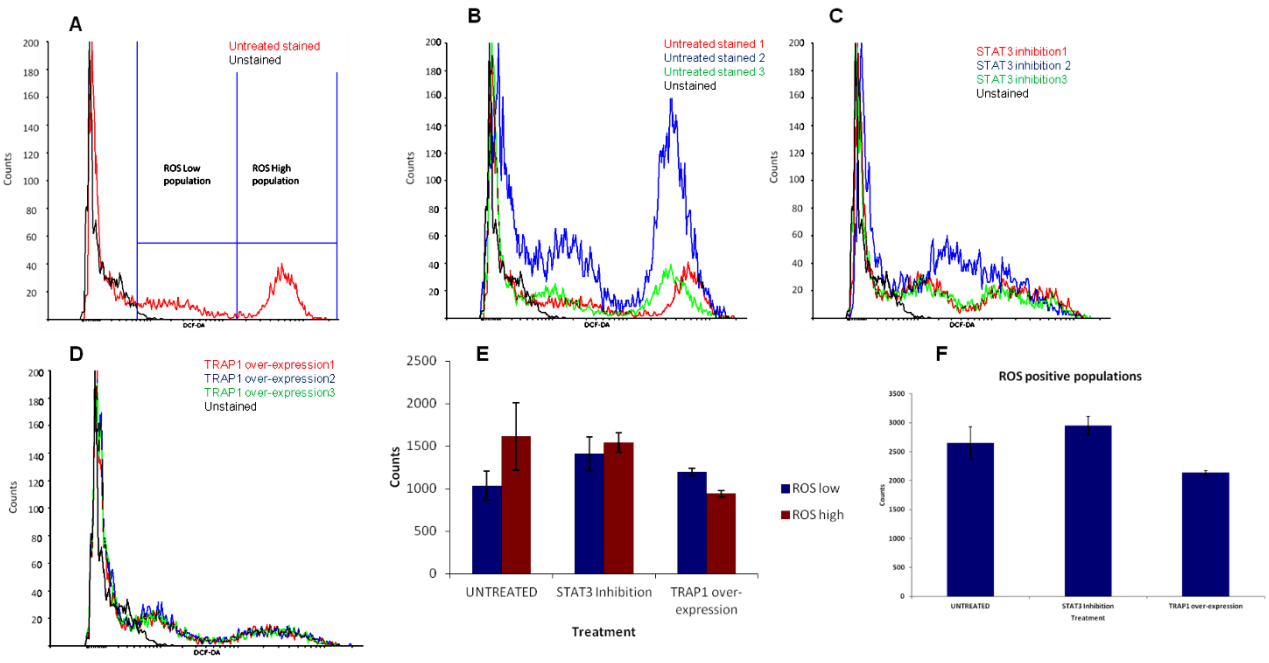

Figure 3.13: Changes in the ROS populations in 3T3L1 treated cells. The ROS populations(A) were defined using unstained and untreated cells as the negative controls (B), STAT3 inhibitor treatment(C) and in TRAP1 over-expression (D) treatment. The geometric means of populations (E) and the ROS positive populations (F) were calculated for the different treatments (n=3).

To assess whether the reduction in the ROS populations was due to a reduction in ROS positive events (H1 population), the percentage of the H1 population to total events, the arithmetic mean, geometric mean and coefficient of variance of the DCF-DA staining fluorescence were calculated from the three replicates (Figure 3.14). The average H1 population was 60.4 %, 62.7 % and 44.7 % of the total events in untreated 3T3L1 cells, in S3I-201 treated cells, in cells over-expressing TRAP1 respectively (Figure 3.14 H1 % of Total Events). The arithmetic and geometric means of the fluorescence were lower in S3I-201 treated cells and in cells over-expressing TRAP1 (Figure 3.14) indicating a reduction in cells with high ROS levels and a shift towards ROS low population.

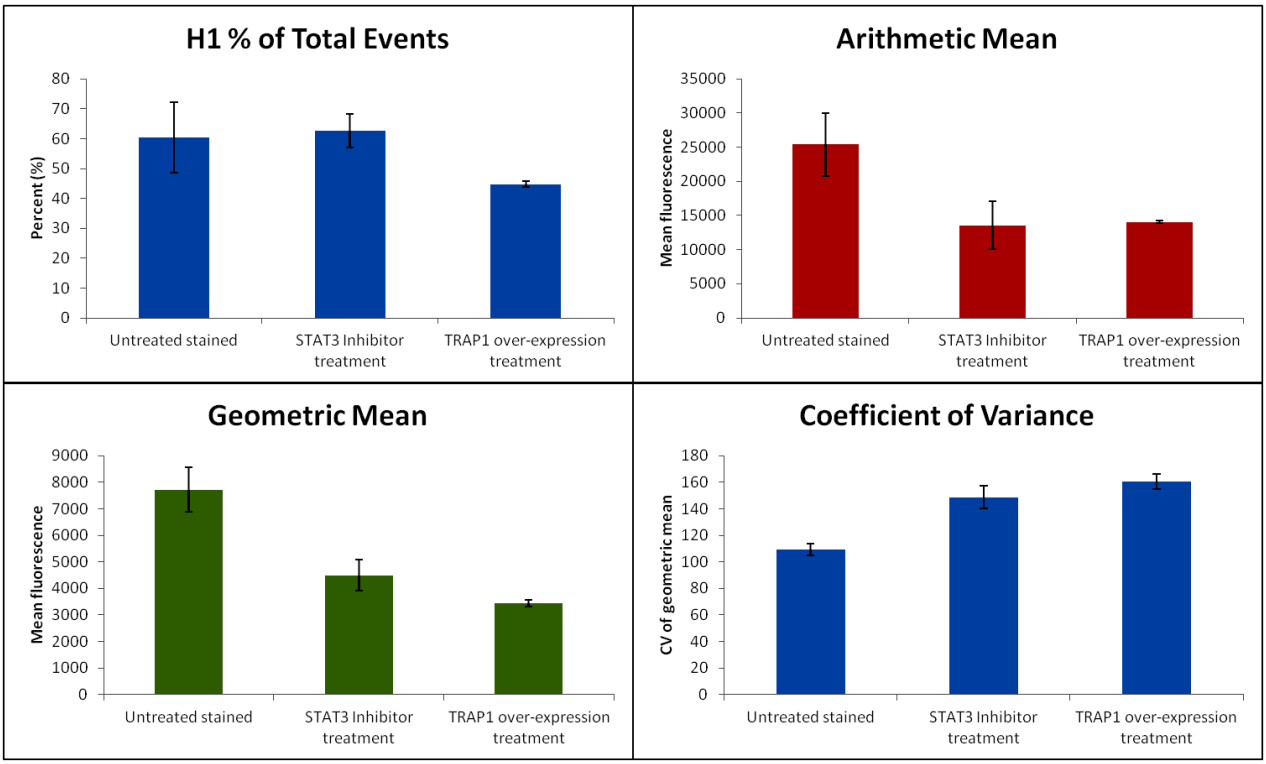

Figure 3.14: Statistical analysis of the H1 population in 3T3L1 cells. The H1 population is the ROS positive population and its percentage in total events was calculated for untreated cells used as the negative control, in STAT3 inhibitor treatment and in TRAP1 over-expression treatment. The arithmetic mean, geometric mean and coefficient of variance were plotted for the different treatments.

3.4 Discussion

Immunofluorescence microscopy was used to study the localization and the effect of either S3I-201 and geldanamycin inhibition or TRAP1 over-expression on the localization of STAT3. The results of this study indicated that STAT3 localized with VDAC (Section 3.3.4), and was detected in the mitochondrial fraction (Section 3.3.5), indicating its potential occurrence in the mitochondria. This observation is in contrast with another study that suggested that STAT3 does not translocate to the mitochondria in human Hep3B hepatocytes (Khan *et al*., 2013). In Khan *et al*. (2013)'s study, the GFP tag on STAT3 may have interfered with the translocation of STAT3 across the mitochondrial membrane. This study's results were therefore potentially consistent with other studies which showed that STAT3 localize within the mitochondria (Gough *et al*., 2009; Wegrzyn *et al*., 2009). These studies have suggested that STAT3 is important in the mitochondria where it both increases the activity of Complex II of the electron transport chain and reduces mitochondrial ROS production (Wegrzyn *et al*., 2009; Shulga and Pastorino, 2012). Furthermore, these studies have suggested that STAT3's translocation to the mitochondria does not require either the DNA binding domain or the phosphorylation of Tyrosine 705, which has been observed as essential for its translocation to the nucleus (Prinsloo *et al*., 2012). Nevertheless, translocation of STAT3 to the mitochondria has been reported to require the phosphorylation of Serine 727 hence one would expect an increase in mitochondrial pSTAT3727 when the levels of its transport machinery was increased (Wegrzyn *et al*., 2009).

Although there are no established STAT3 chaperones for its mitochondrial translocation, molecular chaperones, such as Hsp60, Hsp70 and TRAP1 that occur in the mitochondria, may be involved in such a transfer. These chaperones have been shown to facilitate the translocation of proteins to the mitochondria (Jäättelä, 1999; Liu and Butow, 2006). Hsp90 β has been reported to chaperone STAT3 from the cytoplasm to the nucleus (Prinsloo *et al*., 2012). In this study, over-expression of TRAP1, which is the mitochondria Hsp90 isoform, was found potentially to increase pSTAT3S727 in the nucleus, whereas pSTAT3Y705 had distinct punctate cytoplasm localization that appeared co-localize with VDAC (Section 3.3.4) to support the hypothesis of this study that increasing TRAP1 levels would concurrently increase mitochondrial STAT3. Over-expressed TRAP1 also mis-localizes to the nucleus. Overall, the fluorescence microscopy results therefore strongly suggest that TRAP1 does in fact mediate STAT localization under TRAP1 over-

expression conditions. TRAP1 can therefore potentially also mediate mitochondrial import of STAT3 under normal (non over-expression) conditions.

This study showed that S3I-201's inhibition of the SH2 domain (phosphorylation) and DNA binding potentially reduced cytoplasmic localized pSTAT3Y705 and pSTAT3S727 (Section 3.3.4.3),. Furthermore, this inhibition also appeared to potentially reduce nuclear localized pSTAT3Y705 more than pSTAT3S727 (Section 3.3.4.4), which is the other transactivated Serine 727. Both treated and untreated cells showed cytoplasmic punctuate-staining that indicated potential co-localization of STAT3 and VDAC. This suggests that the inhibitor possibly had less effect on the phosphorylation pathway of Serine 727. Although Tyrosine 705 and Serine 727 have been reported to share similar phosphorylation pathways (Darnell *et al*., 1994), some studies have nonetheless suggested that Serine 727 utilises alternative phosphorylation pathways (Chung *et al*., 1997). These alternative pathways include the MEK pathway that has been shown to phosphorylate Serine 727 (Chung *et al*., 1997). It is therefore likely that inhibiting the SH2 domain by S3I-201, which interferes with the protein-protein interaction domain of STAT3 (Siddiquee *et al.*, 2007), does not appear to have an influence some on the kinases that phosphorylate Serine 727.

STAT3 over-expression is known to inhibit ROS production (Demaria *et al*., 2010; Shin *et al*., 2011). It was assumed that inhibiting STAT3 would increase cellular ROS levels. The results of this study were inconsistent with this observation because they showed that when STAT3 was inhibited, the levels of ROS decreased even though the size of the ROS positive population increased. This therefore suggests a direct role of STAT3 in regulating ROS production, to promote cell survival. Because high ROS levels are associated with dysfunction of cellular processes, including depolarization of the mitochondrial membrane, protein and DNA damage, which ultimately leads to cell death (McBride *et al*., 2006), it is imperative to conduct further studies to determine viability of inhibitor-treated cells for both low and high ROS populations.

TRAP1 has been shown to both inhibit ROS production and protect cells from ROS-induced damage (Kang *et al*., 2007; Montesano *et al*., 2007). The results of this study were consistent with this observation because TRAP1 over-expression was found to increase the low-ROS population, whereas the high-ROS population decreased and overall decreased the size of the ROS positive population. Similar to STAT3, TRAP1 is fundamental in regulating ROS production (Montesano *et al*., 2007). TRAP1 has been found to regulate the metabolic switch from oxidative

phosphorylation, which is associated with ROS production, to aerobic glycolysis (Yoshida *et al*., 2013). Furthermore, TRAP1 plays an important role in improving cell viability under high ROS level by inhibiting ROS-induced apoptosis (Hua *et al*., 2007).

To conclude, this study showed the possibility of a co-occurence of STAT3 with a mitochondrial protein TRAP1, suggesting its mitochondrial localization and a role in ROS regulation. Furthermore, this study also showed a potential role TRAP1 in chaperoning STAT3 to the mitochondria and to the nucleus, which suggests that it could be involved in STAT3 localization and function. Inhibiting STAT3 appeared to have no effect on Serine 727's phosphorylation nuclear accumulation, which suggests the likelihood of alternative phosphorylation pathways, such as serine specific kinases. This therefore suggests that the inhibitor S3I-201 is more specific for tyrosine 705 phosphorylation of STAT3 compared to serine 727. Furthermore, this study showed that both STAT3 and TRAP1 are important inhibitors to ROS production. Therefore, studies on the interactions between STAT3 and TRAP1 are essential.

CHAPTER 4

Investigating the *ex vivo* and *in vitro* interaction between TRAP1 and STAT3

4.1 Introduction

Hsp90 has been reported to interact with STAT3 (Shah *et al.*, 2002; Sato *et al*., 2003; Schoof *et al*., 2009; Prinsloo *et al.*, 2012). Studies on co-localization, co-immunoprecipitation, inhibition assays and biophysical analysis have shown the direct interaction of Hsp90 β and STAT3 in mouse embryonic stem cells and in human Hep3B hepatocytes (Shah *et al.*, 2002; Sato *et al*., 2003; Prinsloo *et al.*, 2012). These studies indicate that the interaction between Hsp90 and STAT3 required the STAT3 DNA binding domain (Sato *et al*., 2003), leukemia inhibitory factor (LIF) stimulation of the JAK/STAT3 pathway (Setati *et al*., 2010), the Hsp90 N-terminal domain and ATP hydrolysis (Schoof *et al*., 2009; Prinsloo *et al.*, 2012). However, the functions of Hsp90 domains had been reported to be cooperative and required its N-terminal domain (Obermann *et al*., 1998).

The translocation of STAT3 to the mitochondria has been reported not to require a DNA binding domain and phosphorylation of Tyrosine 705 (Wegrzyn *et al*., 2009). Nevertheless, studies have shown that TRAP1 may be involved in other functions, including stabilizing phosphorylated STAT3 (Kubota *et al*., 2009). In addition, the previous study (Chapter 3) has shown that these two proteins were involved in regulating ROS production. This therefore suggests a likelihood of their interaction. Little is known about these interactions within the mitochondria.

While fluorescence microscopy can be used to analyze the co-localization of proteins in a cell, co-immunoprecipitation can used to determine if proteins co-occur in common biomolecular complexes. Biophysical analysis such as Surface Plasmon Resonance spectroscopy (SPR) can be employed to assess the direct interaction plus the kinetics of the interaction between two molecules.

4.1.1 Specific Objective

1. To determine if TRAP1 and STAT3 co-localize in the mammalian cells.
2. To determine if TRAP1 and STAT3 occur within the same molecular complex in the mammalian cells.
3. To determine if TRAP1 and STAT3 interact directly *in vitro*.

4.2 Methods

4.2.1 Co-localization analysis of TRAP1 and STAT3

The 3T3L1 cells were stained for immunofluorescence microscopy as described in Chapter 3. MCF7 cells that were grown on microscope cover-slips were fixed in ice-cold methanol, air-dried and blocked with 5 % (w/v) bovine serum albumin in Tris-buffered saline (BSA/TBS) at room temperature. This was followed by incubating the cells with primary antibodies in BSA/TBS at 4 ˚C overnight. Cover slips were washed twice with 1 % (w/v) BSA/TBS and incubated with the appropriate secondary antibodies at room temperature for 1 hr in the dark. The cells were washed twice with PBS for 5 minutes at room temperature (RT) followed by nuclear counterstaining with Hoechst 33342 at a 1:1000 dilution in water for 90 seconds at RT before mounting with Dulbecco's mounting media. Immunofluorescence was captured using a Zeiss LSM 510 Meta Confocal microscope with × 63 oil objective. Co-localization analysis was performed using MacBiophotonics ImageJ co-localization Analysis software. The results of these analyses were presented by Pearson's correlation coefficients (Rr), Manders coefficient (R), and the intensity correlation coefficient (ICQ). Pearson's correlation coefficients (Rr) of -1, 0, and +1 reflected negative co-localization, no co-localization and complete co-localization, respectively. The R values of 0.5 represents 50 % overlap between the pixels in each image (Manders *et al*., 1993; Zinchuk *et al*., 2007) and R values from 0.6 to 1 indicates co-localization (Bolte & Cordelières, 2006). Therefore, two proteins were considered to be co-localized when both their Rr and R were between 0.5 and 1 (Bolte & Cordelières, 2006). Two proteins were considered to be in synchrony when their ICQ was between 0 and 0.5. The intensity of protein fluorescence was represented by channel 1 to channel 2 ratios (Ch1: Ch2).

4.2.2 Co-immunoprecipitation assay

Cell lysate preparation of 3T3L1 cells was conducted as described in Chapter 3.

4.2.2.1 Immunoprecipitation

Lysate aliquots (100 µl) of 1-5 × 10^6 cells were transferred to 2 separate 1.5 ml micro centrifuge tubes. The remaining residual volume was aliquoted (10 µl) and stored at -20 °C to be used as the positive control. A pre-clearing step was performed during which 20 µl of protein A/G PLUS-agarose immunoprecipitation reagent (Santa Cruz Biotechnologies, USA) was added to the lysates

and the resultant slurries were incubated for 1 hr on a rotating shaker at 180-200 rpm at 4°C. Centrifugation at 1000 *g* for 5 minutes was performed, and the supernatants were transferred to a new 1.5 ml micro centrifuge tube. Primary antibody (4 µg of anti- TRAP1) (Appendix Table A1), were added to the test sample and incubated for 2 hrs at 4 °C on a rotating shaker at 180-200 rpm. After incubation, protein A/G PLUS agarose immunoprecipitation beads (40 µl) was added to the sample and incubation was continued overnight on ice on a rocking platform at 180-200 rpm. The control samples included lysate that was subjected to immunoprecipitation without antibody, and protein A/G PLUS-agarose and antibody, without lysate. In each case, the volumes were kept constant by adding the lysis buffer used in lysate preparation.

Following overnight incubation, the complexes were centrifuged at 1000 *g* for 5 minutes at 4 °C, and the pellet washed 4 times with TBS Ph 7.4, repeating the centrifugation steps. The final pellet was re-suspended in 50µl of 5 × SDS sample loading buffer and the sample was boiled for 10 minutes. After boiling, 20 µl of the sample was resolved by 12 % acryl amide SDS-PAGE following Laemmli (1970)'s procedure for Western blot analysis as described in Chapter 3.

4.2.3 Expression and purification of recombinant STAT3

The pET32b-STAT3b-tc bacterial expression construct expressing mouse STAT3 *β* was a kind donation from Dr Christoph Muller (European Molecular Biology Laboratory Heidelberg). STAT3 *β* was expressed and purified following Becker *et al.* (1998)'s procedure. Competent *Escherichia coli (E. coli)* BL21 DE3 (Gold) cells were transformed with a STAT3 *β* construct using a heat shock pulse at 42 °C. *Escherichia coli* BL21 DE3 (Gold) cells (20 µl) that were transformed with pET32-STAT3-tc vector were added to 50 ml of Luria Bertani (LB) broth (10g Trypton, 10g NaCl, 5g Yeast extract in 1 liter double distilled water) containing 200µg/ml amplicillin. The inoculations were cultured overnight as the starter culture at 37 °C with shaking at 180 rpm. From the starter culture, 20 ml were inoculated into 1 L of LB broth with 200µg/ml ampicillin and cultured at 37°C with shaking at 180 rpm until the optical density at 600 nm (OD_{600}) reached 0.3. The culture temperature was then changed to 20°C and cultures grown with shaking at 180 rpm until OD_{600} reached between 0.6-0.7.

STAT3 expression was induced with 1mM IPTG for 5 hours at 20°C and 1 ml samples were collected hourly at 0, 1, 2, 3, 4, 5 hours of induction. After 5 hours of induction, cells were harvested by centrifugation at 1×10^4 rpm for 10 minutes at 4 °C and re-suspended in ice cold

extraction buffer (20mM HEPES-HCl, pH 7.6, 0.1 M KCl, 10 % (v/v) Glycerol, 1 mM EDTA, 10 mM $MnCl_2$, and 0.5 mM PMSF) at a dilution of 10 ml/g of cells pellet. Cells were lysed with 0.5-2 µg/ml lysozyme at 37°C with shaking at 180 rpm for 1 hour and sonicated (6 × 1 minute pulses at 50% power). Cell lysate was clarified by centrifugation at 27000*g* for 45 minutes at 4 °C. Supernatants were treated with 0.1% (v/v) polyethylimine (incubated on ice for 15 minutes with gentle shaking) and further centrifuged at 27000*g* for 20 minutes at 4 °C to remove nucleic acids. To supernatant, 35% (w/v) powdered ammonium sulphate, calculated using software available online at http://www.encorbio.com/protocols/AM-SO4.htm, was added to precipitate soluble protein (Encor Biotechnology Inc.). The precipitate was then centrifuged at 27000*g* (4°C) for 20 minutes. Protein precipitate was re-dissolved in 5 ml dialysis buffer (20mM HEPES-HCl, pH 7.0, 200 mM NaCl, 10 mM $MgCl_2$, 10 mM $MnCl_2$, 0.5 mM PMSF) and dialyzed against 2 changes (2 hours each) of dialysis buffer at a ratio of 1:100 followed by a final exchange at 4°C overnight. STAT3 protein was further purified to homogeneity by gel filtration chromatography using Sephacryl S-200 HR resin in a 16/60 column housing on a ÄKTA (BASIC) FPLC system (Amersham Pharmacia Biotech, UK; GE Healthcare, Life Sciences) system at 1ml/min. Fractions were collected, analyzed by 12% SDS-PAGE and concentrated by Amicon^R Ultra Ultracel^R (10K) Centrifugal Filters (Millipore, Ireland) into 10 mM HEPES, pH 7.4, 150 mM NaCl. Protein was quantified using the NanoDrop 2000 at 280 nm (Thermo Scientific). Hourly samples were treated as follows; 1 ml samples were centrifuged at 1.3×10^4 rpm for 10 minutes at 4 °C, re-suspended in $(OD_{600}Sample/0.5\times150)$ µl of PBS, boiled in 1 × SDS sample buffer for 10 minutes and resolved by SDS-PAGE on a 12 % acryl amide gel. Hourly samples were then analyzed by SDS-PAGE (Laemmli, 1970) and western blot analysis (Towbin *et al*., 1979). The presence of STAT3 was determined by western blot analysis using rabbit polyclonal anti-STAT3 primary antibody (1:500 dilution) and HRP-conjugated anti-rabbit IgG antibodies (1:1000 dilution). Chemiluminescence-based protein detection was achieved using the Clarity^{TM} western ECL substrate (BioRad, USA) in UVIproChemi^{TM} (UVItec, UK).

4.2.4 Expression and purification of recombinant TRAP1 protein

The plasmid construct pQE2-TRAP1 (TRAP1-$(His)_6$) (Michelle Parsons, Department of Biochemistry, Microbiology and Biotechnology, Rhodes University), was transformed into *E. coli* XLI Blue expression cells. The cells were spread onto LB agar plates containing 100 µg/ml

ampicillin and 100 µg/ml kanamycin to select for successfully transformed cells, followed by incubating at 37ºC for approximately 16 hours to select successful transformations. Starter cultures were prepared by inoculating a single colony of each transformation into 5 ml LB broth containing 100 µg/ml of ampicillin and incubated overnight at 37ºC. The starter culture was inoculated into 50 ml fresh LB with 100 µg/ml ampicillin, grown at 37ºC until an OD_{600} of 0.4 to 0.45 was reached before inducing TRAP1 expression for 2 hours with 1 mM IPTG and 1 ml samples were collected hourly at 0, 1, 2 hours of induction.

After 2 hours of induction, cells were harvested by centrifuging at 1×10^4 rpm for 10 minutes at 4 °C and re-suspended in ice cold extraction buffer (20mM HEPES-HCl, pH 7.6, 0.1 M KCl, 10 % (v/v) Glycerol, 1 mM EDTA, 10 mM $MnCl_2$, and 0.5 mM PMSF) at a dilution of 10 ml/g of cells pellet. Cells were lysed with 0.5-2 µg/ml lysozyme at 37°C with shaking at 180 rpm for 1 hour and sonicated (6 × 1 minute pulses at 50 % power). Cell lysate was clarified by centrifuging at 27000*g* for 45 minutes at 4 °C. His-tagged TRAP1 was purified using the His-Spin Protein Miniprep™ kit (ZYMO RESEARCH). Hourly samples were analyzed by SDS-PAGE (Laemmli, 1970) and western blot analysis (Towbin *et al.*, 1979). The presence of TRAP1-$(His)_6$ was determined by western blot analysis using mouse monoclonal anti-His primary antibody (1:500 dilution), HRP-conjugated anti-mouse IgG antibodies (1:1000 dilution). Protein detection was chemiluminescence-based through the use of ClarityTM western ECL substrate (BioRad, USA) in UVIproChemiTM (UVItec, UK).

4.2.5 The *in vitro* analysis of TRAP1/STAT3 interaction using Surface Plasmon Resonance (SPR) spectroscopy

Surface Plasmon resonance spectroscopy is a label-free detection technique that relies on the use of a metallic film sensing surface that reflects light under specific conditions giving rise to a particular electron oscillation phenomenon within that medium referred to as the refractive index. Molecular adsorption or desorption events are therefore measured as changes in the refractive index and SPR can distinguish between surface-bound molecules and unbound material, monitor molecular interactions in real time and are highly sensitive (Englebienne *et al.*, 2003). SPR was performed using a ProteOn™XPR36 instrument (BioRad, USA) on a HTGICB117O1 nickel affinity chip pre-conditioned with vertical and horizontal injections of regeneration buffers (0.5 % SDS, 50 mM NaOH, 100 mM HCl and 300 mM EDTA, pH 8.5), at 30 µl/minute. The poly HIS binding groups on the sensor chip surface was first activated with 250 mM nickel sulphate. SPR

running buffer (40 mM HEPES, pH 7.4; 150 mM KCl; 5 mM $MgCl_2$) was used as the blank solution. Flow cells were activated by 60 µl vertical injections of 250 mM nickel sulphate at 30 µl/minute for 2 minutes. TRAP1 (1 × dilution Flow Through; 10 × dilution Flow Through; 20 × dilution Flow Through; blank solution; 1 × dilution Wash 1; 10 × dilution Wash 1) was then immobilized on the chip as the ligand by 150 µl vertical injections at 30 µl/minute for 5 minutes. Unbound proteins were washed off by 30 µl horizontal injections of SPR running buffer for 60 seconds. This was followed by 50 µl injections of the analyte STAT3 (1 µM; 0.5 µM; 0.25 µM; 0.125 µM; 0.06 µM; 0.03 µM) at 50 µl/minute for 60 seconds in the presence or absence of ATP (1 mM) to determine if STAT3 would associate with the immobilized ligand TRAP1. The dissociation of the ligand analyte complex was achieved by injecting 50 µl of 1 M NaCl at 50 µl/minute for 300 seconds. The surface of the chip was then regenerated by 30 µl injection of 1 mM NaCl for 300 seconds. For an ATP control, 1 mM ATP in SPR running buffer was injected as the analyte at 50 µl/minute for 60 seconds to determine if ATP alone would associate with the immobilized ligand (TRAP1). The TRAP1/STAT3 interaction data was corrected by subtracting the data of the ATP analyte and/or that of the blanking solution (SPR running buffer).The STAT3/TRAP1 interaction study was done in triplicate.

4.3 Results

4.3.1 Co-localization analysis of TRAP1 and STAT3

Analysis of fluorescence signals in an image to determine their co-localization i.e. if two or more different molecules are present in close spatial position in a sample, was employed to quantitatively assess the possibility of the co-occurrence of TRAP1 and STAT3 in mouse 3T3L1 and human MCF7 cells. Although the staining of 3T3L1 cells was sufficient for epi-fluorescence microscopy localization study (Section 3.3), the quality of the confocal microscopy images were of insufficient fluorescence intensity for co-localization analysis of TRAP1 and STAT3 (Section 3.3). Nonetheless, MCF7 cells staining were therefore used since TRAP1 and STAT3 proteins are highly conserved between the two species (Chapter 2). Images of MCF7 cells that were stained for Hsp90 α/β, TRAP1, total STAT3, pSTAT3S727 and pSTAT3Y705 were analyzed for co-localization using the co-staining of Hsp90 α/β (Figure 4.3 Hsp90 α/β panel) with pSTAT3Y705 (Figure 4.1A pSTAT3Y705, STAT3 panel) as a positive control. For two proteins to be considered to be co-localizing, both their Rr and R should be between 0.5 and 1 (Bolte & Cordelières, 2006). The ICQ

value gives an indication of how the two proteins' localization varies in comparison to one another and for the localization to be considered to be in synchrony their ICQ value should be between 0 and 0.5. Ch1: Ch2 gives an indication of the linearity of the fluorescence intensity of the proteins.

Using indirect immunofluorescence and confocal microscopy, Hsp90 α/β was found to be localized mainly in the cytoplasm in all of the MCF7 cells, although apparent weak nuclear localization was also identified (Figure 4.1A Hsp90 α/β panel). On the other hand, pSTAT3Y705 was found to be mostly localized in the nucleus in all of the cells, with some cytoplasmic localization ((Figure 4.1A pSTAT3Y705 panel). The staining profiles for HSP90α/β and pSTAT3Y705 were dissimilar (Figure 4.1B), with HSP90α/β proteins having peak intensities outside the nucleus, in the cytoplasmic region while pSTAT3Y705 had peak intensity in the nucleus. Immunofluorescence and confocal microscopy also suggested that HSP90α/β was situated in a similar location within the cell as pSTAT3Y705 (Figure 4.1 Merged).

Quantitative analysis of the immunofluorescence signals gave a Pearson's correlation coefficient (Rr) of 0.727 (±0.038) and Mander's overlap coefficient (R) of 0.852 (±0.003), suggesting co-localization of HSP90α/β and pSTAT3Y705. Furthermore, the intensity correlation coefficient (ICQ) of 0.397 (±0.023) values indicated that the signals varied in synchrony. . The Ch1:Ch2 ratio was found to be 0.997 (Table 4.1) indicating that expression levels of the proteins were fairly similar. Furthermore, the intensity profiles of Hsp90 α/β and pSTAT3Y705 (Figure 4.1B) showed that nearly all of the immunolocalized pSTAT3Y705 appears to occur in compartments associated with Hsp90 α/β.

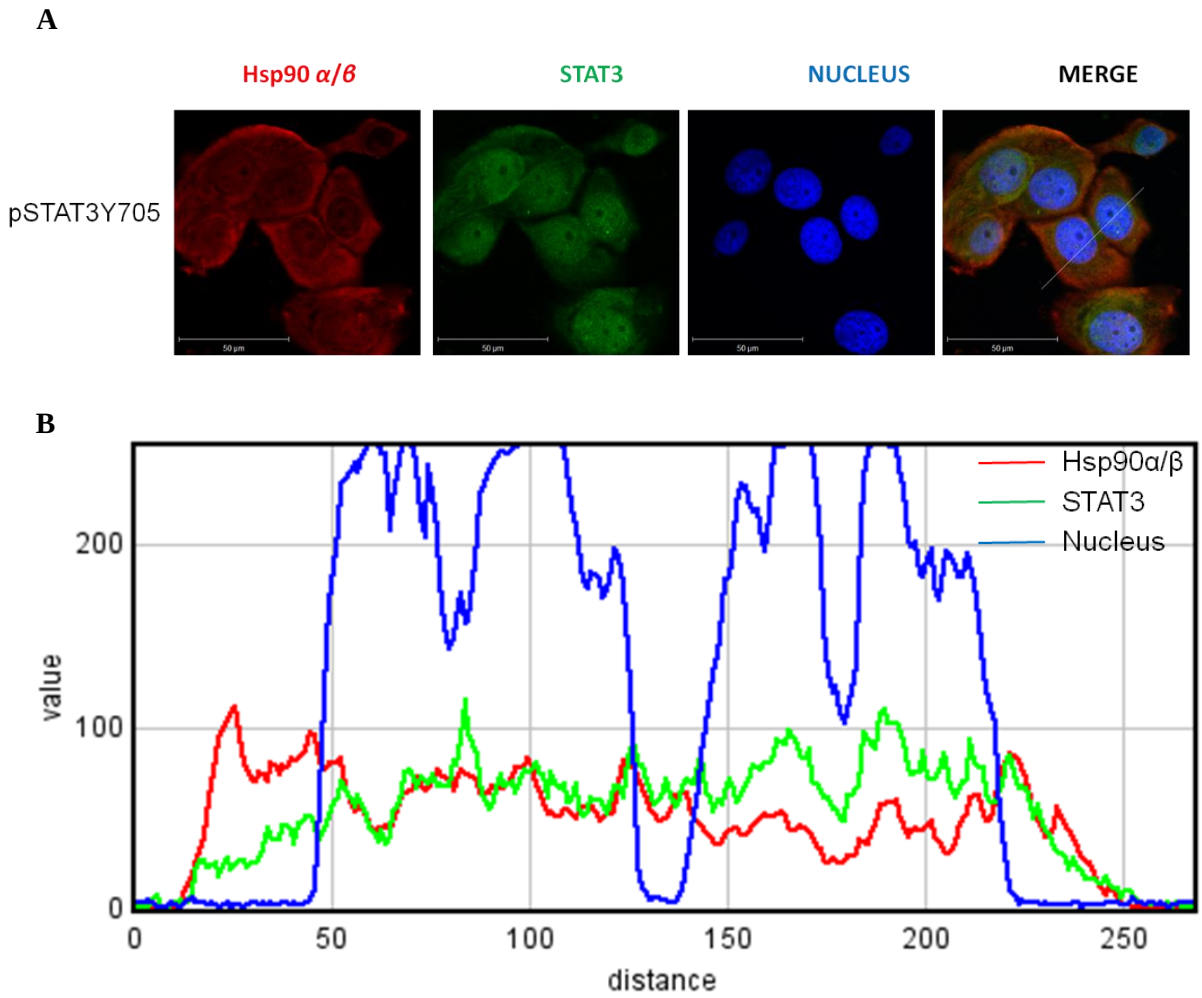

Figure 4.1: Hsp90 *α/β* and pSTAT3Y705 co-localize. Confocal microscopy images of MCF7 cells captured using a Zeiss LSM 510 Confocal Laser scanning microscope at 63× magnification. Scale bars represent 50 µm. Line Profiles were obtained using the program Zeiss LSM Image Browser. White line represents cross section of cell used for intensity line profile. The distance shown on profile is in µm.

TRAP1 and total STAT3 were found to co-localize, with Rr, R and ICQ values of 0.557 (±0.03), 0.638 (±0.018) and 0.264 (±0.027), respectively (Table 4.1). Nevertheless, the co-localization potential was lower than that of the positive control (Table 4.1 Hsp90 *α*/β/pSTAT3Y705 row), indicating that the probability of finding TRAP1 and total STAT3 in the same molecular complex region is lower than that of Hsp90 *α*/β and pSTAT3Y705. The Ch1:Ch2 of TRAP1 and total STAT3 was lower, showing that the expression levels of the two proteins were not the same as highlighted by the fluorescence microscopy images (Figure 4.2A) and the profile plots (Figure 4.2B). Furthermore, although TRAP1 and total STAT3 co-localize, the intensity

profiles showed that the signals were not proportionally co-distributed and would yield unreliable Rr values hence the R values were used to determine co-localization as their calculations are independent of signal proportionality (Dunn *et al.*, 2011). TRAP1 and pSTAT3Y705 co-localized and shared similar predominant perinuclear localization areas as shown by the ICQ value closest to 0.5 (Table 4.1), the fluorescence microscopy images (Figure 4.3A) and the profile plots (Figure 4.3B). Nonetheless, TRAP1 and pSTAT3S727 co-localized although their ICQ was the lowest (Table 4.1). This showed that although the proteins co-localized, they had different predominant localization areas as shown by the fluorescence microscopy images (Figure 4.4A) and the profile plots (Figure 4.4B).

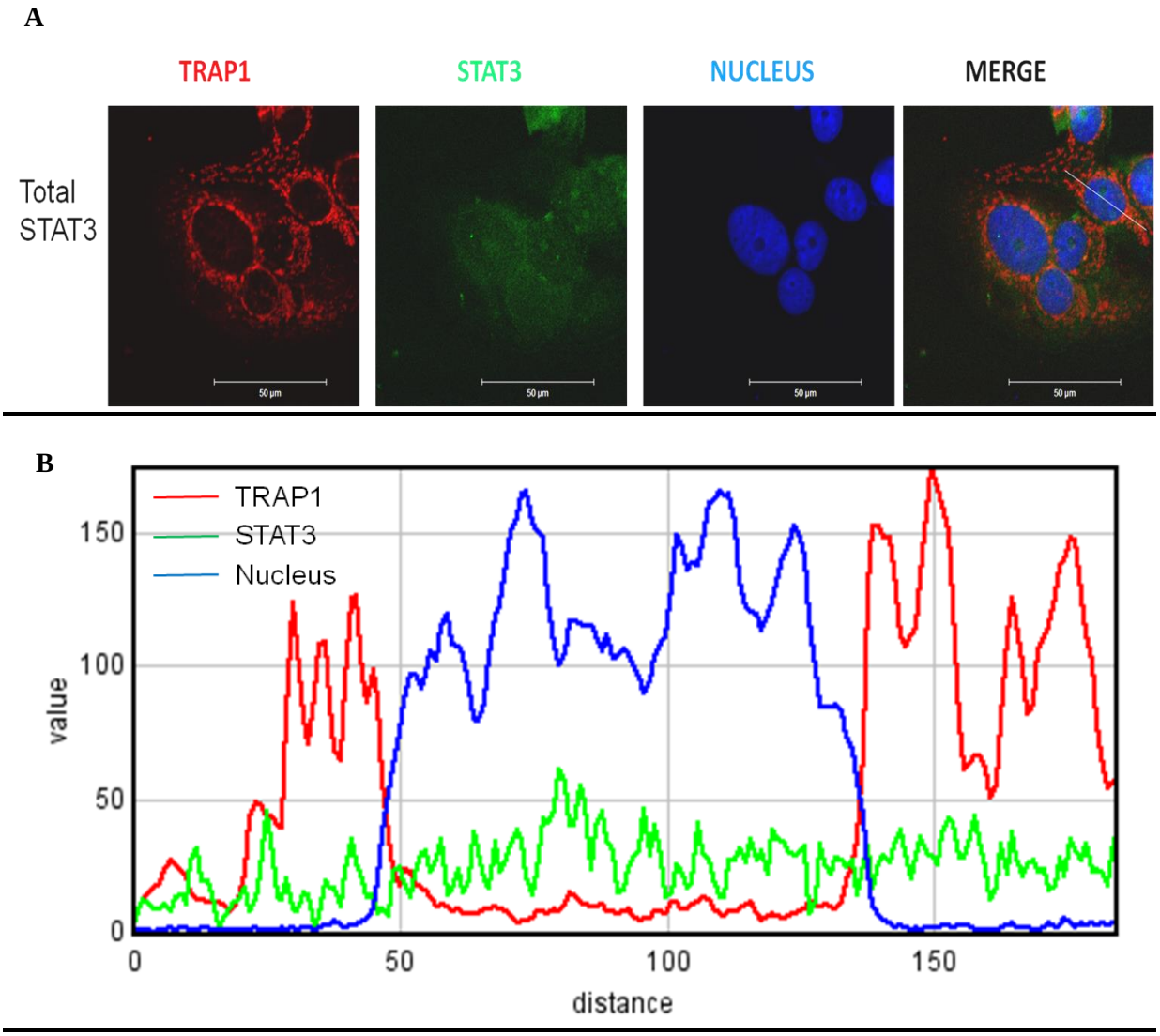

Figure 4.2 TRAP1 and Total STAT3 localization. A. Confocal microscopy images of MCF7 cells captured using a Zeiss LSM 510 Confocal Laser scanning microscope at 63× magnification. Scale bars represent 50 µm. B. Line Profiles were obtained using the program Zeiss LSM Image Browser. White line represents cross section of cell used for intensity line profile. The distance shown on profile is in µm.

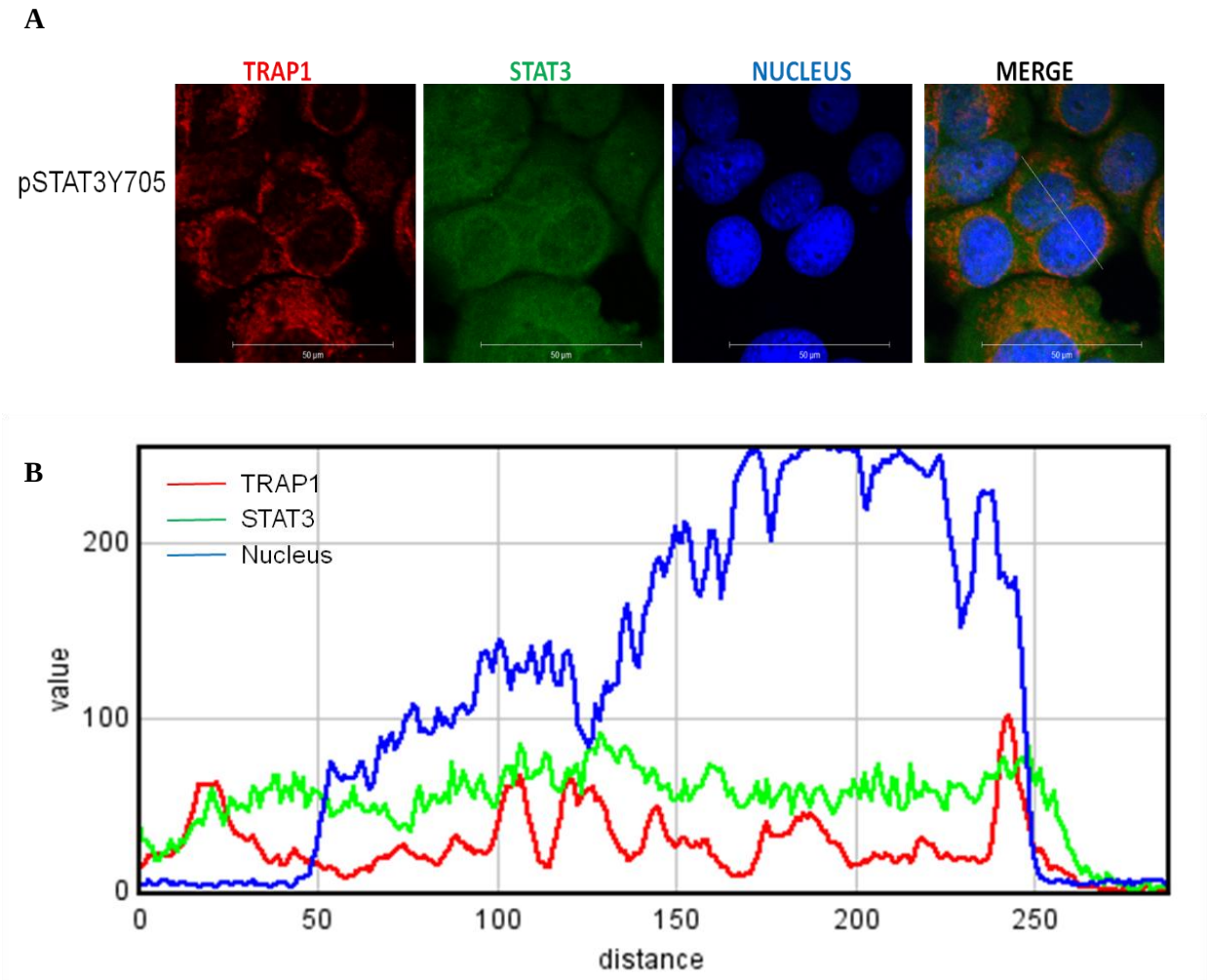

Figure 4.3: TRAP1 and pSTAT3Y705 co-localize. A. Confocal microscopy images of MCF7 cells captured using a Zeiss LSM 510 Confocal Laser scanning microscope at 63× magnification. Scale bars represent 50 µm. B. Line Profiles were obtained using the program Zeiss LSM Image Browser. White line represents cross section of cell used for intensity line profile. The distance shown on profile is in µm.

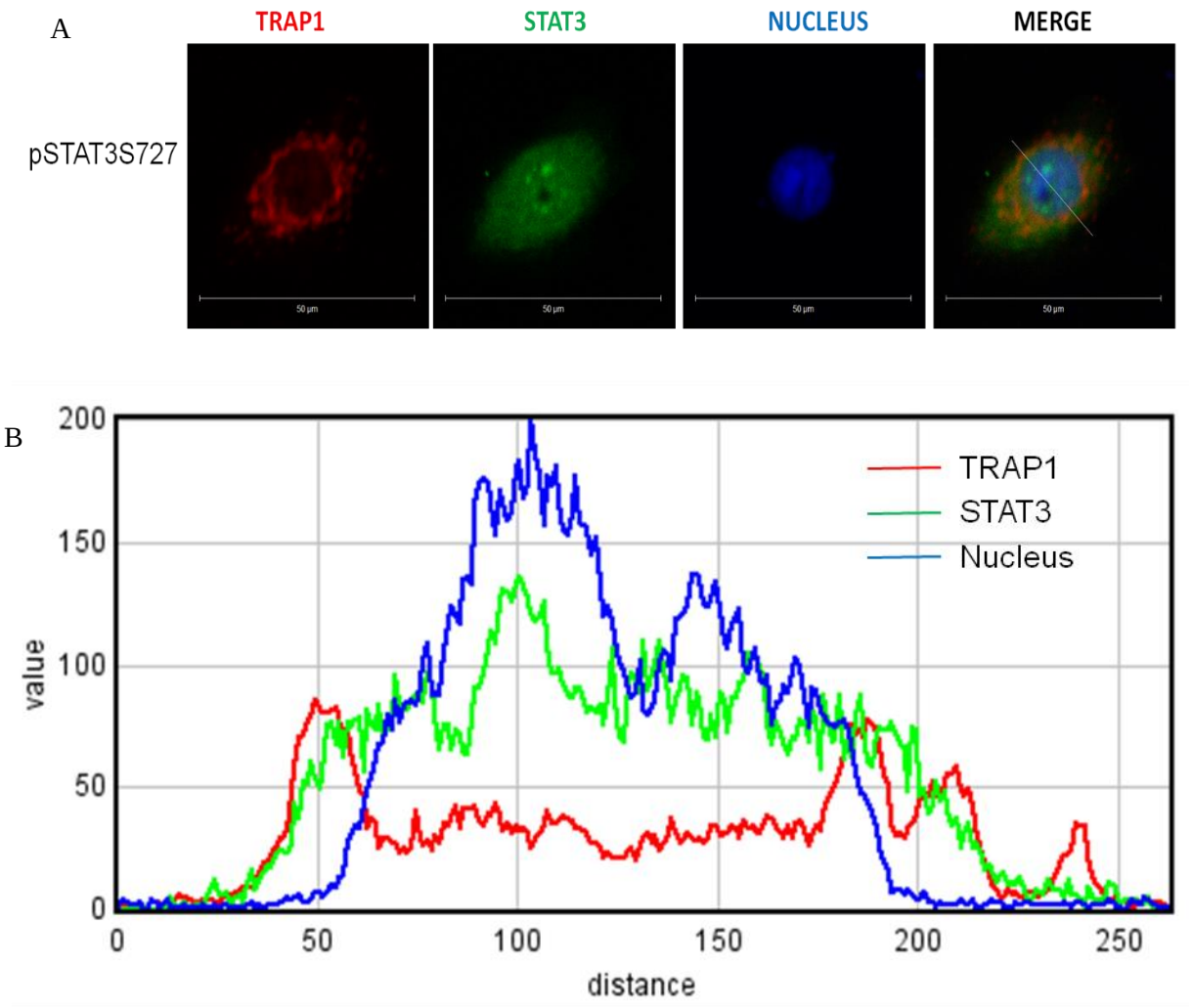

Figure 4.4: TRAP1 and pSTAT3S727 co-localize. A. Confocal microscopy images of MCF7 cells captured using a Zeiss LSM 510 Confocal Laser scanning microscope at 63× magnification. Scale bars represent 50 µm. B. Line Profiles were obtained using the program Zeiss LSM Image Browser. White line represents cross section of cell used for intensity line profile. The distance shown on profile is in µm.

Table 4.1: Co-localization analysis using MacBiophotonics-ImageJ of Confocal images of MCF7 cells (n=3).

Image	Average Pearson's Correlation Coefficient (Rr)	Average Manders' Overlap Coefficient (R)	Intensity correlation quotient (ICQ)	Ch1:Ch2
Hsp90αβ-pStat3-Y705	0.727+/-0.038	0.852+/-0.003	0.397+/-0.023	0.997
TRAP1-Stat3	0.557+/-0.03	0.638+/-0.018	0.264+/-0.027	0.88
TRAP1-pStat3-S727	0.617+/-0.081	0.724+/-0.037	0.176+/-0.056	0.992
TRAP1-pStat3-Y705	0.770+/-0.097	0.788+/-0.053	0.455+/-0.074	0.997

4.3.2 Co-immunoprecipitation TRAP1 by STAT3

Co-immunoprecipitation assays were done the TRAP1 antibody to determine if TRAP1 and STAT3 occurred within the same biological complex. Immunoprecipitates were then tested for TRAP1, total STAT3 and STAT3 phosphorylated at tyrosine 705 (and pSTAT3Y705). No band was detected in the positive control (Figure 4.5 lane 2), two bands estimated to correspond to the heavy and light chain antibody were detected in the no lysate negative control (Figure 4.5 lane 3), no bands were detected in the no antibody negative control (Figure 4.5 lane 4) and four bands were detected for the immunoprecipitation (Figure 4.5 lane 5) western blot. Although the positive control did not pick up the TRAP1 protein, two TRAP1 bands were detected between the 75-150 kDa molecular weights marks in Figure 4.5 lane 5that were not detected in the other lanes, indicating the presence of TRAP1 at detectable levels in that immunoprecipitate.

Total STAT3 was detected in multiple bands in the four samples (Figure 4.6 lanes 2-5) and a band corresponding to the estimated size of STAT3 was detected only in samples containing lysate (Figure 4.6 lanes 2,3,5), indicating that TRAP1 and total STAT3 co-precipitated in a common complex. This was also shown by detecting pSTAT3Y705 (Figure 4.7) just below the 100 kDa molecular weight mark in TRAP1 immunoprecipitation (Figure 4.7 lane 3) and lysate plus antibody sample (Figure 4.7 lane 5). These results indicated a potential for a common complex between TRAP1 and pSTAT3Y705.

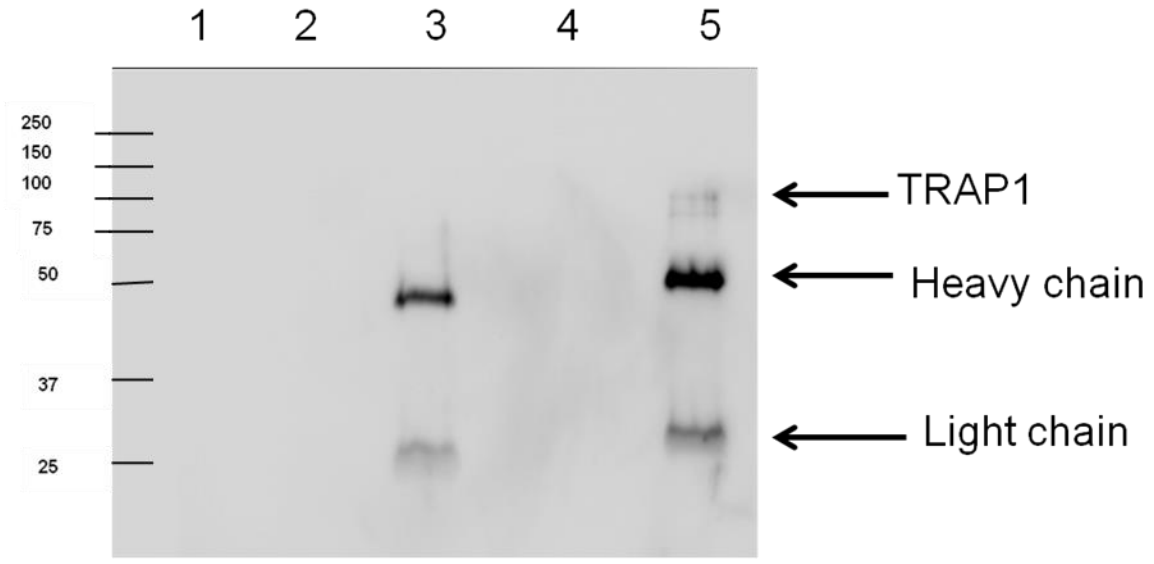

Figure 4.5: Western Blot analyses of immunoprecipitation samples carried out in 3T3L1 cell lysates. Western blot detection of TRAP1 after immunoprecipitation using an anti-mouse TRAP1 antibody. Lane 1: Marker. Lane 2: Free 3T3L1 cell lysate (positive control). Lane 3: Immunoprecipitation of antibody and protein A/G plus agarose beads without lysate (negative control 1). Lane 4: Immunoprecipitation of lysate and protein A/G plus agarose beads without antibody (negative control 2). Lane 5: Immunoprecipitation of lysate and protein A/G plus agarose beads with antibody.

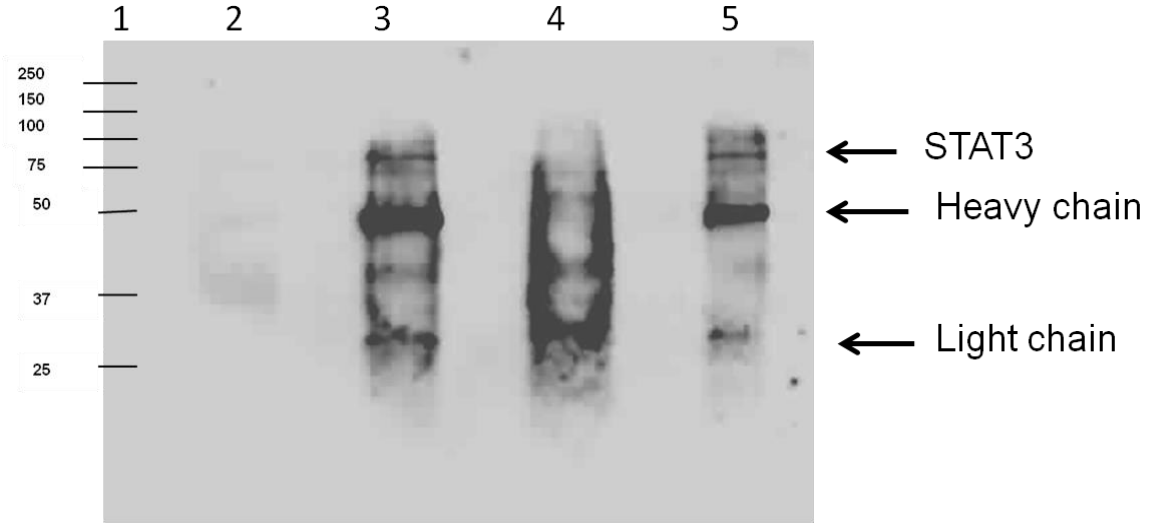

Figure 4.6: Western Blot analyses of immunoprecipitation samples carried out in 3T3L1 cell lysates. Western detection of total STAT3 after immunoprecipitation using an anti-mouse TRAP1 antibody. Lane 1: Marker. Lane 2: Free 3T3L1 cell lysate (positive control). Lane 3: Immunoprecipitation sample. Lane 4: immunoprecipitation of antibody and protein A/G plus agarose beads without lysate. Lane 5: Lysate plus antibody.

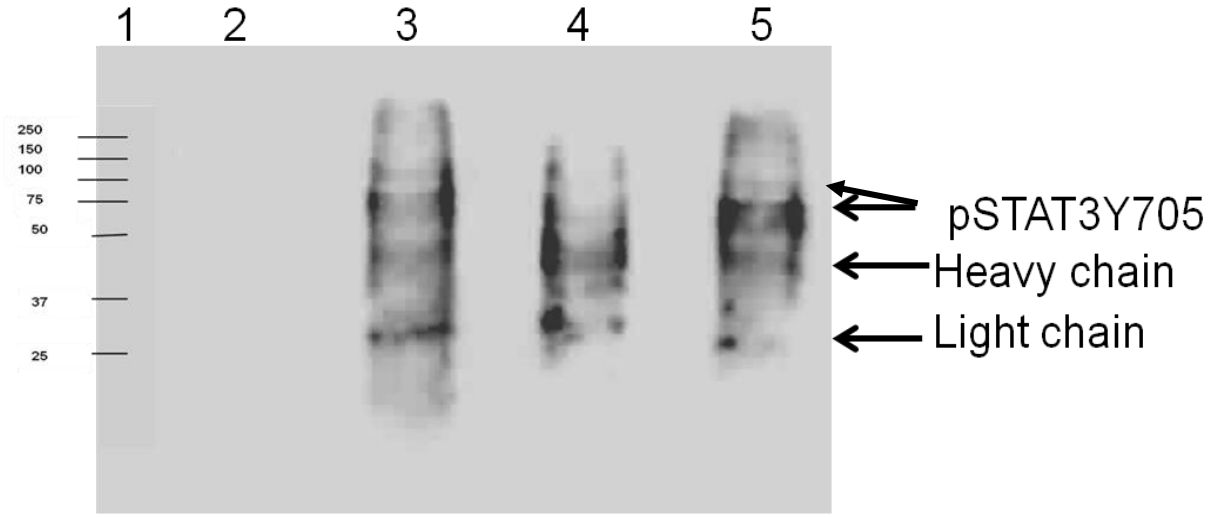

Figure 4.7: Western Blot analyses of immunoprecipitation samples carried out in 3T3L1 cell lysates. Western detection of pSTAT3Y705 after immunoprecipitation using an anti-mouse TRAP1 antibody. Lane 1: Marker. Lane 2: Free 3T3L1 cell lysate (positive control). Lane 3: Immunoprecipitation sample. Lane 4: immunoprecipitation of antibody and protein A/G plus agarose beads without lysate. Lane 5: Lysate plus antibody.

4.3.3 Recombinant expression and purification of STAT3

STAT3 was expressed and purified to use in the *in vitro* interaction study. The induction of STAT3 expression was found to be successful and was detected at about 68 kDa as expected (Figure 4.8), as the construct contained an N and C terminal truncated STAT3 gene. The highest induction was observed after 5 hours on both SDS-PAGE and western blot analysis (Figure 4.8). Western blot analysis showed that proteins with molecular weights lower than the expected were also detected, indicating either translational truncations or degraded products (Figure 4.8).

STAT3 has an FPLC elution profile similar to that of BSA and therefore BSA (Figure 4.9 red profile) was used as a standard for the elution profile and blue dextran was used to determine the void volume (Figure 4.9 green profile). STAT3 (Figure 4.9 black profile; Figure 4.10) was eluted from the FPLC column from 55 ml to 110 ml similar to the BSA elution profile. Analysis by SDS-PAGE and western blot confirmed that the eluted protein was STAT3 (Figure 4.10). The FPLC purified STAT3 was then used for *in vitro* study of the TRAP1/STAT3 interaction.

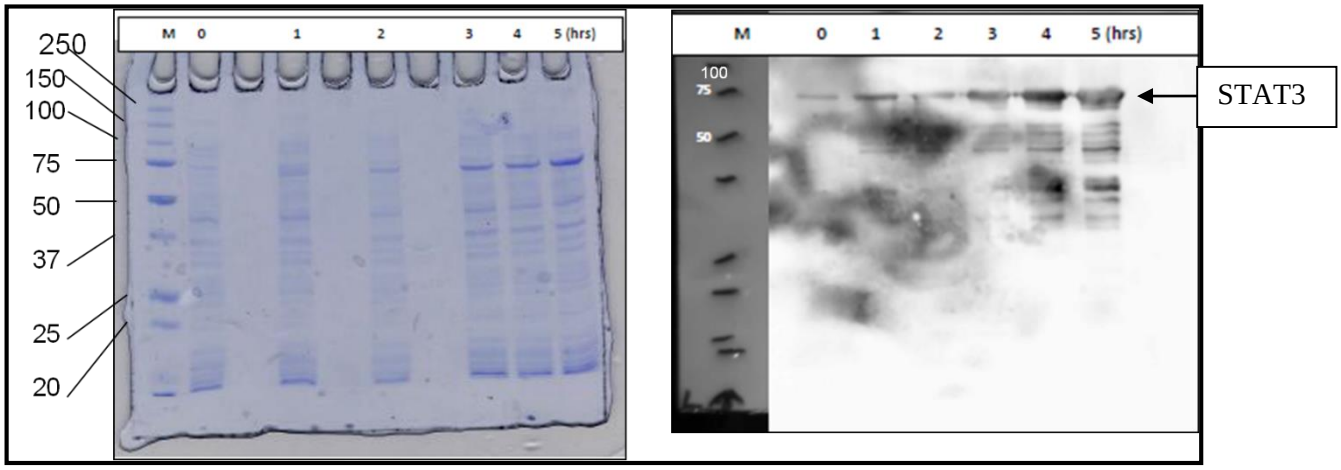

Figure 4.8: Induction of STAT3 expression. Expression of STAT3 (68 kDa) at 21 °C was analyzed by SDS-PAGE and western blot analysis analysis with an anti-STAT3 antibody.

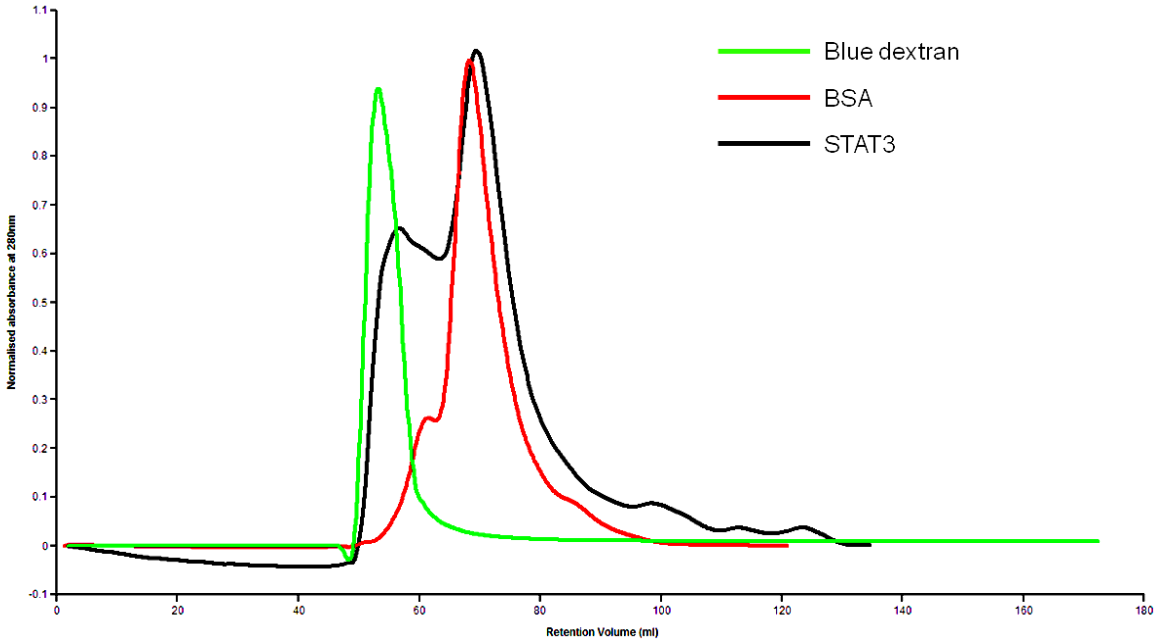

Figure 4.9: The elution profile of STAT3, BSA standard and blue dextran for the void volume, using FPLC purification.

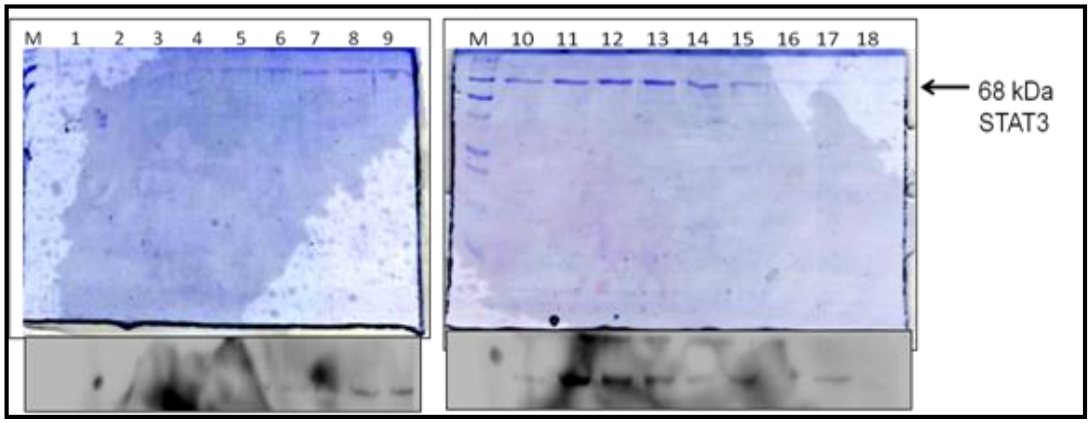

Figure 4.10: Purification of STAT3 to homogeneity using FPLC. Fractions of samples (1.5 ml) were collected from 55-120 ml and then analyzed by SDS-PAGE and western blot analysis with an anti-STAT3 antibody.

4.3.4 Recombinant expression and purification of TRAP1

TRAP1 with a His tag, which had an estimated molecular weight of approximately 70 kDa, was expressed and detected on the western blot using an anti-His antibody (Figure 4.11), indicating that there were no translational truncation products. Nonetheless, His-tagged TRAP1 was detected from the beginning of the experiment and did not appear to increase with induction time, indicating that the plasmid had a leaky promoter and expression required improvement (Figure 4.11). Purification of TRAP1 resulted in loss of detection of proteins at the expected size (Figure 4.12) indicating that the levels of His-tagged TRAP1 were not sufficient to purify or most likely TRAP1 failed to bind to the nickel charged column. Therefore, the flow-through sample was used for the *in vitro* interaction study.

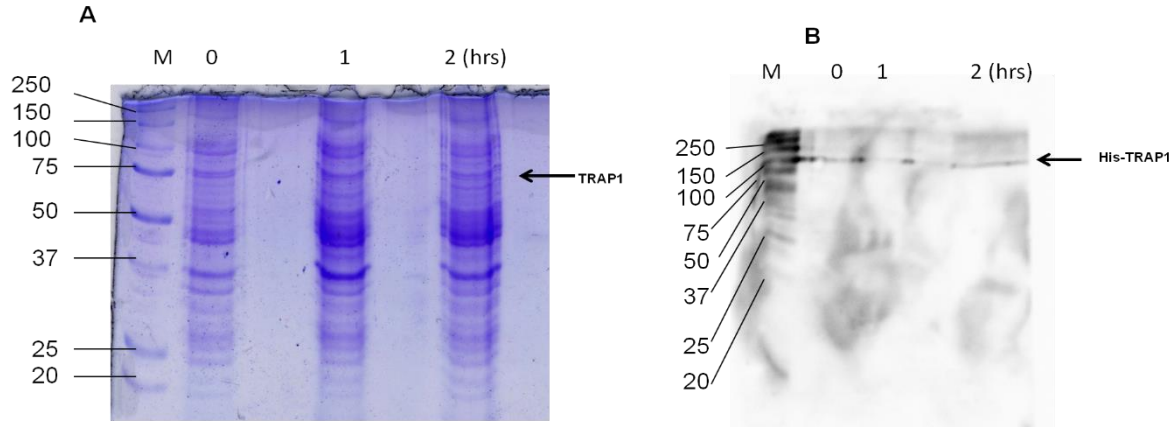

Figure 4.11: Induction of TRAP1 expression. Expression of TRAP1 was conducted at 37 °C for 2 hours and analyzed using SDS-PAGE and western blot analysis with an anti-His antibody of total cell lysate.

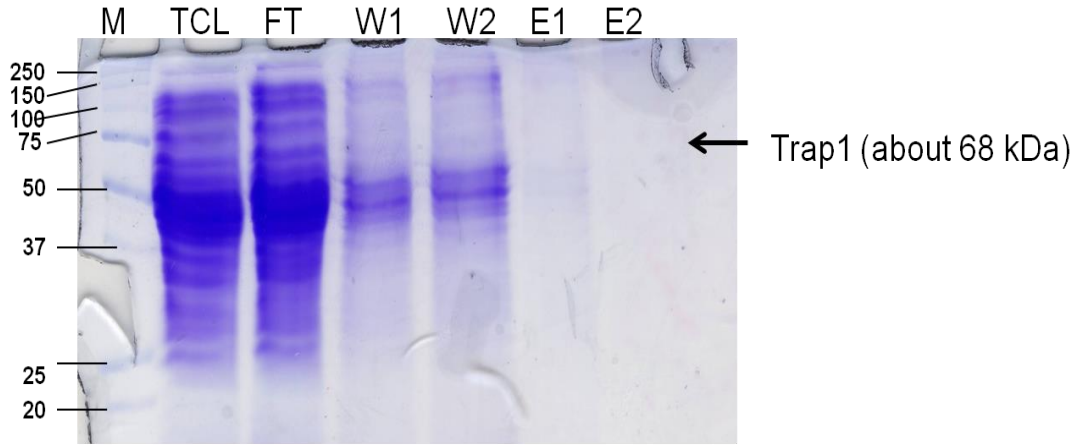

Figure 4.12: Nickel affinity purification of the His-tagged TRAP1. TCL is the total cell lysate; FT is the flow-through; W1 and W2 is the first and second wash respectively; E1 and E2 is the first and second elution respectively.

4.3.5 Analysis of the *in vitro* interaction between TRAP1 and STAT3

Surface plasmon resonance (SPR) spectroscopy was conducted to determine if His-tagged TRAP1 would bind the SPR chip, interact with STAT3 and whether this interaction was ATP dependent. The results showed that proteins in the flow-through from the purification process were bound to the nickel charged chip in a gradual manner as would be expected with specific binding (Figure A6). As nickel is used to selectively purify His-tagged proteins, the specific binding on the nickel charged SPR chip indicates that the bound protein may be the His-tagged TRAP1. However without the crucial control of SPR using chips containing flow-through from *E.coli* not expressing TRAP1, the chip-bound proteins could not confidently be stated to be His-tagged TRAP1 as they can be could be any *E.coli* protein in the column flow-through. STAT3 interacted with a protein in the flow-through bound to the nickel charged chip in a concentration and ATP dependent manner (Figure 4.13). The TRAP1/STAT3 interaction data was corrected by subtracting the data of the ATP analyte and that of the blank (SPR running buffer). In the presence of ATP, the interaction appeared specific in a concentration dependency manner (Figure 4.13). By contrast, in the absence of ATP, this interaction seemed non-specific as the concentration dependency was lost (Figure 4.14). This therefore points to the possibility that the TRAP1 and STAT3 interaction is ATP-dependent. However, the dissociation was not uniform and the data could not be used for kinetics analyses.

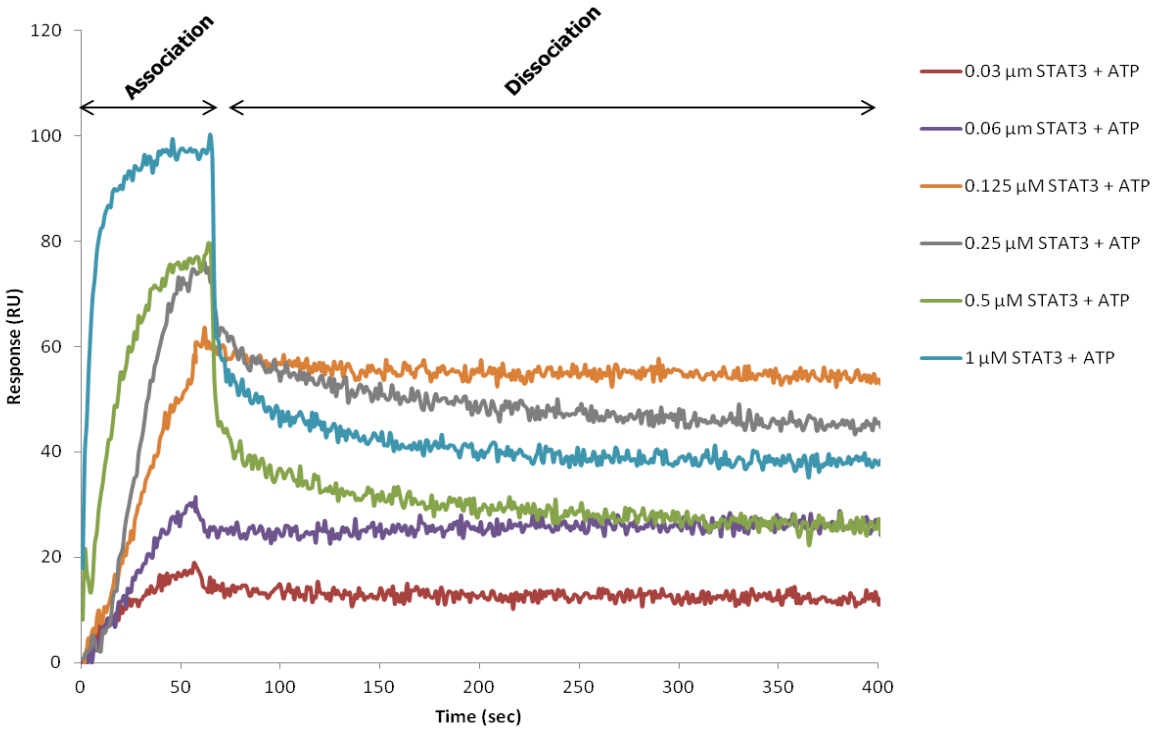

Figure 4.13 SPR analysis of TRAP1 interaction with STAT3 in the presence of ATP.

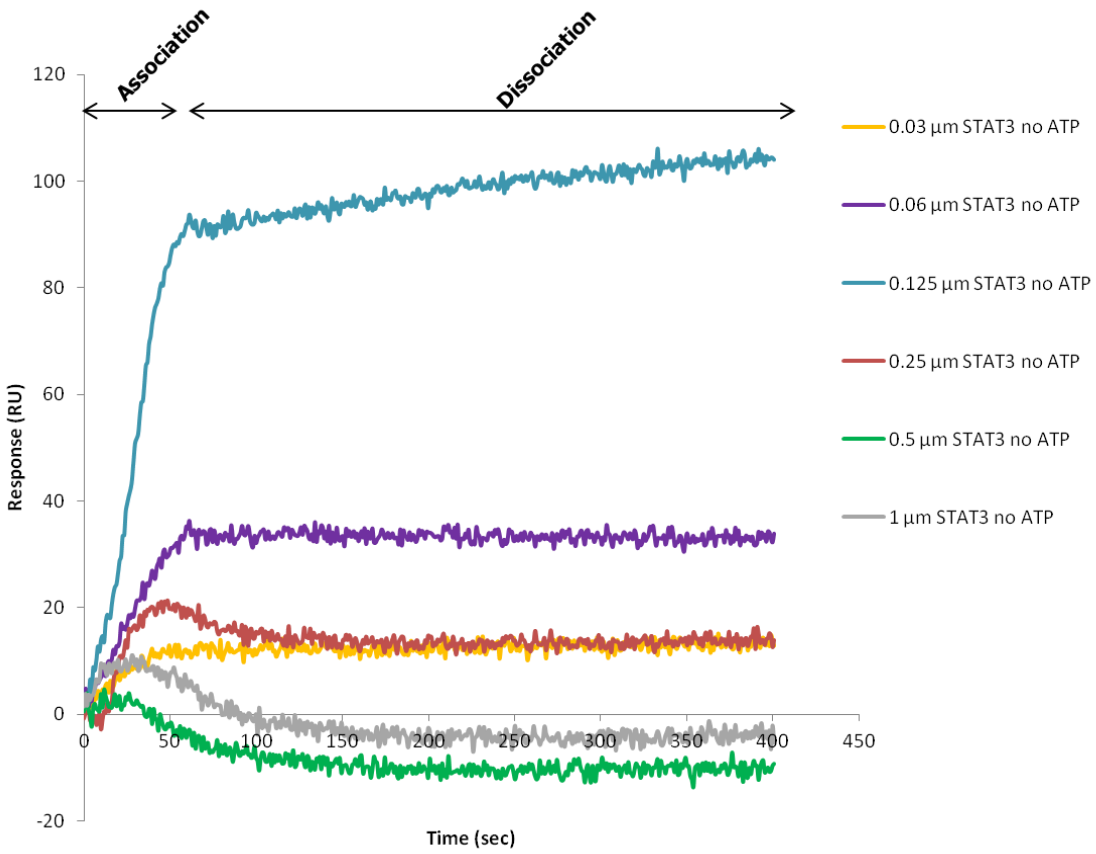

Figure 4.14 SPR analysis of TRAP1 interaction with STAT3 in the absence of ATP.

4.4 Discussion

The results of this study showed that TRAP1 and STAT3 co-localized, potentially confirming the occurrence of STAT3 in the mitochondria, as shown in previous studies (Gough *et al*., 2009). This observation suggests the potential of *in vivo* TRAP1/STAT3 interaction. Studies have shown that cytosolic Hsp90 and STAT3 interact (Sato *et al*., 2003). This interaction has been found to chaperone and stabilize the phospho-activated STAT3 (Schoof *et al*., 2009). Both knockdown and inhibition of Hsp90 isoforms, including TRAP1, have been found to reduce the level of STAT3 phosphorylated at Tyrosine 705 (Kubota *et al*., 2009). In line with the potential role of TRAP1 in chaperoning STAT3 to the mitochondria (Chapter 3), it is, therefore likely that the interaction of these two proteins would be involved in stabilizing phosphorylated STAT3 as suggested by the Kubota *et al*., 2009.

The precipitation of TRAP1 and STAT3 within the same protein complexes as indicated by the detection of STAT3 in TRAP1 immunoprecipitates suggested a potential confirmation of their

co-localization. This suggests that these two proteins occurred within similar protein complexes. Previous studies have suggested that cytosolic Hsp90 and STAT3 share similar protein complexes and would therefore co-immunoprecipitate (Shah *et al*., 2002; Sato *et al*., 2003; Setati *et al*., 2010; Schoof *et al*., 2009). By sharing similar protein complexes, this suggests probable direct protein-protein interactions, such as the chaperoning and stabilizing activated STAT3 (Sato *et al*., 2003; Schoof *et al*., 2009). Therefore, although the co-immunoprecipitation of TRAP1 and STAT3 was done on total cell lysate, it suggests the possibility of this protein-protein interaction within the mitochondria that is analogous to that found in the cytoplasm.

The *in vitro* analyses showed a direct interaction between STAT3 and a protein in the E. coli that was trapped bound onto the nickel charged chip, possibly the His-tagged TRAP1. Furthermore, this interaction was found to be ATP dependent. Similar to the cytosolic Hsp90s, TRAP1 has an N-terminal that hydrolyses ATP (Felts *et al*., 2002). Cytosolic interactions have been found to hydrolyze ATP when binding to STAT3 (Prinsloo *et al*., 2012). This suggests that if the bound ligand protein was TRAP1, the interaction between mitochondrial Hsp90 TRAP1 and STAT3 exhibited an interaction mechanism similar to cytosolic Hsp90. The previous study (Chapter 3) suggested that TRAP1 played a role in translocating STAT3 to the mitochondria and this possible interaction suggested a functional relationship. The possible functional relationships may include stabilizing phosphorylated STAT3, which is important in signal transduction.

To conclude, this study showed that TRAP1 and STAT3 co-localized in MCF7 breast cancer cells. Immunoprecipitation studies suggested possible co-occurrence of these proteins in a common biological complex, whereas the *in vitro* analysis suggests a direct ATP-dependent interaction. Nonetheless, to confirm the direct interaction of TRAP1 and STAT3 and evaluate the kinetics, purified protein should be used for protein pull-down assays and SPR. The results of this study therefore suggest the possibility of a functional relationship between these two proteins.

CHAPTER 5

Conclusions and Future Work

STAT3 signaling has been reported to be crucial in both stem and cancer cells whereby stabilized phosphorylated STAT3 can translocate to the nucleus and activate genes that promote stem cell characteristics and oncogenesis (Demaria *et al*., 2010), respectively. In addition to its cytosolic and nuclear localization, STAT3 has been reported to occur in the mitochondria where it has been proposed to regulate the activities of the electron transport chain and reduce the generation of ROS (Gough *et al*., 2009; Wegrzyn *et al.*, 2009). In this study, STAT3 and its post translational modifications, phosphorylated Tyrosine 705 and phosphorylated Serine 727 were shown to be present in 3T3L1 cells at detectable levels using western blot analysis. Other studies have linked HSP90 β to the JAK/STAT3 signaling pathway because of its involvement in the nuclear translocation of STAT3 phosphorylated at Tyrosine 705 (Shah *et al.*, 2002; Sato *et al*., 2003; Prinsloo *et al*., 2012). However, little is known about the association of TRAP1 with STAT3. In this study, it was hypothesized that STAT3 localized in the mitochondria and its translocation was facilitated by TRAP1, which would have sufficient structural conservation to function like Hsp90 β.

Based on the bioinformatics study, TRAP1 was confirmed to be an Hsp90 homolog. Nevertheless, human TRAP1 was found to be more similar to bacterial Hsp90 and lacked a charged loop region and a TPR-containing co-chaperone binding domain suggesting that the flexibility of TRAP1 would be less compared to Hsp90 β leading to a difference in affinity for substrate binding. In addition, the ATPase domain was confirmed to be the most conserved domain among the Hsp90 homologs, suggesting that TRAP1 may hydrolyse ATP when interacting with substrate (client protein) and would have a different affinity for the same substrate in comparison to Hsp90 β. Secondary structure prediction of TRAP1, in comparison to Hsp90 β, showed that despite the lacking the first charged domain and EEVD motif, the remaining domain's secondary structures were very similar. The function of a protein is dependent on its tertiary structure and the lack of the first charged domain and EEVD motif suggests that the functions of TRAP1 and Hsp90 β may not be conserved. The localization of STAT3 was therefore investigated in relation to TRAP1 and mitochondria to determine if TRAP1 and STAT3 localized in the same regions and if STAT3 was in the mitochondria.

In this study STAT3 was predicted to have cytoplasmic, nuclear and mitochondrial localizations. Furthermore, STAT3 was experimentally found to localize in the nucleus, in the cytoplasm and in similar locations with a mitochondrial protein VDAC. STAT3 was found to co-

localize with a predominantly mitochondrial protein TRAP1, suggesting the possibility of mitochondrial localization of STAT3. The co-immunoprecipitation study revealed that the observed co-localization may have been as a result of STAT3 and TRAP1 co-occurring within the same molecular complexes, suggesting a role of TRAP1 in the STAT3 signaling pathway. Although the results suggested the co-occurrence of these proteins, confirmation of mitochondrial localization was not conclusive. Therefore, further experiments, such as electron microscopy and isolation of pure mitochondria using flow cytometry, could be considered to confirm the mitochondrial localization of TRAP1 and STAT3 conclusively.

Hsp90s play a role in the maturation and stabilizing numerous client proteins, many of which are involved in self-renewal and oncogenesis (Grbovic *et al*., 2006). Of particular interest is that HSP90 β plays a role in nuclear localization of STAT3. However, the involvement of TRAP1, the mitochondrial Hsp90 isoform, in STAT3 signaling pathway has not been clearly defined. Although STAT3 has been reported in the mitochondria (Gough *et al.*, 2009; Wegrzyn *et al*., 2009), its mechanism of translocation to this organelle is still unclear. The over-expression experiment pointed to the possible role of TRAP1 in STAT3 translocation as suggested by an increased in mitochondrial localization of pSTAT3Y705. Furthermore, co-localization and co-immunoprecipitation studies potentially showed that there was a possible association between TRAP1 and STAT3. This was supported by surface plasmon resonance spectroscopy whereby STAT3 directly interacted with a nickel-trapped and immobilized protein, most likely His-TRAP1. This interaction suggest the probable role of TRAP1 in stabilizing STAT3 as suggested by Kubota *et al*., (2009), such as that observed for cytosolic Hsp90 β interactions (Sato *et al*., 2003, Prinsloo et al). Furthermore, the interaction between STAT3 and TRAP1 was found to be ATP dependent. These results suggested that TRAP1 also hydrolyze ATP when binding to substrate as has been described for cytosolic Hsp90 (Sato *et al*., 2003; Schoof *et al*., 2009; Prinloo *et al.*, 2012).

Considering that STAT3 is the JAK/STAT signaling protein that is activated by phosphorylation on Tyrosine 705 and Serine 727 (Darnell *et al.*, 1994; Aaronson *et al.*, 2002; Levy *et al.*, 2002), it was interesting to note that TRAP1 over-expression resulted in a nuclear accumulation of Serine 727 phosphorylated STAT3, potential increase in mitochondrial Tyrosine 705 phosphorylated STAT3 and a reduction in ROS levels. Mitochondrial STAT3 and overexpression have been linked to the reduction of ROS production (Gesualdi *et al*., 2007; Wegrzyn *et al*., 2009; Demaria *et al*., 2010; Shin *et al*., 2011). A possible explanation for this

study's results was that due to the presence of more chaperoning protein, more phosphorylated STAT3 was probably stabilized and entered the nucleus to activate genes that resulted in lower ROS production and also potentially more STAT3 entered the mitochondria and inhibited ROS formation. Kubota *et al.*, 2009 suggested that TRAP1 stabilizes Tyrosine 705 phosphorylated STAT3 when knockdown of TRAP1 resulted in a reduction in Tyrosine 705 phosphorylated STAT3.Therefore, given the suggested role for TRAP1 in mitochondrial localization of STAT3 and the nuclear accumulation of phosphorylated STAT3 in cell over-expressing TRAP1, such a role is possible.

In this study, inhibition of STAT3 resulted in increased ROS levels and appeared to be selective for the STAT3 phosphorylated at Tyrosine 705. This suggested that inhibitors that targeted phosphorylated STAT3 may not be as effective on STAT3 phosphorylated at Serine 727. By comparison, over-expressing TRAP1 was confirmed to result in reduced ROS level (Gesualdi *et al*., 2007). The effect of STAT3 on ROS observed in this study is possible as nuclear STAT3 has been reported to decrease the transcription of mitochondrial proteins and activate the transcription of glycolytic proteins while mitochondrial STAT3 has been reported to bind to ETC complexes supposedly to mop-up excess electrons, all resulting in a reduction in cellular ROS levels (Wegrzyn *et al*., 2009; Demaria *et al*., 2010; Shin *et al*., 2011). Therefore, inhibiting STAT3 would result in increased ROS as observed.

5.1 Future work

In order to acquire conclusive and quantitative data about the TRAP1/STAT3 interaction, future experiments would require the use of purified TRAP1 and STAT3 with the appropriate controls. Preliminary evidence is provided here for a STAT3 mitochondrial chaperoning role for TRAP1, and the observed potential direct interaction suggests other points of contact besides mitochondrial chaperoning such as stabilizing phosphorylated STAT3 in the cytoplasm. Nonetheless, the results of this study suggests that TRAP1 may be directly involved in the STAT3 signaling pathway perhaps through the modulation or stabilization of phosphorylated STAT3 as indicated in Chapter 3. However, further experiments are required to confirm the speculation that TRAP1 stabilizes transactivated phosphorylated STAT3 Tyrosine 705.

To determine how TRAP1 is involved in STAT3 localization, stabilization and signaling, particularly with regards to ROS regulation, experiments can be done which combine modifications of expression of both proteins in mouse models as Chapter 2 highlighted how similar the proteins

are between human and mouse species. As both TRAP1 and STAT3 have been detected in pre-adipocytes, that cell model can therefore be used for such experiments. These experiments would include inhibition or over-expression of STAT3 in combination with TRAP1 expressing, null, inhibited and over-expressing cells. Furthermore STAT3 associated gene expression can be assessed in TRAP1 expressing, null, inhibited and over-expressing cells then assess the ROS levels.

In view of the proposed role of TRAP1 in ROS regulation as a "guardian" of the mitochondria (Kadye *et al.*, 2013), and the established role of STAT3 in activating glycolysis in cancer (Demaria *et al.*, 2010), the synergistic contribution of these two proteins require further study with regards to ROS regulation, gene expression and mitochondrial biogenesis. Figure 5.1 suggest a model for the future experiments.

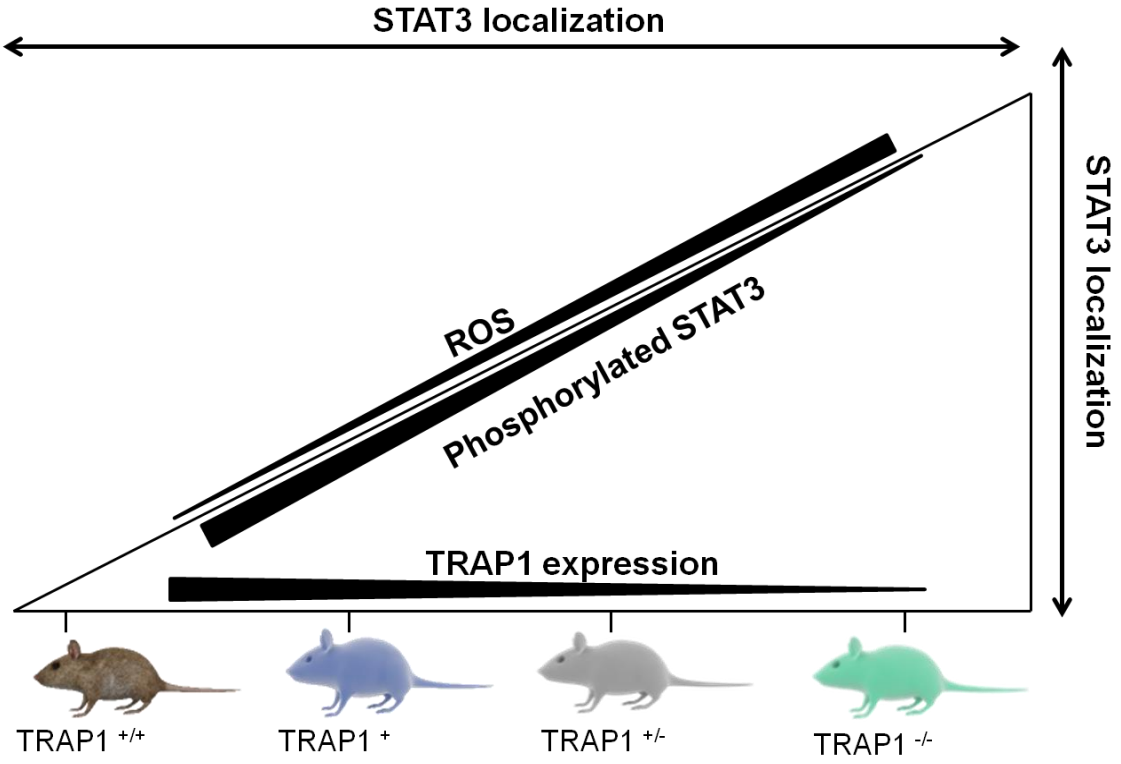

Figure 5.1: Model for the hypothesized role of TRAP1 in STAT3 signaling. This study can be conducted in TRAP1$^{+/+}$ (over-expressing), TRAP1^{+} (endogenously expressing), TRAP1$^{+/-}$ (inhibited endogenously expressing) and TRAP1$^{-/-}$ null cells.

REFERENCES

- Abel, F. Sjöberg, R., Nilsson, S., Kogner, P. and Martinsson T. (2005). Imbalance of the mitochondrial pro- and antiapoptotic mediators in neuroblastoma tumours with unfavourable biology. *Eur. J. Cancer,* 41**,** 635–646.

- Alberts B., Johnson A., Lewis J., Raff M., Roberts K., and Walter P. (1994). Molecular Biology of the Cell. Garland Publishing Inc., New York.
- Al-Hajj, M., Wicha, M. S., Benito-Hernandez, A., Morrison, S. J., & Clarke, M. F. (2003). Prospective identification of tumorigenic breast cancer cells. *Proceedings of the National Academy of Sciences*, *100*(7), 3983-3988.
- Alison, M. R., & Islam, S. (2009). Attributes of adult stem cells. *The Journal of pathology*, *217*(2), 144-160.
- Anderson, S., Bankier, A. T., Barrell, B. G., De Bruijn, M. H. L., Coulson, A. R., Drouin, J., ... & Young, I. G. (1981). Sequence and organization of the human mitochondrial genome. Banerji, U. (2009). Heat shock protein 90 as a drug target: some like it hot. *Clinical Cancer Research*, *15*(1), 9-14.
- Becker, S., Groner, B., & Müller, C. W. (1998). Three-dimensional structure of the Stat3β homodimer bound to DNA. *Nature*, *394*(6689), 145-151.
- Beckmann, R.P. Mizzen, L.E. Welch, W.J. (1990). Interaction of Hsp70 with newly synthesized proteins: implications for protein folding and assembly. *Science, 248*, 850–854.
- Bianco, P., Riminucci, M., Gronthos, S., & Robey, P. G. (2001). Bone marrow stromal stem cells: nature, biology, and potential applications. *Stem cells*, *19*(3), 180-192.

- Bjerkvig, R., Tysnes, B.B., Aboody, K.S., Najbauer, J. and Terzis, A.J. (2005). Opinion: the origin of the cancer stem cell: current controversies and new insights. *Nat Rev Cancer*, *5*(11) p.899-904.
- Bromberg, J. F., Wrzeszczynska, M. H., Devgan, G., Zhao, Y., Pestell, R. G., Albanese, C., & Darnell Jr, J. E. (1999). < i> Stat3</i> as an Oncogene. *Cell*, *98*(3), 295-303.
- Brown, M. A., Zhu, L., Schmidt, C., & Tucker, P. W. (2007). Hsp90—from signal transduction to cell transformation. *Biochemical and biophysical research communications*, *363*(2), 241-246.
- Bullerwell, C. E., & Gray, M. W. (2004). Evolution of the mitochondrial genome: protist connections to animals, fungi and plants. *Current opinion in microbiology*, *7*(5), 528-534.

- Cao, X., Tay, A., Guy, G.R. & Tan, Y.H. (1996). Activation and association of Stat3 with Src in v-Src-transformed cell lines. *Molecular Cell Biology*, 16, 1595-1603.
- Chaudhary, P. M., & Roninson, I. B. (1991). Expression and activity of P-glycoprotein, a multidrug efflux pump, in human hematopoietic stem cells. *Cell*, *66*(1), 85-94.
- Chen, L. B. (1988). Mitochondrial membrane potential in living cells. *Annual review of cell biology*, *4*(1), 155-181.
- Chen, C. F., Chen, Y., Dai, K., Chen, P. L., Riley, D. J., & Lee, W. H. (1996). A new member of the hsp90 family of molecular chaperones interacts with the retinoblastoma protein during mitosis and after heat shock. *Molecular and cellular biology*, *16*(9), 4691-4699.
- Chen, B., Piel, W. H., Gui, L., Bruford, E., & Monteiro, A. (2005). The HSP90 family of genes in the human genome: insights into their divergence and evolution. *Genomics*, *86*(6), 627-637.
- Chuthapisith, S., Eremin, J., El-Sheemey, M. and Eremin, O. (2010). Breast cancer chemoresistance: Emerging importance of cancer stem cells. *Surgical Oncology*, 19, 27-32.
- Clarke, M. F., Dick, J. E., Dirks, P. B., Eaves, C. J., Jamieson, C. H., Jones, D. L., ... & Wahl, G. M. (2006). Cancer stem cells—perspectives on current status and future directions: AACR Workshop on cancer stem cells. *Cancer research*, *66*(19), 9339-9344.
- Cole, C., Barber, J. D., & Barton, G. J. (2008). The Jpred 3 secondary structure prediction server. *Nucleic acids research*, *36*(suppl 2), W197-W201.
- Collins, T. (2007). Introduction to ImageJ for Light Microscopy. *Microscopy and Microanalysis* 13, 1674-1675
- Cooper G. M. and Hausman R. E. (2006). The Cell: a molecular approach. 4th ed. ASM Press and Sinauer Associates, Inc., Sunderland, MA.
- Costantino, E., Maddalena, F., Calise, S., Piscazzi, A., Tirino, V., Fersini, A., ... & Landriscina, M. (2009). TRAP1, a novel mitochondrial chaperone responsible for multi-drug resistance and protection from apoptotis in human colorectal carcinoma cells. *Cancer letters*, *279*(1), 39-46.
- Cuff, J. A., & Barton, G. J. (2000). Application of multiple sequence alignment profiles to improve protein secondary structure prediction. *Proteins: Structure, Function, and Bioinformatics*, *40*(3), 502-511.
- Dalerba, P., Cho, R. W., & Clarke, M. F. (2007). Cancer stem cells: models and concepts. *Annu. Rev. Med.*, *58*, 267-284.

- Darnell Jr, J. E., Kerr, I. M., & Stark, G. R. (1994). Jak-STAT pathways and transcriptional activation in response to IFNs and other extracellular signaling proteins. *Science*, *264*(5164), 1415-1421.
- Dayem, A. A., Choi, H. Y., Kim, J. H., & Cho, S. G. (2010). Role of oxidative stress in stem, cancer, and cancer stem cells. *Cancers*, *2*(2), 859-884. Dick, J.E. (2003**).** Breast cancer stem cells revealed. *PNAS*. **100** (7) p.3547–3549.
- Doyle, L. A., Yang, W., Abruzzo, L. V., Krogmann, T., Gao, Y., Rishi, A. K., & Ross, D. D. (1998). A multidrug resistance transporter from human MCF-7 breast cancer cells. *Proceedings of the National Academy of Sciences*, *95*(26), 15665-15670.
- Dunn, K. W., Kamocka, M. M., & McDonald, J. H. (2011). A practical guide to evaluating colocalization in biological microscopy. *American Journal of Physiology-Cell Physiology*, *300*(4), C723-C742.
- Edgar, R.C. (2004). MUSCLE: multiple sequence alignment of high accuracy and high throughput. *Nucleic Acids Research. 32*(5), 1792-1797.
- Englebienne, P., Van Hoonacker, A., & Verhas, M. (2003). Surface plasmon resonance: principles, methods and applications in biomedical sciences. *Spectroscopy: An International Journal*, *17*(2), 255-273.
- Felts, S. J., Owen, B. A., Nguyen, P., Trepel, J., Donner, D. B., & Toft, D. O. (2000). The hsp90-related protein TRAP1 is a mitochondrial protein with distinct functional properties. *Journal of Biological Chemistry*, *275*(5), 3305-3312.
- Galluzzi, L., Morselli, E., Kepp, O., Vitale, I., Rigoni, A., Vacchelli, E., ... & Kroemer, G. (2010). Mitochondrial gateways to cancer. *Molecular aspects of medicine*, *31*(1), 1-20.
- Garedew, A., & Moncada, S. (2008). Mitochondrial dysfunction and HIF1α stabilization in inflammation. *Journal of cell science*, *121*(20), 3468-3475.
- Gesualdi, M.N., Chirico, G., Pirozzi, G., Costantino, E., Landriscina, M. and Esposito, F. (2007). Tumor necrosis factor-associated protein 1 (TRAP-1) protects cells from oxidative stress and apoptosis, *Stress, 10*(4) 342–350.
- Gough, D. J., Corlett, A., Schlessinger, K., Wegrzyn, J., Larner, A. C., & Levy, D. E. (2009). Mitochondrial STAT3 supports Ras-dependent oncogenic transformation. *Science*, *324*(5935), 1713-1716.

- Gu, L., Vogiatzi, P., Puhr, M., Dagvadorj, A., Lutz, J., Ryder, A., ... & Nevalainen, M. T. (2010). Stat5 promotes metastatic behavior of human prostate cancer cells in vitro and in vivo. *Endocrine-related cancer*, *17*(2), 481-493.

- Hall, T. A. (1999, January). BioEdit: a user-friendly biological sequence alignment editor and analysis program for Windows 95/98/NT. In *Nucleic acids symposium series* (Vol. 41, pp. 95-98).
- Han, D., Williams, E., & Cadenas, E. (2001). Mitochondrial respiratory chain-dependent generation of superoxide anion and its release into the intermembrane space. *Biochem. J*, *353*, 411-416.
- Hanahan, D., & Weinberg, R. A. (2011). Hallmarks of cancer: the next generation. *Cell*, *144*(5), 646-674.
- Hartl, F. U., Bracher, A., & Hayer-Hartl, M. (2011). Molecular chaperones in protein folding and proteostasis. *Nature*, *475*(7356), 324-332.
- Heppner, G. H. (1984). Tumor heterogeneity. *Cancer research*, *44*(6), 2259-2265.
- Hodge, D. R., Hurt, E. M., & Farrar, W. L. (2005). The role of IL-6 and STAT3 in inflammation and cancer. *European journal of cancer*, *41*(16), 2502-2512.
- Imamura, T., Huang, J., Dalle, S., Ugi, S., Usui, I., Luttrell, L. M., ... & Olefsky, J. M. (2001). β-Arrestin-mediated recruitment of the Src family kinase Yes mediates endothelin-1-stimulated glucose transport. *Journal of Biological Chemistry*, *276*(47), 43663-43667.
- Jäättelä, M. (1999). Heat shock proteins as cellular lifeguards. *Annals of medicine*, *31*(4), 261-271.
- Kang, B. H., Plescia, J., Dohi, T., Rosa, J., Doxsey, S. J., & Altieri, D. C. (2007). Regulation of tumor cell mitochondrial homeostasis by an organelle-specific Hsp90 chaperone network. *Cell*, *131*(2), 257-270.

- Karp, P. D. (1998). What we do not know about sequence analysis and sequence databases. *Bioinformatics*, *14*(9), 753-754.

- Katoh, K., Misawa, K., Kuma, K. I., & Miyata, T. (2002). MAFFT: a novel method for rapid multiple sequence alignment based on fast Fourier transform. *Nucleic acids research*, *30*(14), 3059-3066.

- Khan, R., Lee, J. E., Yang, Y. M., Liang, F. X., & Sehgal, P. B. (2013). Live-cell imaging of the association of STAT6-GFP with mitochondria. *PloS one*, *8*(1), e55426.
- Kim, R. H., Kim, R., Chen, W., Hu, S., Shin, K. H., Park, N. H., & Kang, M. K. (2008). Association of hsp90 to the hTERT promoter is necessary for hTERT expression in human oral cancer cells. *Carcinogenesis*, *29*(12), 2425-2431.
- Kondoh, H., Lleonart, M. E., Nakashima, Y., Yokode, M., Tanaka, M., Bernard, D., ... & Beach, D. (2007). A high glycolytic flux supports the proliferative potential of murine embryonic stem cells. *Antioxidants & redox signaling*, *9*(3), 293-299.
- Kubota, K., Inoue, K., Hashimoto, R., Kumamoto, N., Kosuga, A., Tatsumi, M., ... & Tohyama, M. (2009). Tumor necrosis factor receptor-associated protein 1 regulates cell adhesion and synaptic morphology via modulation of N-cadherin expression. *Journal of neurochemistry*, *110*(2), 496-508.
- Landriscina, M., Amoroso, M. R., Piscazzi, A., & Esposito, F. (2010). Heat shock proteins, cell survival and drug resistance: the mitochondrial chaperone TRAP1, a potential novel target for ovarian cancer therapy. *Gynecologic oncology*, *117*(2), 177-182.
- Langer, T., Rosmus, S., & Fasold, H. (2003). Intracellular localization of the 90 kDA heat shock protein (HSP90α) determined by expression of a EGFP–HSP90α-fusion protein in unstressed and heat stressed 3T3 cells. *Cell biology international*, *27*(1), 47-52.
- Leskovar, A., Wegele, H., Werbeck, N. D., Buchner, J., & Reinstein, J. (2008). The ATPase cycle of the mitochondrial Hsp90 analog Trap1. *Journal of Biological Chemistry*, *283*(17), 11677-11688.
- Lindgren, M., Hällbrink, M., Prochiantz, A., & Langel, Ü. (2000). Cell-penetrating peptides. *Trends in pharmacological sciences*, *21*(3), 99-103.
- Liras, A. (2010). Future research and therapeutic applications of human stem cells: general, regulatory, and bioethical aspects. *Journal of translational medicine*, *8*(1), 131. BioMed Central Ltd. doi:10.1186/1479-5876-8-131
- Liu, X., Robinson, G. W., Wagner, K. U., Garrett, L., Wynshaw-Boris, A., & Hennighausen, L. (1997). Stat5a is mandatory for adult mammary gland development and lactogenesis. *Genes & Development*, *11*(2), 179-186.

- Liu, Z., & Butow, R. A. (2006). Mitochondrial retrograde signaling. *Annu. Rev. Genet.*, *40*, 159-185.
- Lonergan, T., Bavister, B., & Brenner, C. (2007). Mitochondria in stem cells. *Mitochondrion*, *7*(5), 289-296.
- Lopez-Lazaro, M. (2008). The warburg effect: why and how do cancer cells activate glycolysis in the presence of oxygen?. *Anti-Cancer Agents in Medicinal Chemistry (Formerly Current Medicinal Chemistry-Anti-Cancer Agents)*, *8*(3), 305-312.
- Malik, K., & Brown, K. W. (2000). Epigenetic gene deregulation in cancer. *British journal of cancer*, *83*(12), 1583.
- Matassa, D. S., Amoroso, M. R., Maddalena, F., Landriscina, M., & Esposito, F. (2012). New insights into TRAP1 pathway. *American journal of cancer research*, *2*(2), 235.
- McBride, H. M., Neuspiel, M., & Wasiak, S. (2006). Mitochondria: more than just a powerhouse. *Current Biology*, *16*(14), R551-R560.
- Mezhybovska, M., Yudina, Y., Abhyankar, A., & Sjölander, A. (2009). β-Catenin is involved in alterations in mitochondrial activity in non-transformed intestinal epithelial and colon cancer cells. *British journal of cancer*, *101*(9), 1596-1605.
- Murakami, H. Pain, D. Blobel, G. (1988). 70-kDa heat shock-related protein is one of at least two distinct cytosolic factors stimulating protein import into mitochondria. *Journal of Cell Biology*, 107, 2051–2057.
- Nakai, K., & Horton, P. (1999). PSORT: a program for detecting sorting signals in proteins and predicting their subcellular localization. *Trends in biochemical sciences*, *24*(1), 34-35.
- Nargund, A. M., Pellegrino, M. W., Fiorese, C. J., Baker, B. M., & Haynes, C. M. (2012). Mitochondrial import efficiency of ATFS-1 regulates mitochondrial UPR activation. *Science*, *337*(6094), 587-590.
- Nesti, C., Pasquali, L., Mancuso, M., & Siciliano, G. (2009). The role of mitochondria in stem cell biology. In *Regulatory Networks in Stem Cells* (pp. 137-143). Humana Press.
- Ni, M., & Lee, A. S. (2007). ER chaperones in mammalian development and human diseases. *FEBS letters*, *581*(19), 3641-3651.
- Nielsen, H., Engelbrecht, J., Brunak, S., & von Heijne, G. (1997). Identification of prokaryotic and eukaryotic signal peptides and prediction of their cleavage sites. *Protein engineering*, *10*(1), 1-6.

- Nowell, P. C. (1986). Mechanisms of tumor progression. *Cancer Res*, *46*(5), 2203-2207.
- Neupert, W., & Herrmann, J. M. (2007). Translocation of proteins into mitochondria. *Annu. Rev. Biochem.*, *76*, 723-749.
- Odorico, J. S., Kaufman, D. S., & Thomson, J. A. (2001). Multilineage differentiation from human embryonic stem cell lines. *Stem cells*, *19*(3), 193-204.
- Okamoto, K., & Shaw, J. M. (2005). Mitochondrial morphology and dynamics in yeast and multicellular eukaryotes. *Annu. Rev. Genet.*, *39*, 503-536.
- Pallis, M., & Russell, N. (2000). P-glycoprotein plays a drug-efflux–independent role in augmenting cell survival in acute myeloblastic leukemia and is associated with modulation of a sphingomyelin-ceramide apoptotic pathway. *Blood*, *95*(9), 2897-2904.
- Pardal, R., Clarke, M. F., & Morrison, S. J. (2003). Applying the principles of stem-cell biology to cancer. *Nature Reviews Cancer*, *3*(12), 895-902.
- Peck, A. R., Witkiewicz, A. K., Liu, C., Stringer, G. A., Klimowicz, A. C., Pequignot, E., ... & Rui, H. (2011). Loss of nuclear localized and tyrosine phosphorylated Stat5 in breast cancer predicts poor clinical outcome and increased risk of antiestrogen therapy failure. *Journal of Clinical Oncology*, *29*(18), 2448-2458.
- Phillips, D., Reilley, M. J., Aponte, A. M., Wang, G., Boja, E., Gucek, M., & Balaban, R. S. (2010). Stoichiometry of STAT3 and Mitochondrial Proteins IMPLICATIONS FOR THE REGULATION OF OXIDATIVE PHOSPHORYLATION BY PROTEIN-PROTEIN INTERACTIONS. *Journal of biological chemistry*, *285*(31), 23532-23536.
- Pieczenik, S. R., & Neustadt, J. (2007). Mitochondrial dysfunction and molecular pathways of disease. *Experimental and molecular pathology*, *83*(1), 84-92.
- Prinsloo, E., Kramer, A. H., Edkins, A. L., & Blatch, G. L. (2012). STAT3 interacts directly with Hsp90. *IUBMB life*, *64*(3), 266-273.
- Rappaport, L., Oliviero, P., & Samuel, J. L. (1998). Cytoskeleton and mitochondrial morphology and function. *Molecular and cellular biochemistry*, *184*(1-2), 101-105.
- Ren, J., Wen, L., Gao, X., Jin, C., Xue, Y., & Yao, X. (2009). DOG 1.0: illustrator of protein domain structures. *Cell research*, *19*(2), 271-273.
- Reya, T., Morrison, S. J., Clarke, M. F., & Weissman, I. L. (2001). Stem cells, cancer, and cancer stem cells. *Nature*, *414*(6859), 105-111.
- Roe, S. M., Prodromou, C., O'Brien, R., Ladbury, J. E., Piper, P. W., & Pearl, L. H. (1999). Structural basis for inhibition of the Hsp90 molecular chaperone by the antitumor antibiotics radicicol and geldanamycin. *Journal of medicinal chemistry*, *42*(2), 260-266.

- Rost, B. (1999). Twilight zone of protein sequence alignments. *Protein engineering*, *12*(2), 85-94.
- Ryan, M. T., & Hoogenraad, N. J. (2007). Mitochondrial-nuclear communications. *Annu. Rev. Biochem.*, *76*, 701-722.
- Sato, N., Yamamoto, T., Sekine, Y., Yumioka, T., Junicho, A., Fuse, H., & Matsuda, T. (2003). Involvement of heat-shock protein 90 in the interleukin-6-mediated signaling pathway through STAT3. *Biochemical and biophysical research communications*, *300*(4), 847-852.
- Scadden, D. T. (2006). The stem-cell niche as an entity of action. *Nature*, *441*(7097), 1075-1079.
- Schoof, N., von Bonin, F., Trümper, L., & Kube, D. (2009). HSP90 is essential for Jak-STAT signaling in classical Hodgkin lymphoma cells. *Cell Commun Signal*, *7*, 17.
- Schumacker, P. T. (2006). Reactive oxygen species in cancer cells: live by the sword, die by the sword. *Cancer cell*, *10*(3), 175-176.
- Sell, S. (1993). Cellular origin of cancer: dedifferentiation or stem cell maturation arrest?. *Environmental health perspectives*, *101*(Suppl 5), 15.
- Setati, M.M., Prinsloo, E., Longshow, V.M. and Murray, P.A. (2010). Leukemia inhibitory factor promotes Hsp90 association with STAT3 in mouse embryonic stem cells. *Life*, *62*(1), 61-66.
- Shah, M., Patel, K., Fried, V. A., & Sehgal, P. B. (2002). Interactions of STAT3 with Caveolin-1 and Heat Shock Protein 90 in Plasma Membrane Raft and Cytosolic Complexes PRESERVATION OF CYTOKINE SIGNALING DURING FEVER. *Journal of Biological Chemistry*, *277*(47), 45662-45669.
- Shulga, N., & Pastorino, J. G. (2012). GRIM-19-mediated translocation of STAT3 to mitochondria is necessary for TNF-induced necroptosis. *Journal of cell science*, *125*(12), 2995-3003.
- Siddiquee, K., Zhang, S., Guida, W. C., Blaskovich, M. A., Greedy, B., Lawrence, H. R. and Turkson, J. (2007). Selective chemical probe inhibitor of Stat3, identified through structure-based virtual screening, induces antitumor activity. *Proceedings of the National Academy of Sciences*, *104*(18), 7391-7396.
- Sreedhar, A. S., & Csermely, P. (2004). Heat shock proteins in the regulation of apoptosis: new strategies in tumor therapy: a comprehensive review. *Pharmacology & therapeutics*, *101*(3), 227-257.
- Stein, W. (2012). *The movement of molecules across cell membranes* (Vol. 6). Elsevier.

- Süel, G. M., Lockless, S. W., Wall, M. A., & Ranganathan, R. (2003). Evolutionarily conserved networks of residues mediate allosteric communication in proteins. *Nature Structural & Molecular Biology*, *10*(1), 59-69.
- Sultan, A.S., Xie, J., LeBaron, M.J., Ealley, E.L., Nevalainen, M.T. and Rui, H. (2005) Stat5 promotes homotypic adhesion and inhibits invasive characteristics of human breast cancer cells. *Oncogene,* 24, 746–760.

- Tammineni, P., Anugula, C., Mohammed, F., Anjaneyulu, M., Larner, A. C., & Sepuri, N. B. V. (2013). The import of the transcription factor STAT3 into mitochondria depends on GRIM-19, a component of the electron transport chain. *Journal of Biological Chemistry*, *288*(7), 4723-4732.

- Tamura, K., Peterson, D., Peterson, N., Stecher, G., Nei, M. and Kumar, S. (2011). MEGA5: Molecular Evolutionary Genetics Analysis Using Maximum Likelihood, Evolutionary Distance, and Maximum Parsimony Method. *Molecular Biology and Evolution*, 28**,** 2731-2739.

- Thompson JD, Higgins DG, Gibson TJ *(11-Nov-1994)* CLUSTAL W: improving the sensitivity of progressive multiple sequence alignment through sequence weighting, position-specific gap penalties and weight matrix choice. *Nucleic acids research, 22*(22) 4673-4680
- Thomson, J.A., Itskovitz-Eldor, J., Shapiro, S.S., Waknitz, M.A., Swiergiel, J.J., Marshall, V.S. and Jones, J.M. (1998). Embryonic stem cell lines derived from human blastocysts. *Science,* 282, 1145.

- Timofeeva, O. A., Chasovskikh, S., Lonskaya, I., Tarasova, N. I., Khavrutskii, L., Tarasov, S. G., ... & Dritschilo, A. (2012). Mechanisms of unphosphorylated STAT3 transcription factor binding to DNA. *Journal of Biological Chemistry*, *287*(17), 14192-14200.
- Trepel, J., Mollapour, M., Giaccone, G., & Neckers, L. (2010). Targeting the dynamic HSP90 complex in cancer. *Nature Reviews Cancer*, *10*(8), 537-549.
- Turrens, J. F. (2003). Mitochondrial formation of reactive oxygen species. *The Journal of physiology*, *552*(2), 335-344.
- Visvader, J. E., & Lindeman, G. J. (2008). Cancer stem cells in solid tumours: accumulating evidence and unresolved questions. *Nature Reviews Cancer*, *8*(10), 755-768.
- Wang, X. (2001). The expanding role of mitochondria in apoptosis. *Genes & development*, *15*(22), 2922-2933.

- Wang, Y., Yang, J., Zheng, H., Tomasek, G. J., Zhang, P., McKeever, P. E., ... & Zhu, Y. (2009). Expression of mutant p53 proteins implicates a lineage relationship between neural stem cells and malignant astrocytic glioma in a murine model. *Cancer cell*, *15*(6), 514-526.
- Warburg, O., Wind, F., & Negelein, E. (1927). The metabolism of tumors in the body. *The Journal of general physiology*, *8*(6), 519-530.
- Warburg, O. (1956). On the origin of cancer cells. *Science*, *123*(3191), 309-314.
- Wegrzyn, J., Potla, R., Chwae, Y. J., Sepuri, N. B., Zhang, Q., Koeck, T., ... & Larner, A. C. (2009). Function of mitochondrial Stat3 in cellular respiration. *Science*, *323*(5915), 793-797.

- Wen, Z., & Darnell, J. E. (1997). Mapping of Stat3 serine phosphorylation to a single residue (727) and evidence that serine phosphorylation has no influence on DNA binding of Stat1 and Stat3. *Nucleic acids research*, *25*(11), 2062-2067.
- Whitesell, L., & Lindquist, S. L. (2005). HSP90 and the chaperoning of cancer. *Nature Reviews Cancer*, *5*(10), 761-772.
- Wicha, M. S., Liu, S., & Dontu, G. (2006). Cancer stem cells: an old idea—a paradigm shift. *Cancer research*, *66*(4), 1883-1890.
- Weiss, M. L., & Troyer, D. L. (2006). Stem cells in the umbilical cord. *Stem cell reviews*, *2*(2), 155-162.
- Xu, F., Mukhopadhyay, S., & Sehgal, P. B. (2007). Live cell imaging of interleukin-6-induced targeting of "transcription factor" STAT3 to sequestering endosomes in the cytoplasm. *American Journal of Physiology-Cell Physiology*, *293*(4), C1374-C1382.
- Yokogami, K., Wakisaka, S., Avruch, J. & Reeves, S.A. (2000). Serine phosphorylation and maximal activation of STAT3 during CNTF signaling is mediated by the rapamycin target mTOR. *Current Biology*, *10* (1), 47–50.
- Yuan, Z.L., Guan, Y.J., Wang, L., Wei, W., Kane, A.B. & Chin, Y.E. (2004). Central role of the threonine residue within the p+1 loop of receptor tyrosine kinase in STAT3 constitutive phosphorylation in metastatic cancer cells. *Molecular Cell Biology*, 24, 9390–9400.
- Zhang, X., & Darnell, J. E. (2001). Functional importance of Stat3 tetramerization in activation of the α2-macroglobulin gene. *Journal of Biological Chemistry*, *276*(36), 33576-33581.

- Zhou, S., Schuetz, J. D., Bunting, K. D., Colapietro, A. M., Sampath, J., Morris, J. J., ... & Sorrentino, B. P. (2001). The ABC transporter Bcrp1/ABCG2 is expressed in a wide variety of stem cells and is a molecular determinant of the side-population phenotype. *Nature medicine*, *7*(9), 1028-1034. ClustalW2 FAQs http://www.ebi.ac.uk/Tools/clustalw2/

- http://www.ncbi.nlm.nih.gov/ cdsearch/cdd

APPENDIX

A1: Reagents, Chemicals and Sources

Table A1: Reagents, Chemicals and Sources

Tissue culture Reagent	**Company**	**Country**
6 well culture plates	Corning	USA
Dako fluorescent mounting medium	Dako	USA
Dimethyl sulphoxide (DMSO)	Sigma-Aldrich	USA
Dulbecco's Modified Eagle Medium (DMEM) with 4.5 g/L D-glucose, L-glutamine, pyruvate	Gibco, Invitrogen	USA
Fetal calf serum (FCS)	PAA Laboratories	USA
Hoechst 33342	Invitrogen	USA
L-glutamine	Gibco	USA
Penicillin-Streptomycin solution stabilizer (5 000U and 5 mg strep)	Sigma-Aldrich	USA
T25 (25 cm3) tissue culture flasks	Corning	USA
T75 (75 cm3) tissue culture flasks	Corning	USA
Trypan Blue solution (0.4 %)	Sigma-Aldrich	USA
Trypsin/ ethylenediaminetetraacetic acid (EDTA)	Sigma-Aldrich	USA
EDTA	Saarchem	USA
Ethidium bromide	Sigma-Aldrich	USA
Fermentas Marker Plus	Fermentas	USA
Geldanamycin	BioMol International	USA
Glacial acetic acid	SAARCHEM	South Africa
Glycerol	SAARCHEM	South Africa
Glycine	Sigma-Aldrich	South Africa
HCl	Merck	South Africa
KCl	SAARCHEM	South Africa
NaCl	Sigma-Aldrich	South Africa
NP40	Roche	Germany
Ponceau S	Sigma-Aldrich	USA
Potassium diydrogen phosphate	Merck	South Africa
Protease inhibitor cocktail	Sigma-Aldrich	USA
Protein A/G PLUS-agarose immunoprecipitation reagent	Santa Cruz Biotechnologies	USA
Sodium diodecyl sulphate	Sigma-Aldrich	USA
TEMED	Sigma-Aldrich	USA
Trans-Blot® nitrocellulose membrane	Bio-Rad	South Africa
Triton X-100	Sigma-Aldrich	USA
Trizma base	Sigma-Aldrich	USA
Tryptone (pancreatic digestion of casein)	Biolab, Merck	UK
Tween-20	SAARCHEM, MERCK	South Africa

Table A2: List of primary antibodies used for Western analysis and Fluorescence microscopy.

Antibody	**Company**	**Catalogue Number**	**Dilution for Western detection**	**Dilution for confocal microscopy**
Goat polyclonal anti- VDAC antibody	Santa Cruz Biotechnologies	sc 13119	1:500	1:500
Mouse monoclonal anti-HSP75 (TR1) antibody	Santa Cruz Biotechnologies	sc13557	1:500	1:500
Rabbit polyclonal anti- STAT3 (H-190) antibody	Santa Cruz Biotechnologies	sc -7179	1:500	1:500
Rabbit polyclonal anti-pSTAT3Y705 antibody	Santa Cruz Biotechnologies	sc-7993-R	1:500	1:500
Rabbit polyclonal anti-pSTAT3S727 antibody	Santa Cruz Biotechnologies	sc-8001-R	1:500	1:500
Mouse monoclonal anti-Histone H4(F-9) antibody	Santa Cruz Biotechnologies	sc-25260	1:500	N/A
Mouse anti-Actin antibody	Santa Cruz Biotechnologies	sc-8032	1:500	N/A

Table A3: Secondary antibodies used for Western detection.

Antibody	**Company**	**Catalogue**	**Dilution**
HRP Donkey anti-mouse IgG,	Santa Cruz Biotechnologies	sc-2014	1:1000
HRP Donkey anti-rabbit IgG,	Santa Cruz Biotechnologies	sc-2013	1:1000
HRP Donkey anti-goat IgG,	Santa Cruz Biotechnologies	sc-2020	1:1000

Table A4: Secondary antibodies used for fluorescence microscopy and confocal microscopy.

Antibody	**Company**	**Catalogue**	**Dilution**	**Excitation wavelength**
Alexa Fluor® 488 chicken anti-rabbit IgG (H+L)	Invitrogen	A21441	1:1000	488 nm
Alexa Fluor® 546 donkey anti-mouse IgG (H+L)	Invitrogen	A10036	1:1000	546 nm
Alexa Fluor® 633 donkey anti-goat IgG (H+L)	Invitrogen	A21082	1:1000	630 nm

A.2 *Mycoplasma* detection protocol

Mycoplasma were tested for using immunofluorescent microscopy. Cells were seeded and grown on sterile glass cover slips overnight at 37 °C. The media was removed rinsed off with 10 mM PBS. Cells were fixed with ice cold methanol and the cover slip were dipped Hoechst 33342 (1:1000 dilution in water) for 15 seconds and left to dry on paper towel. Cover slip were mount onto glass slide with mounting medium and sealed with nail varnish. Negative detection would be clean blue nuclei without any other speckled staining around and positive detection would be blue specks (nuclear staining) around and on top of the area on the cytoplasm (Figure A1).

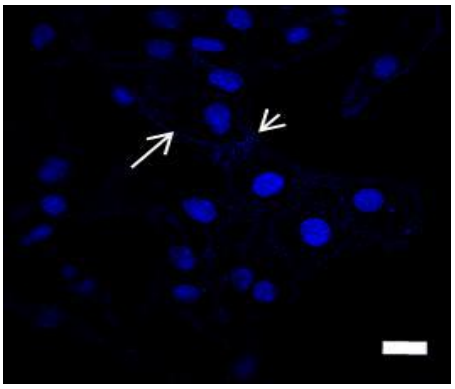

Figure A1: Confocal microscopy image of Caco2 cells contaminated with *Mycoplasma*. Caco2 cell nuclei stained with Hoechst. Scale bar represents 20 μM. Arrows point toward *Mycoplasma*.

A.3 Verification of recombinant TRAP1 gene by sequencing

>pRC_CMV-TRAP1 _T7 forward

TCCCRRRCTCGGATYCCACTAGTAACGGCCGCCAGTGTGCTGGTWATTCTGCAGATATCCATCACACTGGTGGCMGCGSAGC
CAACATGGCGCGCGAGCTGCGGGCGCTGCTGCTGTGGGGCCGCCGCCTGCGGCCTTTGCTGCGGGCGCCGGCGCTGGCGGCC
GTGCCGGGAGGAAAACCAATTCTGTGTCCTCGGAGGACCACAGCCCAGTTGGGCCCCAGGCGAAACCCAGCCTGGAGCTTG
CAGGCAGGACGACTGTTCAGCACGCAGACCGCCGAGGACAAGGAGGAACCCCTGCACTCGATTATCAGCAGCACAGAGAGC
GTGCAGGGTTCCACTTCCAAACATGAGTTCCAGGCCGAGACAAAGAAGCTTTTGGACATTGTTGCCCGGTCCCTGTACTCAG
AAAAAGAGGTGTTTATACGGGAGCTGATCTCCAATGCCAGCGATGCCTTGGAAAAACTGCGTCACAAACTGGTGTCTGACGG
CCAAGCACTGCCAGAAATGGAGATTCACTTGCAGACCAATGCCGAGGAAGGCACCATCACCATCCAGGATACTGGTATCGG
GATGACACAGGAAGAGCTGGTGTCCAACCTGGGGACGATTGCCAGATCGGGGTCAAAGGCCTTCCTGGATGCTCTGCAGAA
CCAGGCTGAGGCCAGCAGCAAGATCATCGGCCAGTTTGGAGTGGGTTTCTACTCAGCTTTCATGGTGGCTGACAGAGTGGAG
GTCTATTCCCGCTCGGCAGCCCCGGGGAGCCTGGGTTACCAGTGGCTTTCAGATGGTTCTGGAGTGTTTGAAATCGCCGAAGC
TTCGGGAGTTAGAACCGGGACAAAAATCATCATCCACCTGAAATCCGACTGCAAGGAGTTTTCCAGCGAGGCCCGGGTGCGA
GATGTGGTAACGAAGTACAGCAACCTCGTCAGCTTCCCCTTGTACTCGAATGGAAGGCGGATGAGCACCTTGCAGSCCATCT
GGATGATGGACCCCAAGGATGTCCGTGAGTGGCAACATGAGGAGTTCTACCGCTACGTCGCGCAAGGCCTCACGACAGCCCC
GCTACMCCCTGCACTWTAGACGGACGCCMACCGCYTYAACATCCGCAGCCATCTCTACGTGACCGGAMCATGAACCGGTTC
CATGGTTTTTKGAAAKGTGTGRARGA

Table A4: Top 10 pRC_CMV-TRAP1 _T7 forward BLAST search result sequences producing significant alignments.

Blast result	Description	Max score	Total score	Query cover	E value	Max ident	Accession
1	Homo sapiens TNF receptor-associated protein 1 (TRAP1), nuclear gene encoding mitochondrial protein, transcript variant 1, mRNA	1840	1840	91%	0.0	98%	NM_016292.2
2	Synthetic construct Homo sapiens clone IMAGE:100010806; FLH193498.01L; RZPDo839G1168D TNF receptor-associated protein 1 (TRAP1) gene, encodes complete protein	1840	1840	91%	0.0	98%	DQ896346.2
3	Synthetic construct clone IMAGE:100006106; FLH193502.01X; RZPDo839G1178D TNF receptor-associated protein 1 (TRAP1) gene, encodes complete protein	1840	1840	91%	0.0	98%	DQ893476.2
4	Homo sapiens TNF receptor-associated protein 1, mRNA (cDNA clone MGC:15157 IMAGE:4131231), complete cds	1840	1840	91%	0.0	98%	BC018950.2
5	Homo sapiens cDNA clone IMAGE:2822999, containing frame-shift errors	1840	1840	91%	0.0	98%	BC000406.2
6	Homo sapiens cDNA clone IMAGE:2822999, containing frame-shift errors	1840	1840	91%	0.0	98%	BC002994.1
7	Synthetic construct DNA, clone: pF1KB9972, Homo sapiens TRAP1 gene for TNF receptor-associated protein 1, without stop codon, in Flexi system	1838	1838	91%	0.0	98%	AB528744.1
8	Synthetic construct Homo sapiens heat shock protein 75 (TRAP1) mRNA, partial cds	1836	1836	91%	0.0	98%	AY335656.1
9	Homo sapiens TNF receptor-associated protein 1, mRNA (cDNA clone MGC:23363 IMAGE:4648083), complete cds	1834	1834	91%	0.0	98%	BC023585.2
10	Homo sapiens mRNA for TNF receptor-associated protein 1 variant, clone: REC08044	1834	1834	91%	0.0	98%	AK223205.1

>pRC_CMV-TRAP1 _SP6 reverse

CGWTATCMTGGGAACATCWTATGGGTATCAGTGTCGCTCTTGGGCTTGACAGCAGCTCATTCAAGGGGAGGGAGGTGGCCC
TAGGGTCGTCAACAAGTCCAGCAGCAMTCWTGGCGTTCTCGTATATCTGATCCACCAGCAGCTGAGCCAGGCCAGGCTCGCT
TGCGCGCAGCTGATCCAGCTTCTTGATGAGCGCGTGCCTGGGGTTGATCTCCAGCGTGGGCTGCAGGAGCTGTGCGCGCTCCT
CCTGGGTCTTGGCCAGCTGCTGCATGCGCAGGAAGTGGCGGGCAGCCCCCATCTCCAGCACGGTGACCATGGCAGGGTGGGT
GTCCAGTCGGAGGGTCACCTTCACGTTGGTGACACGCGACCCCAGCACATTTCTCATCCAGGCCATGAGCTCCTCCGTCTCCT
TCTCTGATAGGCACTCGGCGGCTGGGGACCTGTCCTCAAACTTCTCCTCCTTGTAGTGATCCACGACTATGTCCGTCTCCACA
GAGATCAGCTTCTTCTTGTCAAACTCACGAAGGTGCAGCAGGGTGAGCTCATCAAACTGCTCAAAGCAGAAGAGAACCTCTG
CGTCTTTCTTCTTCATGGCCTCATAGTAGGGTGAGTGCTCTGCCAGGTGACGGTTGGGGGCGCACAGGTARTAGATGTTGCGG
GTGCCGGCCCGCATGCGGCTGGCGTATTCTGAGAGGCTGGTTARCTGCCCGGAGGGCAGCGCCGAGGACTCGTAGCGCAGCA
GCTTTGCTATGTCCTCYTTGACCTCCTGCTCGGTGGCGGTCACAATGCCCTCCCCGCATGAACARGGCCCGTAATCCTTCMMA
AAAACTTTGCATACCTTTCTCAASCATCCTTTTTTTTACYCCTGGYCAATGAAGAATTTTGATCMACCCCTCYGGCTGTAAAA
CGTCCCCGGGARTTTYCCTGATGARTTGCSCTCTYCCTGCRGCAGCTCCCCGGCTGAGGYTYMGGGGGSAAATGTTCYTCMCT
GGTCCAMCCMCACCTCGGAATGRAASCSGMACCCACTTGGGGCCAGGAWGSTCCSGKGGSMYCTTKGGTCCTGGAWTRRAG
RAMMYTTTKCCG

Table A5: Top 10 pRC_CMV-TRAP1 _SP6 reverse BLAST search sequences producing significant alignments.

Blast result	Description	Max score	Total score	Query cover	E value	Max ident	Accession
1	Homo sapiens TNF receptor-associated protein 1 (TRAP1), nuclear gene encoding mitochondrial protein, transcript variant 2, mRNA	1482	1482	92%	0.0	93%	NM_001272049.1
2	Homo sapiens cDNA FLJ58608 complete cds, highly similar to Heat shock protein 75 kDa, mitochondrial precursor	1482	1482	92%	0.0	93%	AK299127.1
3	Homo sapiens TNF receptor-associated protein 1 (TRAP1), nuclear gene encoding mitochondrial protein, transcript variant 1, mRNA	1482	1482	92%	0.0	93%	NM_016292.2
4	Homo sapiens TNF receptor-associated protein 1, mRNA (cDNA clone MGC:23363 IMAGE:4648083), complete cds	1482	1482	92%	0.0	93%	BC023585.2
5	Homo sapiens TNF receptor-associated protein 1, mRNA (cDNA clone MGC:15157 IMAGE:4131231), complete cds	1482	1482	92%	0.0	93%	BC018950.2
6	Homo sapiens tumor necrosis factor type 1 receptor associated protein mRNA, complete cds	1482	1482	92%	0.0	93%	AF154108.1
7	Synthetic construct Homo sapiens clone IMAGE:100010806; FLH193498.01L; RZPDo839G1168D TNF receptor-associated protein 1 (TRAP1) gene, encodes complete protein	1478	1478	92%	0.0	93%	DQ896346.2
8	Synthetic construct clone IMAGE:100006106; FLH193502.01X; RZPDo839G1178D TNF receptor-associated protein 1 (TRAP1) gene, encodes complete protein	1478	1478	92%	0.0	93%	DQ893476.2
9	Homo sapiens TNF receptor-associated protein 1, mRNA (cDNA clone IMAGE:3138548), partial cds	1476	1476	92%	0.0	93%	BC001455.2
10	Homo sapiens cDNA FLJ36025 fis, clone TESTI2016701, highly similar to TUMOR NECROSIS FACTOR TYPE 1 RECEPTOR ASSOCIATED PROTEIN	1476	1476	92%	0.0	93%	AK093344.1

A.4 Real time cell analysis

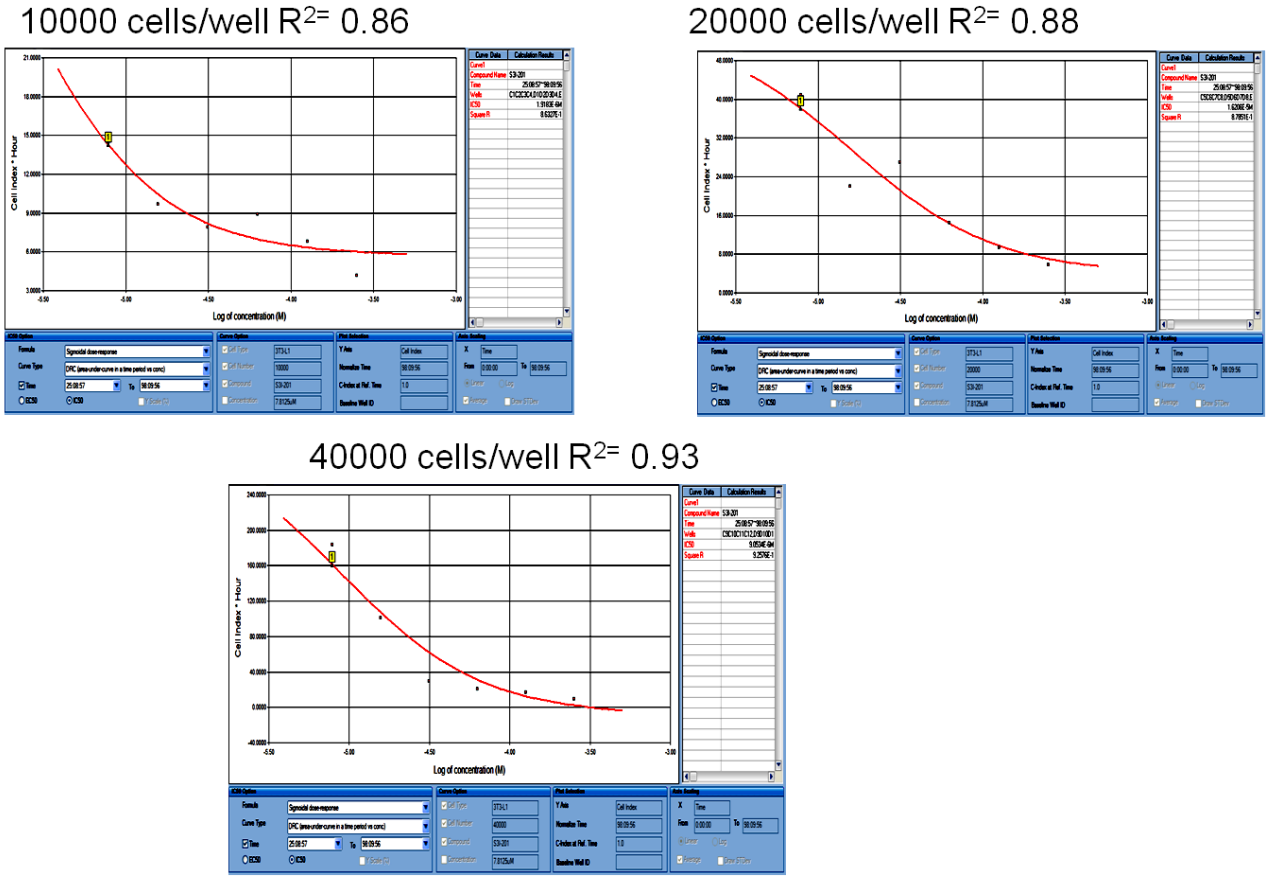

Figure A3: IC50 plots at different 3T3L1 cell densities

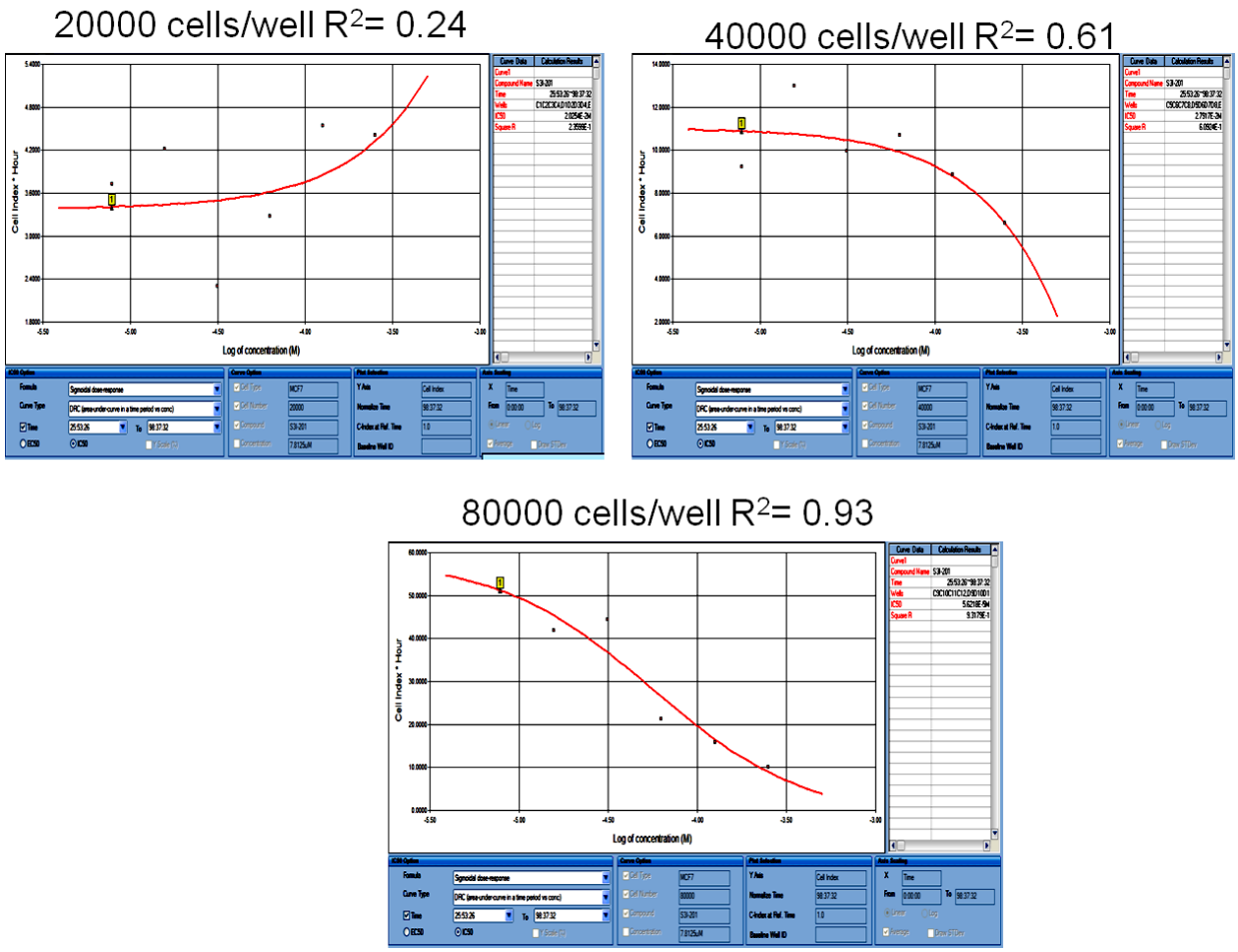

Figure A4: IC50 plots at different MCF7 cell densities

A5 Immobilization of TRAP1 for SPR

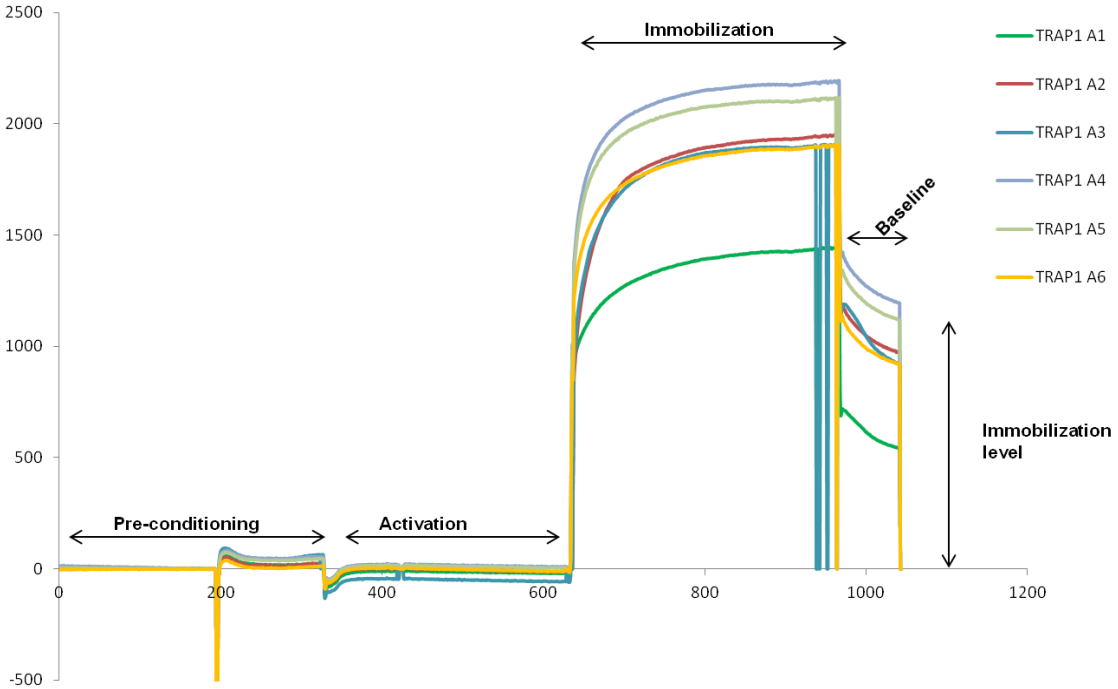

Figure A5: Immobilization of His-tagged TRAP1

Hypothesis

Guardian of the Furnace: Mitochondria, TRAP1, ROS and Stem Cell Maintenance

Rose Kadye
Adam H. Kramer
Julia Joos-Vandewalle
Michelle Parsons
Zikhona Njengele
Heinrich Hoppe
Earl Prinsloo*

Biomedical Biotechnology Research Unit, Department of Biochemistry, Microbiology and Biotechnology, Rhodes University, Grahamstown, South Africa

Abstract

Mitochondria are key to eukaryotic cell survival and their activity is linked to generation of reactive oxygen species (ROS) which in turn acts as both an intracellular signal and an effective executioner of cells with regards to cellular senescence. The mitochondrial molecular chaperone tumor necrosis factor receptor associated protein 1 (TRAP1) is often termed the cytoprotective chaperone for its role in cancer cell survival and protection from apoptosis. Here, we hypothesize that TRAP1 serves to modulate mitochondrial activity in stem cell maintenance, survival and differentiation. © 2013 IUBMB Life, 66(1):42–45, 2014

Keywords: *mitochondria; stem cells; cancer; TRAP1; reactive oxygen species*

Introduction

Tightly regulated external and internal signal processing control the two basic characteristics of stem cells: first, the ability to self-renew and second, differentiation into diverse specialized cells. Extensively interlinked signaling pathways control self-renewal through activation of defined sets of genes regulating the fine balance between self-renewal and differentiation (1, 2). Under normal physiological conditions, controlled imbalances in these signaling systems induce differentiation. Similarly in differentiated cells uncontrolled changes in these signaling systems can induce and drive cellular transformation and oncogenesis (3). Seemingly, stem cell phenotypes have also been observed in cancer as so-called cancer stem cells (4, 5).

Abbreviations: *ROS, reactive oxygen species; TRAP1, tumor necrosis factor receptor associated protein 1*

Volume 66, Number 1, January 2014, Pages 42–45

**Address correspondence to: Earl Prinsloo, Biomedical Biotechnology Research Unit, Department of Biochemistry, Microbiology and Biotechnology, PO Box 94, Rhodes University, Grahamstown, 6140, South Africa. Tel: +27466038082. Fax: +27466223984; E-mail: e.prinsloo@ru.ac.za*

Received 19 September 2013; Accepted 14 November 2013

DOI 10.1002/iub.1234

Published online 30 December 2013 in Wiley Online Library (wileyonlinelibrary.com)

Homeostatic balance in normal aerobic eukaryotic cells is required to maintain mitochondria, and fine-tuning the bioenergetic systems within stem cells becomes extremely important to maintain phenotype (6). Reactive oxygen species (ROS) produced as a by-product of mitochondrial activity, is often detrimental to cells as it causes DNA and protein damage, but this viewpoint is shifting slightly due to the role ROS plays in signaling and differentiation (7–9). Under hypoxic conditions, cells can shift from mitochondrial oxidative phosphorylation to cytosolic aerobic glycolysis, known as the Warburg effect, to produce ATP (10–12). The Warburg effect, thought to provide the building blocks required by the rapidly proliferating cells and protect the mitochondria from ROS-induced membrane damage and initiation of apoptosis, has been reported in rapidly proliferating cancer, cancer stem cells and normal stem cells (13–16). Molecular chaperones play a strong role in preventing apoptosis and the mitochondrial molecular chaperone, TRAP1, has been shown to protect cells against ROS-induced damage in cancer cell models (17–20).

Mitochondria and ROS—The Cellular Furnace

Beside their vital role in energy generation, mitochondria also play essential roles in processes such as apoptosis, cellular proliferation, calcium homeostasis and steroid metabolism (21). During oxidative phosphorylation, the respiratory complexes leak electrons to oxygen producing the free radical superoxide

(O_2^-) that is typically converted to a nonradical ROS (H_2O_2) by spontaneous dismutation or by superoxide dismutase (9). ROS leads to arrest of biosynthetic pathways and mitochondrio-cytosolic translocations which activate caspase-dependent and -independent mechanisms that together mediate apoptosis (22). Oxidative stress resulting from a disturbance of the equilibrium between ROS and endogenous antioxidant defence mechanisms causes DNA damage leading to senescence in normal cells and may result in a detrimental effect on the self-renewal ability of stem cells. Molecular chaperones, particularly of the heat shock protein 90 (Hsp90) family play a strong cytoprotective role during oxidative stress, to prevent apoptosis and promote survival. Hsp90 expression is increased to ensure and maintain proper folding and assembly of protein complexes (18, 19). Changes in the expression levels of the nuclear encoded mitochondrial located TRAP1 are suggested to regulate mitochondrial mediated apoptosis in cancer (20).

Stem Cell Mitochondria

Balancing self-renewal, maintenance and differentiation against apoptosis is vital to stem cell survival. Bioenergetics plays a crucial role in regulating stem cell fate (23, 24). An excellent example of ROS regulation in stem cells is in hematopoietic stem cells (HSCs) where overproduction of ROS affects the stem cell phenotype. HSCs exist within a well protected hypoxic niche in the bone marrow where they possess lower ROS levels than those of the subsequent progeny and are thrust into the highly oxygenated circulatory system when needed (25, 26). The stem cell niche is pushed toward decreasing ROS to prevent differentiation and hence promote an environment that is conducive to maintaining self-renewal (27).

Stem cell mitochondria are thought to play important roles in maintaining stemness and differentiation as well as cancer stem cell survival through a number of ways, for example, the regulation of the oxidative stress in the cell (11, 12, 28). The volume and efficacy of mitochondria within human embryonic stem cells determine the cell type's ability to regulate ROS and respond to oxidative stress conditions (28). Competent active mitochondria enable *in vitro* cultured embryonic stem cells to resist oxidative stress better than differentiated cells (29). Suggestions have been made that stem cell stability and differentiation state can be tested using functional mitochondrial characteristics such as subcellular localization, metabolic activity and mitochondrial mass (30). The increase in mitochondrial mass in differentiated cells would be accompanied by an increased ATP production and therefore higher ROS levels. To prevent differentiation and maintain self-renewal, the mitochondria need to be stabilized against loss of homeostasis.

TRAP1—Guarding the Furnace

As a member of the Hsp90 family of heat shock proteins known for the familial role played in signal transduction, TRAP1, an intramitochondrial protein, takes a more specialized approach to its molecular chaperone activity by acting as a cytoprotective chaperone (17, 19, 31, 32). Phosphorylation of TRAP1 by PTEN-induced putative kinase 1 protects cancer cells against oxidative stress-induced apoptosis. TRAP1, together with Hsp90α/β and immunophilin cyclophilin D (cypD), form a mitochondrial chaperone system that maintains mitochondrial homeostasis by controlling the cypD regulated mitochondrial permeability transition and appears to be actively involved in the inhibition of proapoptotic proteins (33–35). Interestingly, Hua *et al.* (35) showed that the silencing of TRAP1 through siRNA increased ROS accumulation, whereas TRAP1 overexpression decreased ROS production in cancer cell models. Recently, Yoshida *et al.* (36) have shown that TRAP1 downregulation results in altered mitochondrial activity, specifically resulting in increased complex IV activity in, among others, human cervical HeLa cells and mouse adult fibroblasts derived from TRAP1−/− knockout mice. Seemingly, this indicates conserved mammalian function and tight regulation of the shift between oxidative phosphorylation and aerobic glycolysis. The mechanism appears to be through TRAP1 interaction with the mitochondrial c-Src (Tyrosine-protein kinase CSK). Furthermore, Sciacovelli *et al.* (37) have shown that TRAP1 inhibits complex II enzymatic activity in colorectal cancer and in turn decreases cellular oxygen consumption effectively halting

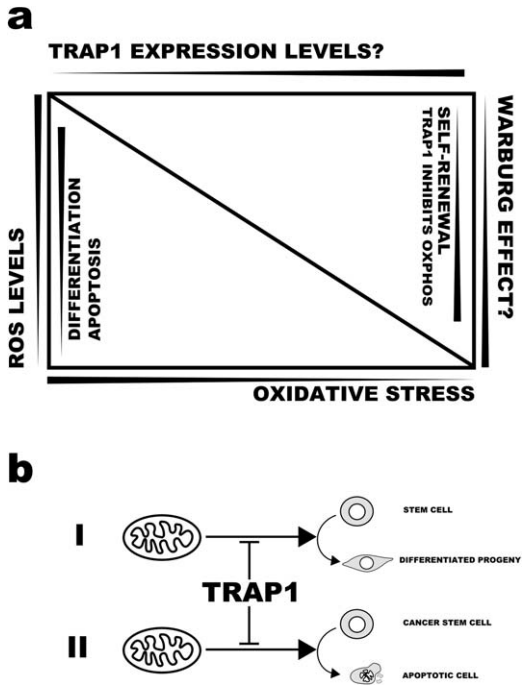

Fig 1 *A model for the role of TRAP1 modulation of ROS in stem cell fate. (A) TRAP1 expression levels are potentially linked to hypoxia, leading to increased self-renewal, decreased oxidative stress and a potential switch to the Warburg effect. This in turn decreases differentiation and/or apoptosis. (B) The "TRAP1 Buffer" maintains (I) stem cell and (II) cancer stem cell phenotypes. See text for further details.*

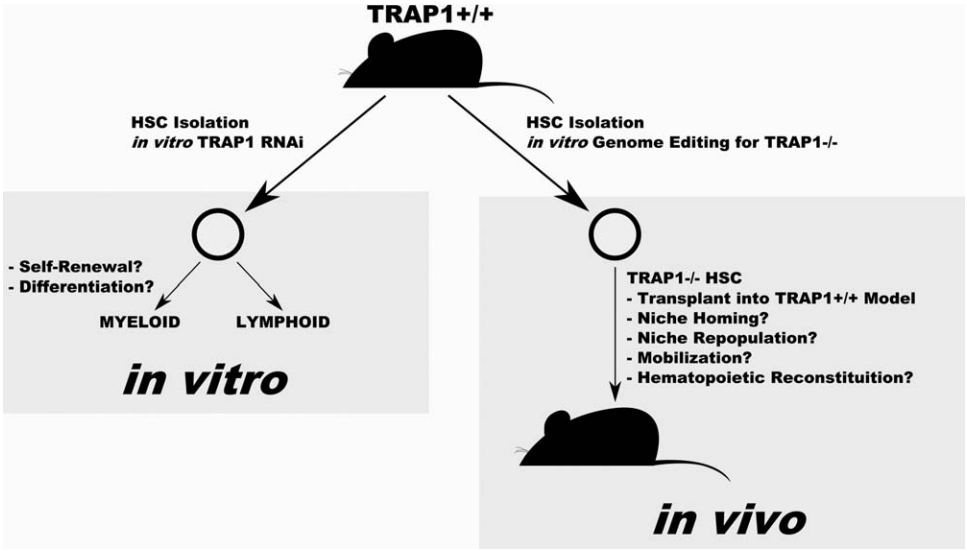

Fig 2 *Potential experimental approaches in investigating the role of TRAP1 in HSC self-renewal and differentiation. (A)* In vitro *differentiation following TRAP1 RNAi, and (B)* In vivo *homing, repopulation and mobilization of TRAP1−/− genome edited HSCs in a mouse model. See text for further details.*

oxidative phosphorylation. These critical findings point to the importance of TRAP1 in maintaining the integrity of the mitochondria under oxidative stress.

The HSC model provides us with a glimpse into the relationship (in stem cells) between hypoxia and TRAP1 by comparing genomic and proteomic expression levels (38, 39). Interestingly the response appears to be at the translational level where lower TRAP1 protein levels are found in the differentiated progenitor cell population (approximately 1.5× decrease) compared to the multipotent hematopoietic stem cell population (38, 39). The increased expression in the HSCs of the cytosolic stress inducible Hsp90α (∼1.2×) and constitutive Hsc70 (∼1.2×) was also observed suggesting a shift from a protected niche to a more stressful environment on differentiation. Proteomic data for the Myeloid Gr-1^+ and Erythroid Ter-119^+ populations would provide a clearer picture of the dynamic changes to TRAP1 expression that may occur on differentiation and also potentially reflect the switch from hypoxia (in the bone marrow) to normoxia. Linked to this Leav *et al.* (40) have shown increased TRAP1 protein expression in hypoxic basal compartment of the prostate which is known to be the prostate stem cell niche.

The buffer effect of TRAP1 in stem cells (Fig. 1), and its relationship to the molecular chaperone network, requires clarification. The HSC model provides a perfect system to test the hypothesis whether the TRAP1 buffer regulates hematopoiesis by regulation of mitochondrial ROS levels from the hypoxic stem cell niche to a less protected oxygenated environment. As TRAP1 specific inhibitors are nonexistent and effectively Hsp90 family inhibitors, directed TRAP1 knockdown in the HSC model via RNA interference is a more viable approach in understanding function and may yield interesting insight into the contribution of the protein to hematopoietic differentiation *in vitro*. Furthermore, genome editing for TRAP1 knockout and transplantation of HSCs in a mouse model (TRAP1+/+ as opposed to TRAP1−/−) may permit a more comprehensive understanding of the role of TRAP1 in homing to, repopulation of and recruitment from the hypoxic bone marrow niche *in vivo*. Figure 2 serves to illustrate these research approaches to proving/disproving the hypothesis presented here.

Conclusions

Based on available information and extrapolation from other models, questions surrounding the mitochondrial contribution to stem cell self-renewal, survival and differentiation are far from answered. Beyond the need for maintaining stable mitochondria and balancing oxidative stress, the mechanisms of regulation and modulation in stem cells (both normal and cancer) requires description. The link between molecular chaperones and oxidative stress regulation is well established in cancer and needs investigation in stem cells to further understand stem cells within their respective niche environments and to exploit this to understand stem cell differentiation i*n vitro* and *in vivo*. TRAP1 represents a model protein for asking such questions by looking at the novel interactions it mediates to regulate ROS production, its degree of upregulation (or downregulation), role it plays in the modulation of "the Warburg effect" and novel protein translocations it facilitates within the stem cell framework.

Acknowledgements

The authors would like to acknowledge Rhodes University, National Research Foundation (NRF) of South Africa, and the

Medical Research Council (MRC) of South Africa and the Kresge Foundation for financial support. R.K. is the recipient of a Rhodes University Andrew Mellon Foundation Masters Scholarship, A.H.K. is the recipient of an NRF Scarce Skills MSc Scholarship, and J.J.V.W. is the recipient of a MRC Masters Scholarship.

References

[1] Blank, U., Karlsson, G., and Karlsson, S. (2008) Signaling pathways governing stem-cell fate. Blood 111, 492– 503.

[2] Dalton, S. (2013) Signaling networks in human pluripotent stem cells. Curr. Opin. Cell. Biol. 25, 241– 246.

[3] Clevers, H. and Nusse, R. (2012) Wnt/β-catenin signaling and disease. Cell 149, 1192– 1205.

[4] Schepers, A. G., Snippert, H. J., Stange, D. E., Van den Born, M., Van Es, J. H., et al. (2012) Lineage tracing reveals Lgr5+ stem cell activity in mouse intestinal adenomas. Science 337, 730– 735.

[5] Driessens, G., Beck, B., Caauwe, A., Simons, B. D., Blanpain, C., et al. (2012) Defining the mode of tumour growth by clonal analysis. Nature 488, 527– 530.

[6] Yu, W-M., Liu, X., Shen, J., Jovanovic, O., Pohl, E. E., et al. (2013) Metabolic regulation by the mitochondrial phosphatase PTPMT1 is required for hematopoietic stem cell differentiation. Cell Stem Cell 12, 62– 74.

[7] Le Belle, J. E., Orozco, N. M., Paucar, A. A., Saxe, J. P., Mottahedeh, J., et al. (2011) Proliferative neural stem cells have high endogenous ROS levels that regulate self-renewal and neurogenesis in a PI3K/Akt-dependant manner. Cell Stem Cell 8, 59– 71.

[8] Tormos, K. V., Anso, E., Hamanaka, R. B., Eisenbart, J., Joseph, J., et al. (2011) Mitochondrial complex III ROS regulate adipocyte differentiation. Cell Metab. 14, 537– 544.

[9] Murphy, M. P. (2009) How mitochondria produce reactive oxygen species. Biochem. J. 417, 1– 13.

[10] Kobayashi, C. I. and Suda, T. (2012) Regulation of reactive oxygen species in stem cells and cancer stem cells. J. Cell. Physiol. 227, 421– 430.

[11] Chaudhari, P., Ye, Z., and Jang, Y-Y. (2012) Roles of reactive oxygen species in the fate of stem cells. Antioxid. Redox. Signal DOI: 10.1089/ars.2012.4963.

[12] Shi, X., Zhang, Y., Zheng, J., and Pan, J. (2012) Reactive oxygen species in cancer stem cells. Antioxid. Redox. Physiol. 16, 1215– 1228.

[13] Kondoh, H., Lleonart, M. E., Nakashima, Y., Yokode, M., Tanaka, M., et al. (2007) A high glycolytic flux supports the proliferative potential of murine embryonic stem cells. Antioxid. Redox. Physiol. 9, 293– 299.

[14] Menendez, J. A., Joven, J., Cufí, S., Corominas-Faja, B., Oliveras-Ferraros, C., et al. (2013) The Warburg effect version 2.0: metabolic reprogramming of cancer stem cells. Cell Cycle 12, 1166– 1179.

[15] Ruckenstuhl, C., Büttner, S., Carmona-Gutierrez, D., Eisenberg, T., Kroemer, G., et al. (2009) The Warburg effect suppresses oxidative stress induced apoptosis in a yeast model for cancer. PloS One 4, e4592.

[16] Gogvadze Gogvadze, V., Zhivotovsky, B., and Orrenius, S. (2010) The Warburg effect and mitochondrial stability in cancer cells. Mol. Aspects Med. 31, 60– 74.

[17] Montesano Gesualdi, N., Chirico, G., Pirozzi, G., Costantino, E., Landriscina, M., et al. (2007) Tumor necrosis factor-associated protein 1 (TRAP-1) protects cells from oxidative stress and apoptosis. Stress 10, 342– 350.

[18] Sreedhar, A. S. and Csermely, P. (2004) Heat shock proteins in the regulation of apoptosis: new strategies in tumor therapy: a comprehensive review. Pharmacol. Ther. 101, 227– 257.

[19] Kang, B. H., Plescia, J., Dohi, T., Rosa, J., Doxsey, S. J., et al. (2007) Regulation of tumor cell mitochondrial homeostasis by an organelle-specific Hsp90 chaperone network. Cell 131, 257– 270.

[20] Masuda, Y., Shima, G., Aiuchi, T., Horie, M., Hori, K., et al. (2004) Involvement of tumor necrosis factor receptor-associated protein 1 (TRAP1) in apoptosis induced by beta-hydroxyisovalerylshikonin. J. Biol. Chem. 279, 42503– 42515.

[21] McBride, H. M., Neuspiel, M., and Wasiak, S. (2006) Mitochondria: more than just a powerhouse. Curr. Biol. 16, R551 – R560.

[22] Green, J. C. and Reed, D. R. (1998) Mitochondria and apoptosis. Science 281, 1309– 1312.

[23] Vieira, H. L., Alves, P. M., Vercelli, A. (2011) Modulation of neuronal stem cell differentiation by hypoxia and reactive oxygen species. Prog. Neurobiol. 93, 444– 455.

[24] Wang, K., Zhang, T., Dong, Q., Nice, E. C., Huang, C., et al. (2013) Redox homeostasis: the linchpin in stem cell self-renewal and differentiation. Cell Death Dis. 4, e537.

[25] Parmar, K., Mauch, P., Vergilio, J-A., Sackstein, R., Down, J. D. (2007) Distribution of hematopoietic stem cells in the bone marrow according to regional hypoxia. Proc. Natl. Acad. Sci. USA 104, 5431– 5436.

[26] Miao, W., Xufeng, R., Park, M-R., Gu, H., Hu, L., et al. (2013) Hematopoietic stem cell regeneration enhanced by ectopic expression of ROS-detoxifying enzymes in transplant mice. Mol. Ther. J. Am. Soc. of Gene Ther. 21, 423– 432.

[27] Mohyeldin, A., Garzón-Muvdi, T., and Quiñones-Hinojosa, A. (2010) Oxygen in stem cell biology: a critical component of the stem cell niche. Cell Stem Cell 7, 150– 161.

[28] Cho, Y. M., Kwon, S., Pak, Y. K., Seol, H. W., Choi, Y. M., et al. (2006) Dynamic changes in mitochondrial biogenesis and antioxidant enzymes during the spontaneous differentiation of human embryonic stem cells. Biochem. Biophys. Res. Commun. 348, 1472– 1478.

[29] Saretzki, G., Armstrong, L., Leake, A., Lako, M., and Von Zglinicki, T. (2004) Stress defense in murine embryonic stem cells is superior to that of various differentiated murine cells. Stem Cells 22, 962– 971.

[30] Nesti, C., Pasquali, L., Vaglini, F., Siciliano, G., Murri, L., et al. (2007) The role of mitochondria in stem cell biology. Biosci. Rep. 27, 165– 171.

[31] Landriscina, M., Laudiero, G., Maddalena, F., Amoroso, M. R., Piscazzi, A., et al. (2010). Mitochondrial chaperone Trap1 and the calcium binding protein Sorcin interact and protect cells against apoptosis induced by antiblastic agents. Cancer Res. 70, 6577 – 6586.

[32] Matassa, D. S., Amoroso, M. R., Maddalena, F., Landriscina, M., and Esposito, F. (2012) New insights into TRAP1 pathway. Am. J.Cancer Res. 2, 235– 248.

[33] Altieri, D. C., Stein, G. S., Lian, J. B., and Languino, L. R. (2012) TRAP-1, the mitochondrial Hsp90. Biochim. Biophys. Acta 1823, 767– 773.

[34] Pridgeon, J. W., Olzmann, J., Chin, L-S., and Li, L. (2007) PINK1 protects against oxidative stress by phosphorylating mitochondrial chaperone TRAP1. PLoS Biol. 5, e172.

[35] Hua, G., Zhang, Q., and Fan, Z. (2007) Heat shock protein 75 (TRAP1) antagonizes reactive oxygen species generation and protects cells from granzyme M-mediated apoptosis. J. Biol. Chem. 282, 20553– 20560.

[36] Yoshida, S., Tsutsumi, S., Muhlebach, G., Sourbier, C., Lee, M-J., et al. (2013) Molecular chaperone TRAP1 regulates a metabolic switch between mitochondrial respiration and aerobic glycolysis. Proc. Natl. Acad. Sci. USA 110, E1604– E1612.

[37] Sciacovelli, M., Guzzo, G., Morello, V., Frezza, C., Zheng, L., et al. (2013) The mitochondrial chaperone TRAP1 promotes neoplastic growth by inhibiting succinate dehydrogenase. Cell Metab. 17, 988– 999.

[38] Gerrits, A., Li, Y., Tesson, B. M., Bystrykh, L. V., Weersing, E., et al. (2009) Expression quantitative trait loci are highly sensitive to cellular differentiation state. PLoS Gen. 5, e1000692.

[39] Klimmeck, D., Hansson, J., Raffel, S., Vakhrushev, S. Y., Trumpp, A., et al. (2012) Proteomic cornerstones of hematopoietic stem cell differentiation, distinct signatures of multipotent progenitors and myeloid committed cells. Mol. Cell. Proteomics 11, 286– 302.

[40] Leav, I., Plescia, J., Goel, H. L., Li, J., Jiang, Z., et al. (2010) Cytoprotective mitochondrial chaperone TRAP-1 as a novel molecular target in localized and metastatic prostate cancer. Am. J. Pathol. 176, 393– 401.